ENGINEERING RESEARCH INSTITUTE
THE UNIVERSITY OF MICHIGAN
ANN ARBOR

Technical Report

A SIMPLIFIED FALLING-SPHERE METHOD FOR UPPER-AIR DENSITY

Submitted for the Project

by

L. M. Jones
F. L. Bartman

Department of Aeronautical Engineering

The research reported in this document has been sponsored by the Geophysics Research Directorate of the Air Force Cambridge Research Center, Air Research and Development Command, under Contract No. AF 19(604)-999.

Project 2215

DEPARTMENT OF THE AIR FORCE
AIR FORCE CAMBRIDGE RESEARCH CENTER
GEOPHYSICS RESEARCH DIRECTORATE
M/F CONTRACT AF 19(604)-999

June 1956

ERRATA

Page	Line	Should read (Correction is underscored.):
vii	2 from bottom	45 Acceleration vs time, DAN No. 2 sphere 59
vii	1 from bottom	46 Horizontal range vs time, DAN No. 2 nose cone 62
ix	3 from top	experiment for upper-air density and a suitable ...
2	5 from bottom	In this equation a_D and V are the magnitudes of vectors ...
3	14 from bottom	much as the four-foot spheres of References 4 and 5 ...
10	3 from top	seconds from start of record
11	3 from top	seconds from start of record
15	8 from bottom	v_o, it may be seen by (16) ...
40	6 from top	means, the 10-kc signal marks take-off ...
40	14 from bottom	the frequency by 6 ...
59	1 from bottom	Fig. 45. Acceleration vs time, DAN No. 2 sphere.
62	8 from bottom	Fig. 46. Horizontal range vs time, DAN No. 2 nose cone.
71	top curve	(See graph.)
86	8 from top	square root of the number of points ...
88	10 from top	July, 1956.

TABLE OF CONTENTS

TABLE OF CONTENTS (Concl.)

LIST OF TABLES

LIST OF FIGURES

LIST OF FIGURES (Cont.)

LIST OF FIGURES (Concl.)

OBJECTIVE

The project objective is to develop the small-sphere experiment for upper-air density for a suitable rocket system to the point where the combination can be used for synoptic surveys.

ABSTRACT

The successful development and field test of the small-sphere rocket experiment for upper-air density and temperature was carried out. The general aerodynamics of the method was applied specifically to the small-sphere case. An accelerometer for measuring drag acceleration directly was developed. A telemetering and ground-station system was designed, built, and operated. The Nike-Deacon rocket system was adapted to sounding purposes. Two flights, one carrying the complete experiment, were carried out. Densities to 260,000 feet and temperatures to 228,000 feet were obtained. The errors were evaluated.

UNIVERSITY OF MICHIGAN PROJECT PERSONNEL

Both Part Time and Full Time

Bartman, Frederick L., M.S., Research Engineer

Filsinger, Edward A., Instrument Maker

Finkbeiner, Richard G., Electronic Technician

Gleason, Kermit L., Instrument Maker

Hansen, William H., B.S., Associate Research Engineer

Harrison, Lillian M., Secretary

Harwit, Martin O., M.A., Research Assistant

Jones, Leslie M., B.S., Project Supervisor

Liu, Vi Cheng, Ph.D., Research Engineer

Pattinson, Theodore R., Electronic Technician

Reddy, Gopal K., M.S., Assistant in Research

Schaefer, Edward J., M.S., Research Engineer

Titus, Paul A., Research Associate

Wenk, Norman J., B.S., Research Engineer

1. INTRODUCTION

The general profile of upper-air density, pressure, and temperature based on rocket measurements is given in the Panel Atmosphere.[1] Synoptic data, i.e., with temporal and geographic variations, are desirable for the purpose of establishing a standard atmosphere. The preparation of a standard atmosphere to 500 kilometers has been undertaken by the Air Force Cambridge Research Center.[2] This model atmosphere is a proposed extension to the ICAO Standard Atmosphere,[3] a revised version of which will be published shortly.

A technique for obtaining upper-air density and temperature by measuring the drag of a falling sphere was developed by the upper-atmosphere research group in the Department of Aeronautical Engineering at the University. Rocket-borne aerodynamic methods for density, pressure, and temperature used previously by the group required the calibration and telemetering of end-organ outputs as well as accurate tracking of the rocket for velocity, position, and angle of attack. It was thought that if the velocity and drag accelerations of a falling sphere were obtained from the measured trajectory, ambient density could be calculated directly from the drag equation, thus eliminating the necessity of obtaining data from end organs and avoiding angle-of-attack problems. The first approach[4,5] was to eject inflatable spheres four feet in diameter from Aerobee rockets and measure their trajectories by means of the DOVAP[6] tracking system and a DOVAP transponder in the sphere. This experiment was performed with a satisfactory degree of success on four occasions. The inflatable-sphere technique, while simpler than some other methods, required the use of an Aerobee rocket and the elaborate ground array of the DOVAP system and therefore could not be considered a "synoptic" method. Further simplifications of the sphere experiment were conceived and studied for feasibility. The development and field use of these ideas is the subject of this report.

The most important change was to measure directly, within the sphere, the drag acceleration. This is in contrast to measuring the total acceleration by DOVAP and subtracting the acceleration of gravity to find the small difference, which is the drag acceleration. An accelerometer was developed which would make the desired drag measurement. It was hoped that the accelerometer could be designed to fit in a sphere which would in turn

fit in the Deacon rocket of the Nike-Deacon combination. This two-stage, all-solid-propellant rocket was being investigated as an inexpensive alternative to the Aerobee for carrying payloads one-third that of the Aerobee to Aerobee altitudes. As developed, the accelerometer sensitivity is such as not only to permit use of a small sphere but also ultimately to extend the altitude range of the experiment by a significant amount. The Nike-Deacon also showed promise and the work with it resulted in the successful adaptation to upper-air sounding purposes.

This report describes the aerodynamics of the sphere experiment, the development of the accelerometer, sphere, ground station, and rocket. It describes the successful flights in April and June, 1955, of two Nike-Deacons carrying the small sphere and gives the density and temperature results of the second flight which are in good agreement with other rocket results.

2. AERODYNAMICS

The forces acting on a free-falling sphere, the density of which is large compared to that of the ambient atmosphere, are gravitational attraction and aerodynamic drag. Since the necessity for knowing the gravity force can be eliminated by the proper choice of measurement reference system (see Section 3), the drag force only is of interest. The lateral force induced by spinning is negligible compared to drag in this experiment because the rotational circumferential velocity is negligible compared to the translational velocity. From the drag equation we have

$$\rho = \frac{2ma_D}{V^2AC_D}, \tag{1}$$

where

ρ = ambient-air density,
m = mass of sphere,
a_D = drag acceleration,
V = velocity of sphere relative to air,
A = cross-sectional area of sphere, and
C_D = drag coefficient, a dimensionless parameter.

In this equation a_D and V are vectors having opposite directions. For high angle firings the velocity vector throughout most of the trajectory will be in the same direction as the acceleration of gravity. At the top of the trajectory where V is small, a correction must be made for the horizontal component which is known from auxiliary tracking (radar) or from the launching

angle of the rocket. For low-angle firings, such as DAN 2, this correction must be applied throughout. Also, when V is small, winds may cause an error but it can be shown that for typical winds the error is negligible. Estimated values of typical winds have been given by Bartman, Liu, and Schaefer.[7]

The drag coefficient, C_D, is a function of the dimensionless parameters M and λ/d, which are the Mach number and Knudsen number, respectively.

M = Mach number = V/a,
V = sphere velocity,
a = ambient sound velocity,
λ/d = Knudsen number,
λ = mean free path, and
d = a characteristic dimension, i.e., diameter of the sphere.

A third dimensionless parameter of significance to the experiment is Reynolds number, $Re = V\rho d/\mu$, where μ is the coefficient of viscosity of air. It is known from kinetic theory that μ is proportional to $\rho a\lambda$, which leads to the relation

$$\frac{\lambda}{d} \sim \frac{M}{Re} .$$

Thus C_D depends on Mach number and Reynolds number. Values of C_D are obtained from ballistic-range, wind-tunnel, and other measurements. The values are then used for the spheres of the experiment at the same values of M and Re. The close agreement of results from the falling-sphere method with the Panel atmosphere and with balloon results may be construed as evidence of the validity of the assumption, consistent with the requirements of dimensional analysis, that the drag coefficient of a sphere in a rarefied gas is primarily a function of Mach number and Reynolds number of the flow. Inasmuch as the four-foot spheres of References 5 and 6 yielded reasonable results, it may be argued that the coefficients of drag for the seven-inch spheres of this report are quite good because the dimensional extrapolation from the 1/2-inch test spheres of, say, a ballistic tunnel to the seven-inch size used in the rocket flights is much less than in the case of the four-foot spheres.

Spheres, because of their geometrical simplicity, are commonly used to calibrate flow devices such as ballistic ranges and wind tunnels. In spite of this, the "map" of C_D as a function of M and Re had significant gaps in the region of interest to the sphere experiment. At the request of The University of Michigan, the Naval Ordnance Laboratory at White Oak, Maryland, undertook to fill in some of the blank areas. The result is seen in Fig. 1.[8] At the further request of the University, NOL is currently measuring sphere drag coefficient in the cross-hatched area of Fig. 1. These

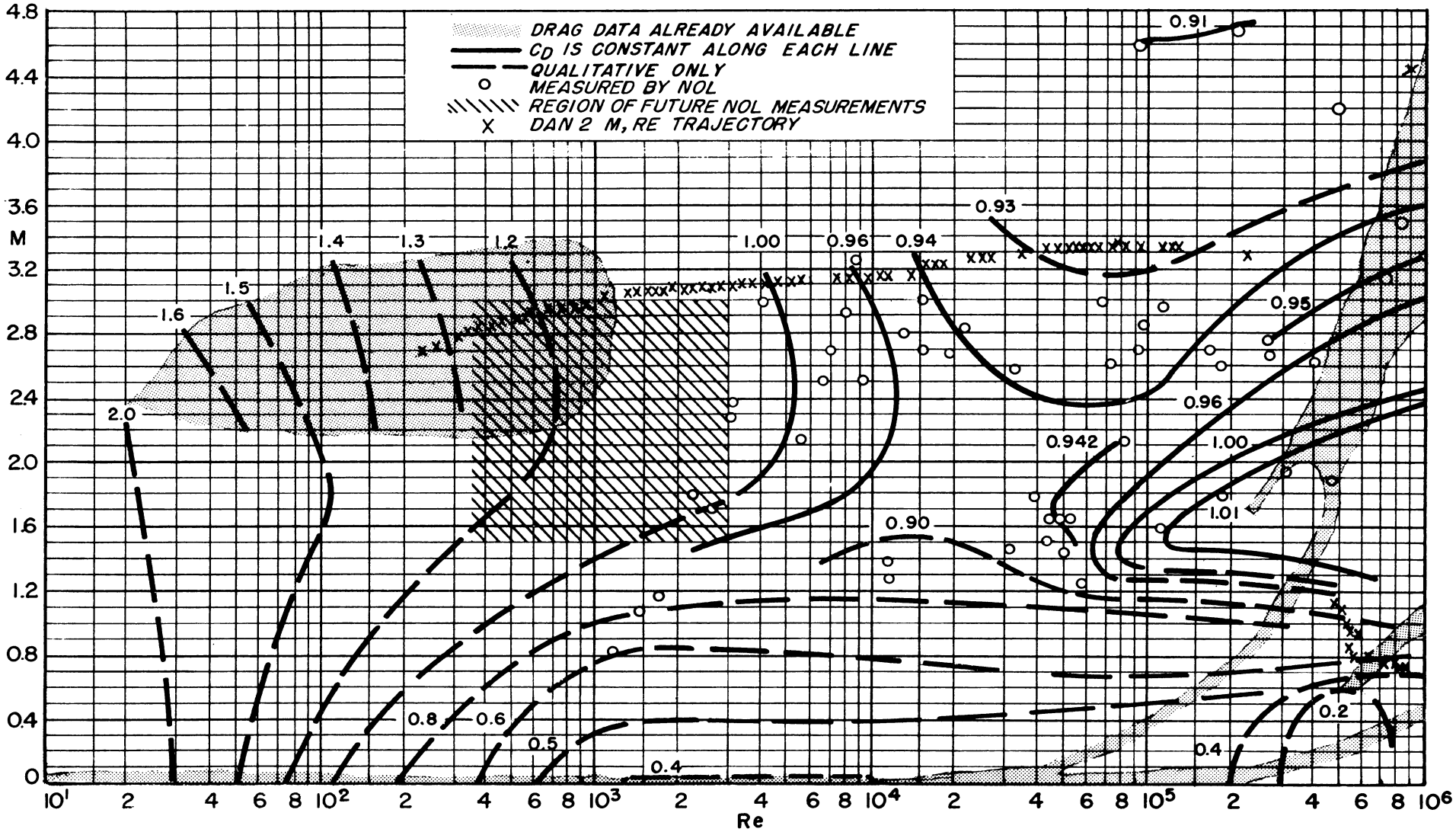

Fig. 1. Contour map of drag coefficient as a function of Mach number and Reynolds number.

data will be useful in extending the sphere experiment to higher altitudes and in bridging the gap between the previous NOL points and the data in the upper-left-hand corner which were obtained in the hypersonic wind tunnel at the University of California.[9,10] A tie-in of the wind-tunnel data with ballistic-range data is desirable, not only to make more C_D values available but also to shed some light on the magnitude of the effect of the sting and turbulence on wind-tunnel results. The ballistic-range data are not subject to difficulties from these two factors and the range conditions are thought to be an excellent simulation of the falling-sphere conditions.

The drag-coefficient function of Fig. 1 shows no evidence of a critical Reynolds number in the supersonic flow. It appears from the shadowgraphs taken in connection with the NOL experiments that the point of separation on spheres at supersonic speeds is marked by a shock wave, the location of which is sensitive neither to the Reynolds number nor to the Mach number. The fact that the separation phenomena on spheres at supersonic speeds are no longer controlled by the boundary-layer conditions (as in subsonic flow) may be considered as the reason that the drag coefficient of a sphere is insensitive to the Reynolds number.

3. PREDICTED TRAJECTORIES[11]

Predicting the trajectory of a sphere, i.e., position, velocity, and acceleration, is a straightforward process which can be done on a desk calculator. A family of trajectories for different spheres dropped from various altitudes is often useful for such things as estimating temperature rise, determining maximum acceleration to be encountered, making an error analysis, and so on. In order to assemble a catalog of sphere trajectories without laborious calculation, the problem was worked out on an analog computer (Reeves REAC C101). The computer prediction process is of course significantly different from the calculation of final results, i.e., density and temperature, from the data of a flight. The latter process is digital and is described in Section 9.

3.1. EQUATIONS

The equation of motion of the falling sphere is written as

$$\vec{a} = \vec{g} + \frac{C_D \rho A |\vec{V}| \vec{V}}{2m} , \qquad (2)$$

where g is the acceleration of gravity and the other symbols are as in (1). The frame of reference is a right Cartesian coordinate system at sea level on the earth's surface. Coriolis acceleration is neglected.

Assuming that the motion takes place in a vertical plane, the following are the equations for the two components of motion:

Vertical

$$\ddot{x}_3 = -g - \frac{C_D \rho A}{2m} (\dot{x}_3 - w_3) \sqrt{(\dot{x}_1 - w_1)^2 + (\dot{x}_3 - w_3)^2}$$

$$= -g - \rho g \frac{C_D \beta}{2} (\dot{x}_3 - w_3) \sqrt{(\dot{x}_1 - w_1)^2 + (\dot{x}_3 - w_3)^2} \quad (3)$$

Horizontal

$$\ddot{x}_1 = -\frac{C_D \rho A}{2m} (\dot{x}_1 - w_1) \sqrt{(\dot{x}_1 - w_1)^2 + (\dot{x}_3 - w_3)^2}$$

$$= -\rho g \frac{C_D \beta}{2} (\dot{x}_1 - w_1) \sqrt{(\dot{x}_1 - w_1)^2 + (\dot{x}_3 - w_3)^2} \quad (4)$$

where

$g = |g|$,
$\beta = A/mg$,
$\dot{x}_1 = \frac{dx_1}{dt}$
t = time, and
w_1, w_3 = wind-velocity components.

Although g decreases approximately 0.5% for each 50,000-foot increase in altitude, it is assumed to be constant at its average value over the altitude range. C_D is assumed to be constant at 0.95. The air density, ρ, is taken from the UARRP atmosphere. In most cases, especially with small spheres, the wind effect is negligible. The wind terms are left in the equations below, however, to show how they can be handled on the computer. The equations are used in the following form:

$$X_3'' = \frac{g}{60} - \frac{C_D \beta}{2} \rho_1 (X_3' - W_3) \sqrt{(X_1' - W_1)^2 + (X_3' - W_3)^2} \quad (5)$$

$$X_1'' = \frac{C_D \beta}{2} \rho_1 (X_1' - W_1) \sqrt{(X_1' - W_1)^2 + (X_3' - W_3)^2} \quad (6)$$

where

a computer unit (1 volt) = 1500 feet,
computer time τ = t/5, and
ρ_1 = 1500 ρg.

Thus:

$$x_1 = 1500\ X_1 \tag{7}$$

$$x_3 = 1500\ X_3 \tag{8}$$

$$\dot{x}_1 = \frac{dx_1}{dt} = 300\ \frac{dX_1}{d\tau} = 300\ X_1' \tag{9}$$

$$\dot{x}_3 = \frac{dx_3}{dt} = 300\ \frac{dX_3}{d\tau} = 300\ X_3' \tag{10}$$

$$\ddot{x}_1 = \frac{d^2x_1}{dt^2} = 60\ \frac{d^2X_1}{d\tau^2} = 60\ X_1'' \tag{11}$$

$$\ddot{x}_3 = \frac{d^2x_3}{dt^2} = 60\ \frac{d^2X_3}{d\tau^2} = 60\ X_3'' \tag{12}$$

$$w_1 = 300\ W_1 \tag{13}$$

$$w_3 = 300\ W_3\ . \tag{14}$$

3.2. COMPUTER CIRCUIT

Figure 2 is a schematic of the computer circuit. For simplicity, buffer amplifiers used to prevent loading are not shown. Voltages are scaled up or down to use effectively the range of the computer. The complete circuit setup enables one to calculate simultaneously a vacuum trajectory for a sphere, a drag trajectory for a second sphere, and the relative position and velocity of the two.

The Reeves input table was used to generate the density function. In this type of function generator, a wire on a graph mounted on a drum serves as the arm of a linear potentiometer to pick off a voltage proportional to the ordinate of the graph. The ordinate of the density curve varies by a factor of 10^5 over the range of altitudes 40,000 to 400,000 feet. Since it would have been difficult to fasten a wire accurately on such a graph, the square root of the density was generated and then squared. Figure 3 shows the density function.

One-second time marker pulses were used to mark the trajectory data. A relay was used to start the solution on one of the time pulses. The time

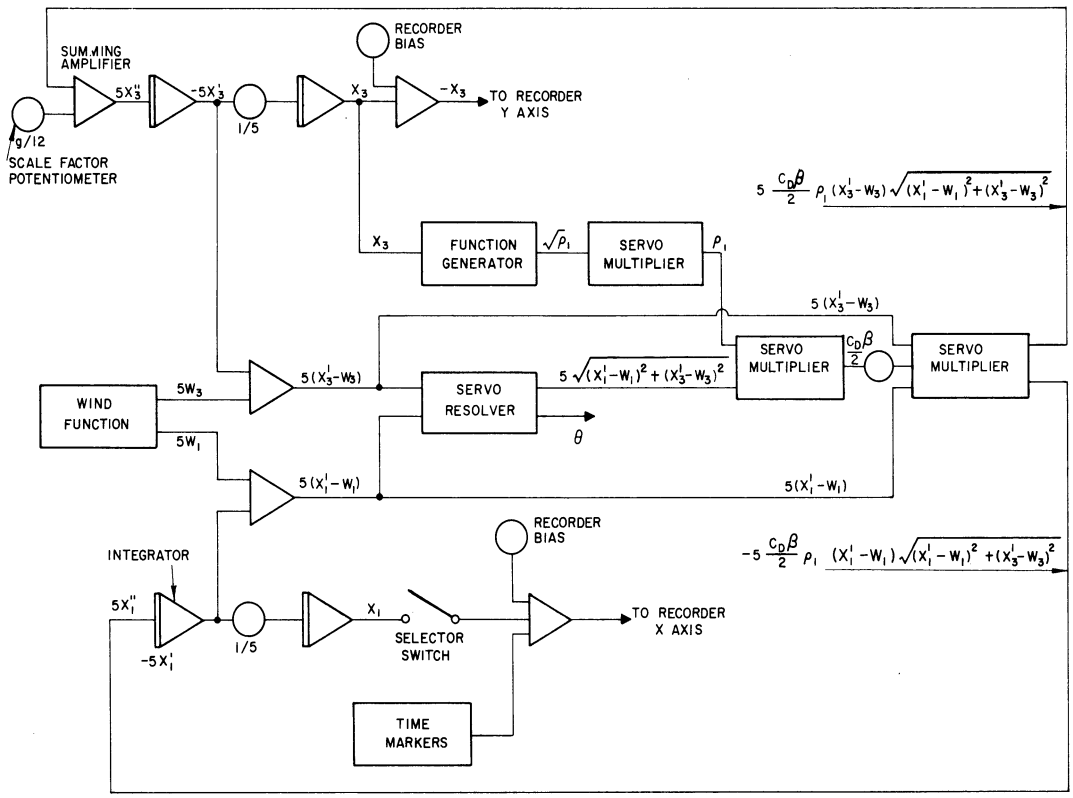

Fig. 2. Analog computer circuit for sphere trajectories.

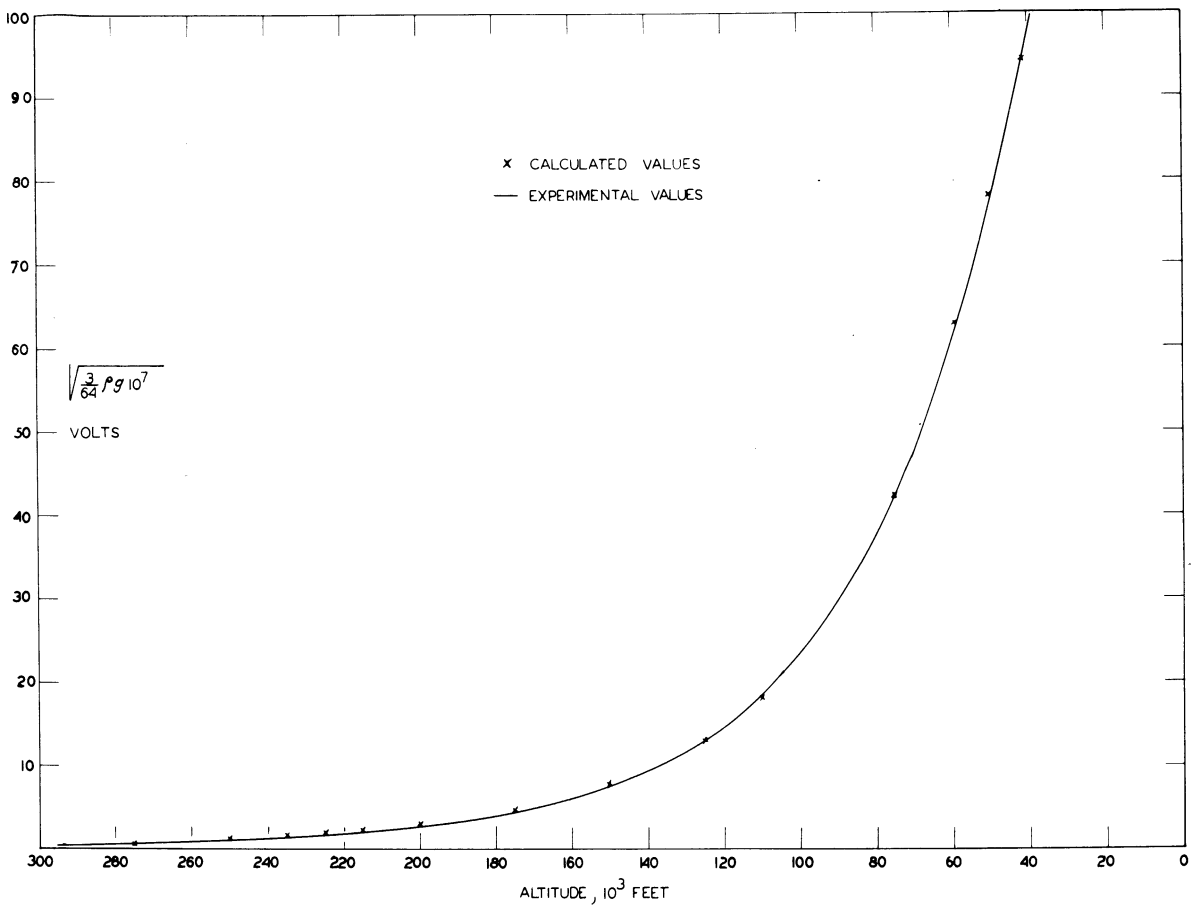

Fig. 3. Density function for computer.

marks indicate 5-second intervals in problem time. Initial altitudes and velocities were set in the appropriate integrators.

3.3. RESULTS

Figure 4 shows the trajectories of spheres of different area-to-weight ratios (β) dropped from an altitude of 350,000 feet. Figure 5 shows the trajectories of a sphere with $\beta = .031$ (which is the one used in the flights of this report) dropped from various altitudes.

The analog computer has proved extremely useful in obtaining trajectories for various purposes. Its use will be extended to large, light spheres, higher trajectories, and the small accelerations encountered near peak.

4. ACCELEROMETER

The acceleration of a sphere might be measured with respect to various reference bodies. In the DOVAP case the earth is used. This permits the measurement of the total acceleration of the sphere and thus has the advantage of permitting, in theory at least, the measurement of wind. A distinct disadvantage is that the acceleration of gravity must be subtracted from the total acceleration to get the drag acceleration. Since, throughout much of the flight, the drag acceleration is small it is obtained by differencing two large quantities, a notoriously poor process. Also, the DOVAP system requires a tremendous array of ground equipment as well as a flight unit. If the measuring reference body is carried along in the rocket and dropped with the sphere, they will both experience the acceleration of gravity. Thus the relative acceleration of sphere and reference body is the difference in their respective drag accelerations. Then, if the drag of the reference body is made negligibly small, the difference will be the drag acceleration of the sphere. The reference bodies may be either free-falling or constrained and may be either external to the sphere or internal. The internal constrained-body type, for example, would correspond to a conventional spring-mass accelerometer. The external free-falling reference system could be realized by a two-body arrangement in which the drag of a large, light sphere is measured by an rf link with respect to a small, dense, nearly free-falling body released from the rocket simultaneously. Considerations of aerodynamic and mechanical simplicity, range of measurement, and accuracy led to the choice of the free-falling internal-reference-body system, which arrangement constitutes a transit-time accelerometer. The drag on the reference body in this case is completely negligible.

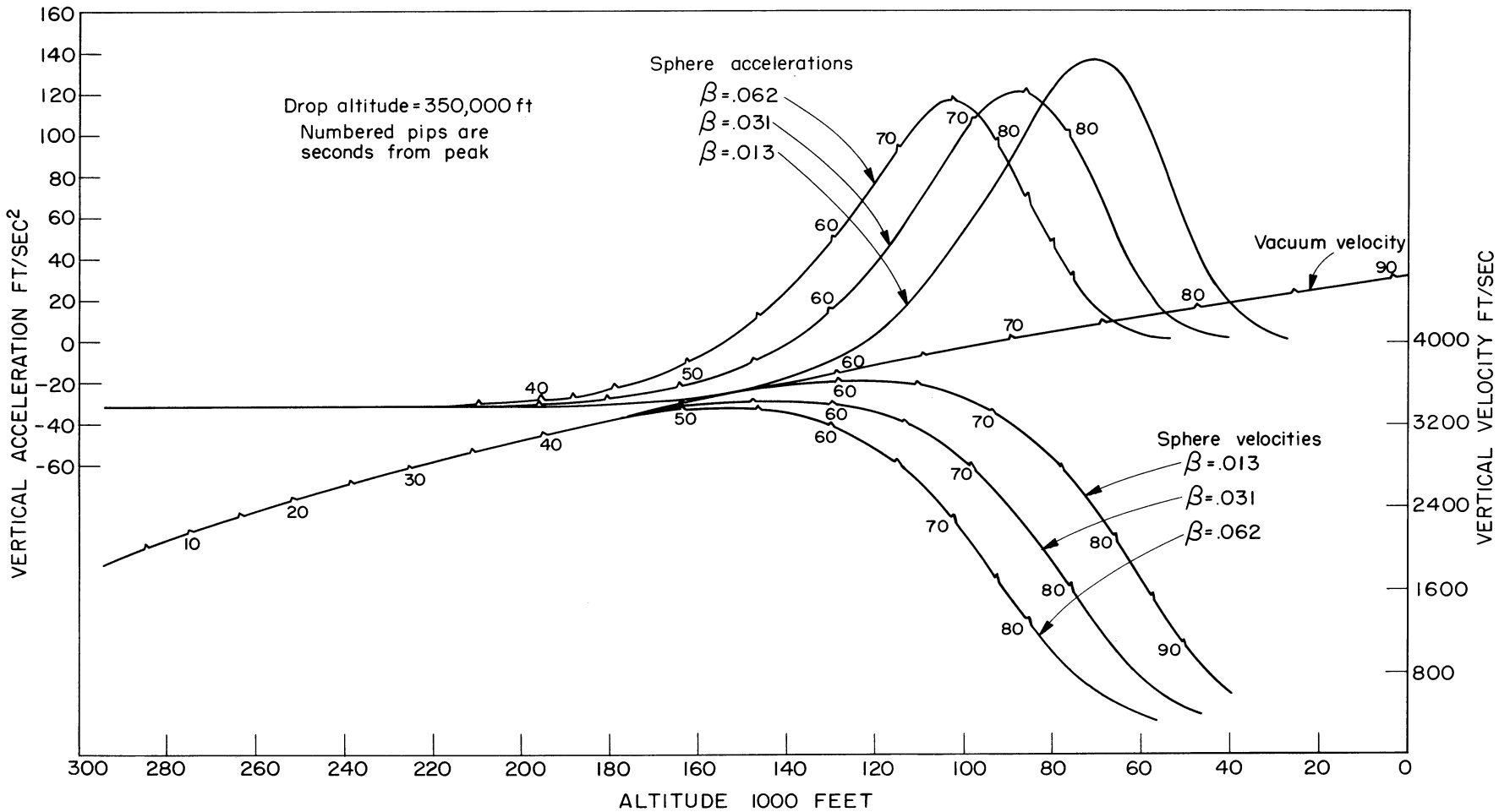

Fig. 4. Predicted trajectories for spheres of different β dropped from 350,000 feet.

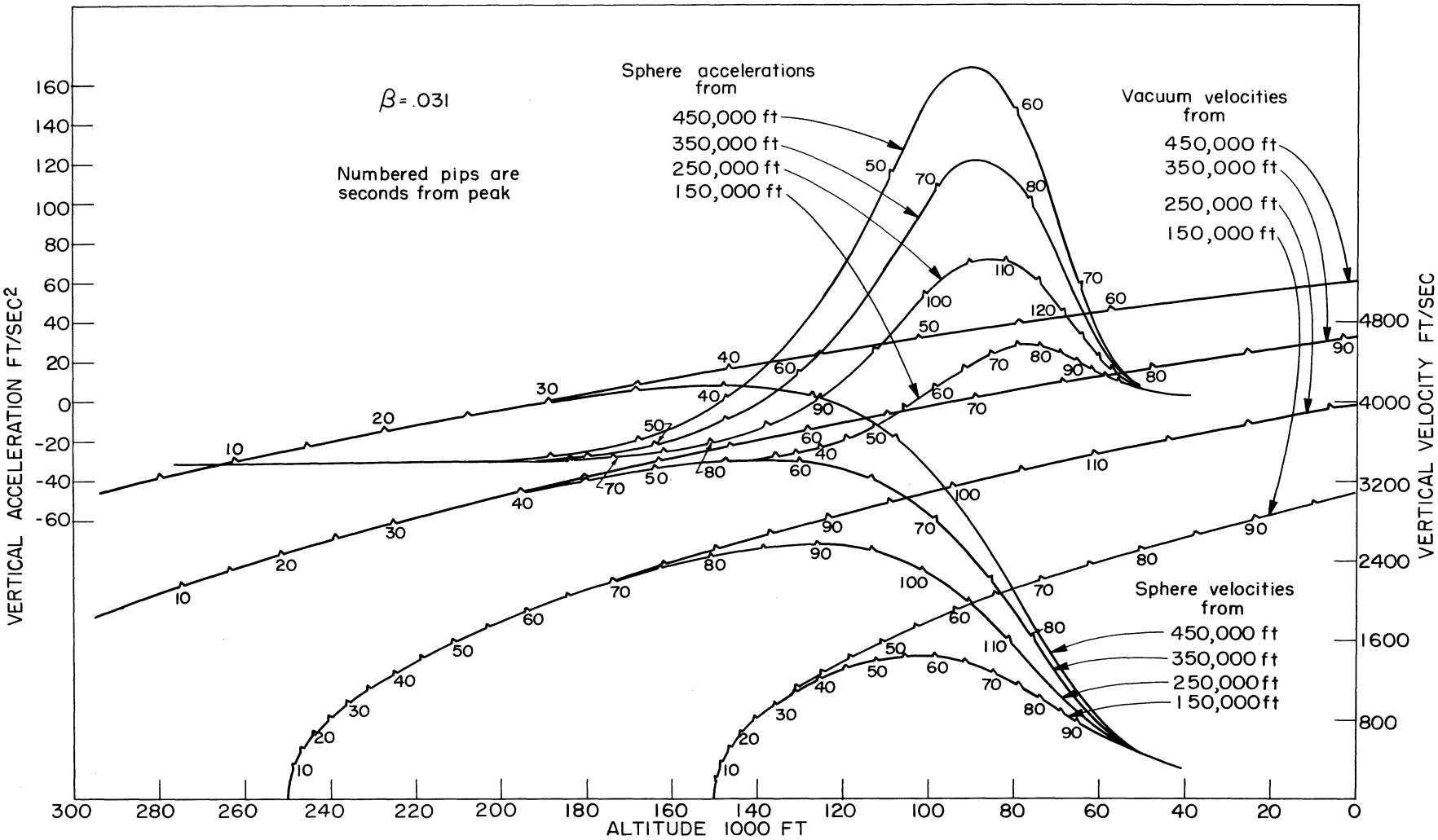

Fig. 5. Predicted trajectories for spheres of β = .031 dropped from various altitudes.

4.1. OPERATION

Figure 6 is a schematic of the device. Figures 7 and 8 show the construction. In operation, the coils are energized from a battery through an intervalometer switch. The fingers move toward each other, thus picking up the bobbin and centering it in the cavity. When the switch opens, the decay of the field in the field coils sends a large current through the moving coils, thus accelerating them rapidly outward and releasing the bobbin. The bobbin then accelerates freely toward the cavity. The time from the release of the bobbin to the instant of contact with the cavity is a measure of the relative acceleration of the cavity and bobbin, provided the center of rotation of the entire device (sphere) lies on the center of the caged bobbin. Electrical contact to the bobbin is made through a fine "cat's whisker" wire. Both the cavity and bobbin are figures of revolution shaped so that the distance traveled by the bobbin is the same in any direction (0.188 inch). In the rocket flight, the cycling time of the accelerometer was about 150 milliseconds for pickup, and about 450 milliseconds for maximum transit time. The transit times are telemetered from the sphere to the ground by means of a transmitter in the sphere. The electronics of the sphere and ground station are described in Sections 5 and 6.

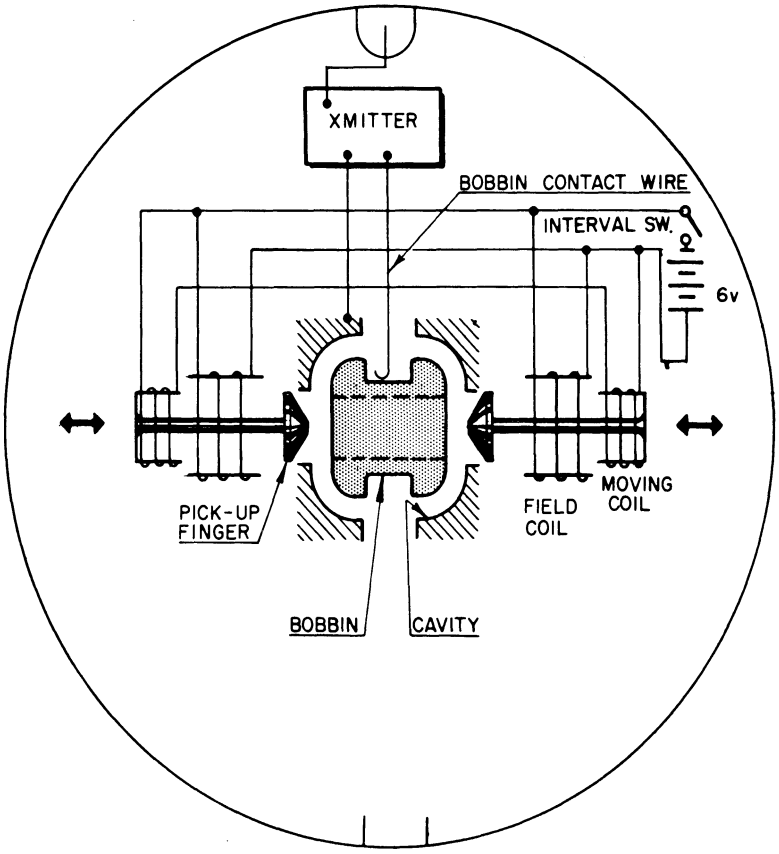

Fig. 6. Schematic of accelerometer.

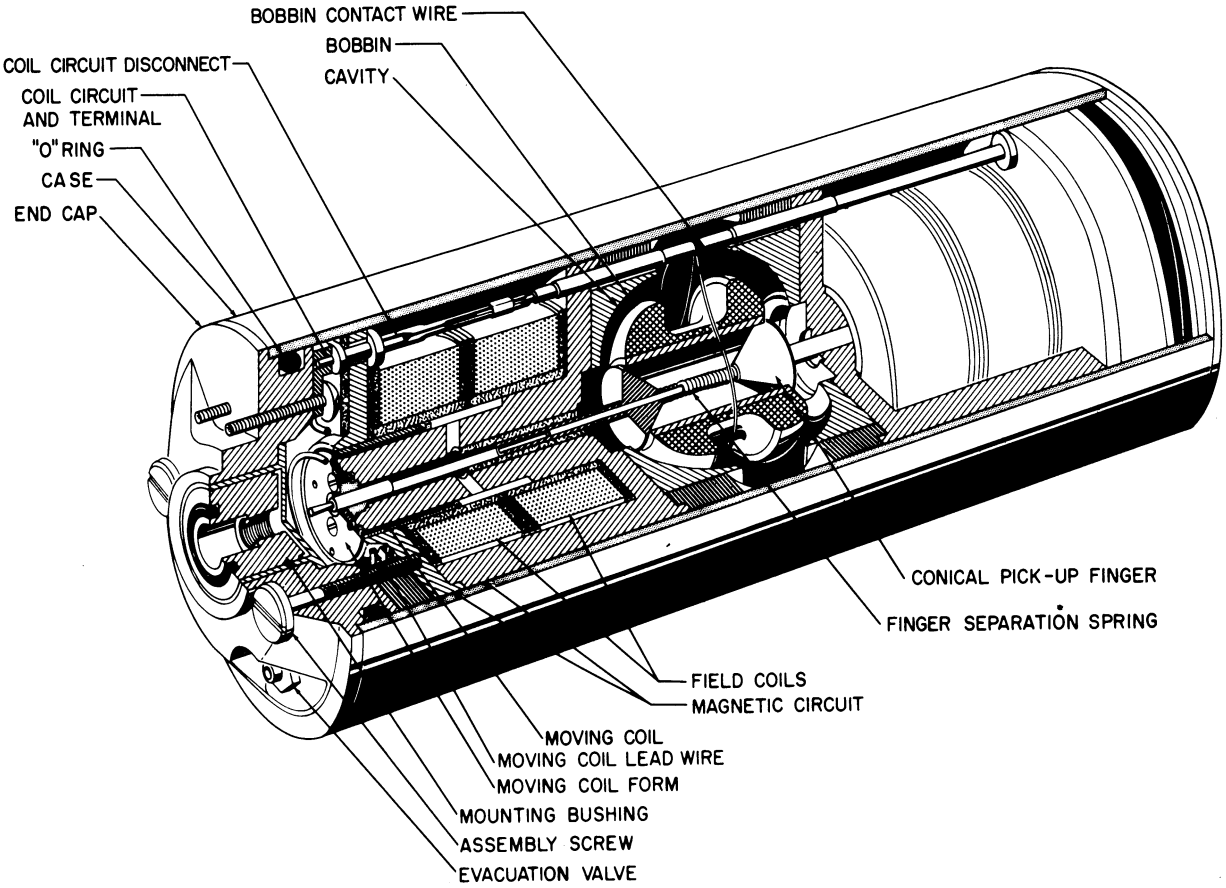

Fig. 7. Construction of transit-time accelerometer.

4.2. DESIGN AND CONSTRUCTION

Many of the design limits were set by the size of the sphere, which in turn was determined by the size of the rocket. The Deacon is 6 inches in diameter so that its payload nose cone must be about the same. The sphere was finally designed 7 inches in diameter, and the accelerometer 6 inches long. In order to provide room within the sphere for batteries, interval switch, transmitter, etc., the accelerometer diameter was limited to 2.25 inches. Within the accelerometer in turn, having allowed for coils and other components, the transit distance of .188 inch was arrived at. Calculations showed that densities to nearly 300,000 feet could be obtained if accelerations as low as 10^{-2}g were measured. The trajectory predictions from the computer (Section 3) indicated that maximum accelerations of about 5g would be encountered, although 3g would cover the region above 100,000 feet, which is of primary interest. The transit times corresponding to accelerations of 5g, 1g, and 10^{-2}g for a transit distance of 0.188 inch are approximately 14, 31, and 312 milliseconds, respectively.

The cavity and magnetic circuit were constructed of soft steel, the bobbin of aluminum with a stainless-steel center bushing. The pickup fingers were made also of stainless steel. The cavity and bobbin were silver plated for

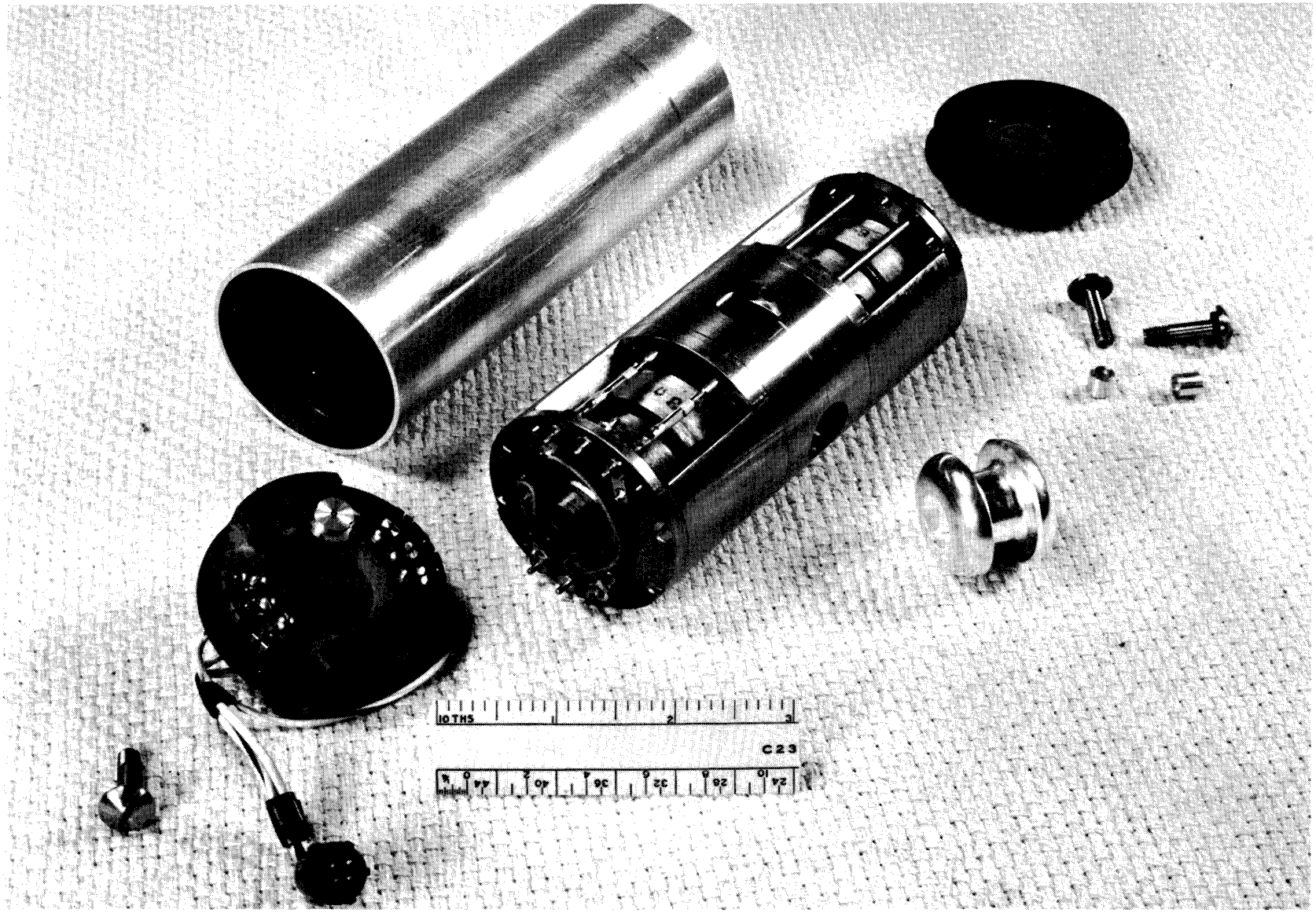

Fig. 8. Completed accelerometer.

electrical conductivity. Contact to the bobbin was made through a silver-wire spring 0.002 inch in diameter. The moving coils were wound with 80 turns each of AWG 28 wire. The field coils were taken from commercial relays. In order to minimize magnetic disturbances to the bobbin, the cavity was made of soft steel. In order to minimize turbulent air disturbances to the bobbin, provision was made to evacuate the accelerometer; but this was found to be unnecessary.

4.3. ERRORS

Four primary sources of error were anticipated in making and operating the accelerometer. These are: initial velocity imparted to the bobbin during release, error in time measured, error in distance traveled, and centrifugal acceleration due to off-center mounting of the bobbin in the spinning sphere. The equation of motion of the bobbin is

$$a = \frac{2(s - v_o t)}{t^2} , \tag{15}$$

where

a = acceleration,
s = distance,
v_o = initial velocity, and
t = time.

The percent error in acceleration due to v_o is

$$\delta a_{v_o} = \frac{200 v_o}{at} \left(\frac{v_o}{\sqrt{v_o^2 + 2as}} - 1 \right) . \tag{16}$$

The total systematic and probable errors measured in the laboratory at 5g, 1g, and .01g were about 1 percent. Even if all of this error were due to v_o, it may be seen by (2) that $v_o \ll \sqrt{2as}$. This leads to the following simple expressions for percent errors in acceleration due to v_o and errors in t and s:

$$\delta a_{v_o} = 200\ v_o/at, \tag{17}$$

$$\delta a_t = 200\ \Delta t/t, \text{ and} \tag{18}$$

$$\delta a_s = 100\ \Delta s/s. \tag{19}$$

Actual values of v_o were not determined directly, but the magnitude of v_o required to cause a 1-percent error in acceleration is seen from (17) to be

Acceleration (g)	v_o (inch/sec)
5	.13
1	.060
.01	.006

The transit times were measured with an electronic counter (Hewlett-Packard Model 522B) capable of measuring time intervals to $\pm 10^{-5}$ seconds. From (18), the percent errors in acceleration due to an error of 10^{-5} seconds in time are

Acceleration (g)	Percent Error
5	.14
1	.064
.01	.006

The accelerometer was constructed with shop tolerances of ± 0.001 inch or better on critical dimensions. It is reasonable to say that it could be assembled and adjusted so that the bobbin transit distance was within ± 0.002 inch of the design value. This would cause a 1-percent error at any acceleration.

If the center of the caged bobbin does not lie on the center of rotation (CG) of the spinning, tumbling sphere, an error due to centrifugal acceleration will be present. A rocket is said to spin about its longitudinal axis and tumble about a transverse axis through the CG. These motions are conserved by the sphere if the ejection is gentle. The sphere was mounted in the rocket in such a way that rocket spin would cause the sphere to spin about the longitudinal axis of the accelerometer and tumble about a transverse axis. Tumble periods are very large and may be ignored. Spin periods for the Nike-Deacon are of the order of 10 seconds. In order that centrifugal accelerations be 1 percent or less of the .01g lower limit of measurement, it was necessary to locate the CG of the sphere within 0.1 inch of the common geometrical centers of the sphere and caged bobbin. Measurements with a theodolite on the sphere suspended on a fine wire showed that the CG was within 0.05 inch of any diameter. This could have been improved with balancing masses, but it was not thought necessary to do so.

4.4. LABORATORY TESTS

The accelerometer is an absolute device which requires no calibration once it has been shown to be working correctly. Tests at 1.0g showed that the omnidirectional characteristic was good. Tests at 0.01g were made by retarding the free fall of the entire accelerometer very slightly by means of a pulley. The accelerometer was attached to a massive bullet, which was

dropped through a distance of 4 feet. The air drag of the combination was calculated to be negligible. A thread attached to the accelerometer was wound around the pulley so that its moment of inertia provided a small retarding acceleration. The moment of inertia of the pulley was measured accurately by timing the fall rates of various light masses attached to the thread. The pulley friction was estimated by measuring the angular deceleration during spinning. The friction was found to be negligible. Figure 9 is a schematic of the setup, which is an Attwood's machine. First, a small mass (M_1) is substituted for M and the drop time T over measured distance S is noted. From this the moment of inertia of the pulley I is

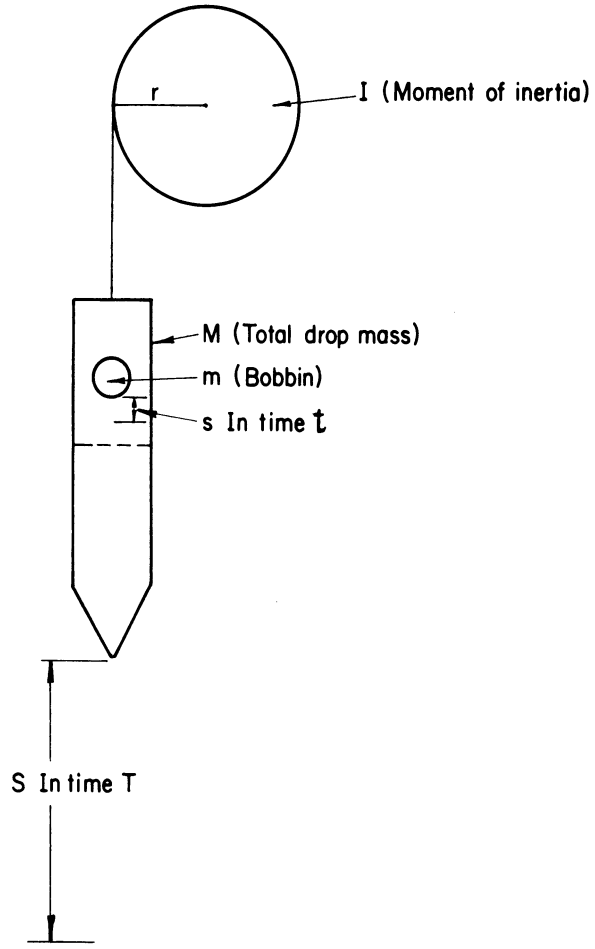

Fig. 9. Schematic of low-acceleration check.

$$I = \frac{Mr^2 T^2 \left(g - \frac{2S}{T^2}\right)}{2S} . \quad (20)$$

Then M (the heavy accelerometer plus bullet) is used and the relative acceleration of m and M measured. This corresponds to the drag acceleration and is given by

$$a = \frac{gI}{Mr^2 + I} . \quad (21)$$

The time t for bobbin m to move the transit distance s is read on the counter and is

$$t = \frac{2s(Mr^2 + I)}{gI} . \quad (22)$$

Figure 10 is a photograph of the experimental setup, showing the bullet of which the accelerometer is the upper part. The pulley is on the platform above the bullet. A second accelerometer is seen on the bench and the electronic counter in the upper part of the rack.

Prior to flight, no tests were made at accelerations greater than 1g, except to substitute a steel bobbin for the aluminum one to show that the fingers would cage the tripled weight, and hence be capable of caging the aluminum bobbin under a drag acceleration of 3g. The flight test showed the desirability of insuring operation up to 5g. See Section 9. Consequently a centrifuge was built for extending the test accelerations. The apparatus, which is seen in Fig. 11, consists of an I-beam 110 inches long mounted at the center on a ball bearing. The accelerometer is mounted on the right end and the batteries and intervalometer switch on the left. Signals to the

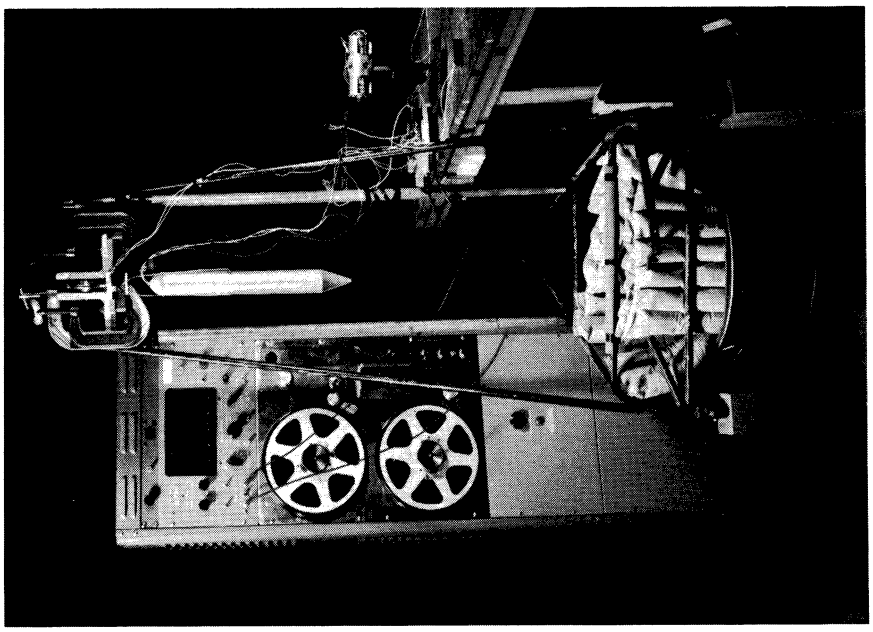

Fig. 10. Setup of low-acceleration check.

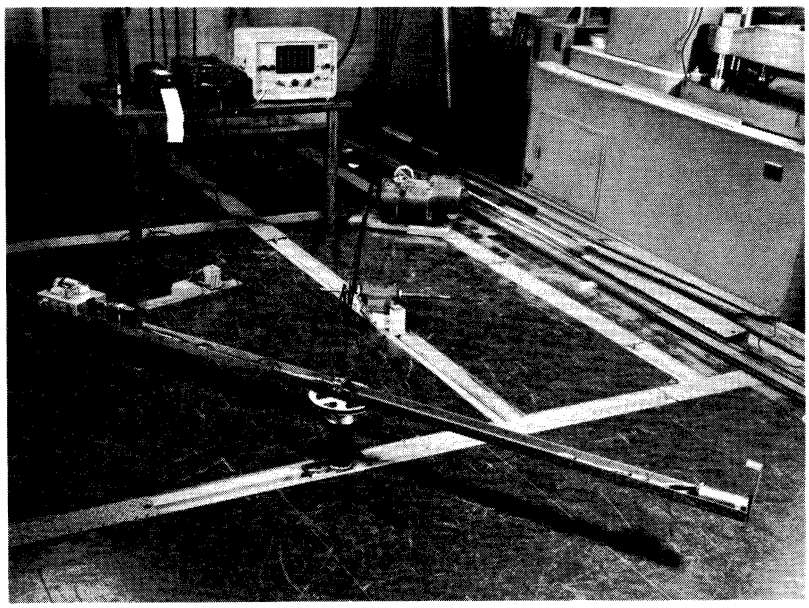

Fig. 11. Centrifuge for high-acceleration check.

counter (on the table) were taken through a plug and jack acting as slip rings. The beam was rotated by a variable-speed drive with pulleys and v-belts. The period of the centrifuge was recorded on the Brush Recorder. Successful runs up to 5g were carried out. They showed that, provided the battery and intervalometer switch were in excellent condition, the errors at 5g are about the same as at 1.0g and 0.01g.

In summary, the laboratory tests on two accelerometers showed that systematic errors and standard deviations (in 10 runs) are ± 1 percent or better between 5g and 0.01g.

5. THE SPHERE AND NOSE-CONE INSTRUMENTATION

5.1. SPHERE

The seven-inch diameter of the sphere was mutually determined by the size of the Deacon rocket and the design possibilities of the accelerometer. With careful design it was possible to pack within this size sphere the acessory components which included batteries, intervalometer switch and motor, transmitter, ejection or starting switch, and miscellaneous small parts. A further design requirement of the sphere was that it serve as an antenna to radiate about 1 watt at 217 mc. It was also required to be pressurized. Figure 12 is a schematic of the sphere circuit. Figures 13 and 14 show the sphere components and assembly.

The sphere halves were machined from a solid Dural bar. They were separated and insulated from each other by a half-inch equatorial ring of Teflon. The intervalometer switch was a standard 12-position, single-circuit wafer driven by a 6-volt, d-c, gear-reduction motor (Globe Industries) with a shaft speed of 1 revolution per 0.6 second. The B-battery supply was made up of Burgess U-15 batteries, 180 volts total. The A battery consisted of 3 Willard BR-1B lead-acid cells, 6 volts total. The battery life with everything operating was about 20 minutes. The control switch had positions for "off," "transmitter only on," "transmitter and accelerometer on," and "flite." In the latter position the transmitter was on but the accelerometer was turned off by a switch held open as long as the sphere was within the nose cone. This switch closed upon ejection. It was mounted on the equatorial insulation ring. Other items mounted flush in the ring were contacts for monitoring voltages, a pressurizing fitting, antenna timing control, and fittings for suspending the sphere in balancing checks. Figure 15 shows the sphere suspended for a balance check which was accomplished with a Wild T-3 theodolite, also shown. As noted in Section 4, provision was made to add balancing weights, but these were not required. The sphere was sealed by O-rings at four joints, two between the halves and the ring and two at the poles where the halves were screwed to the accelerometer, which was the main structural

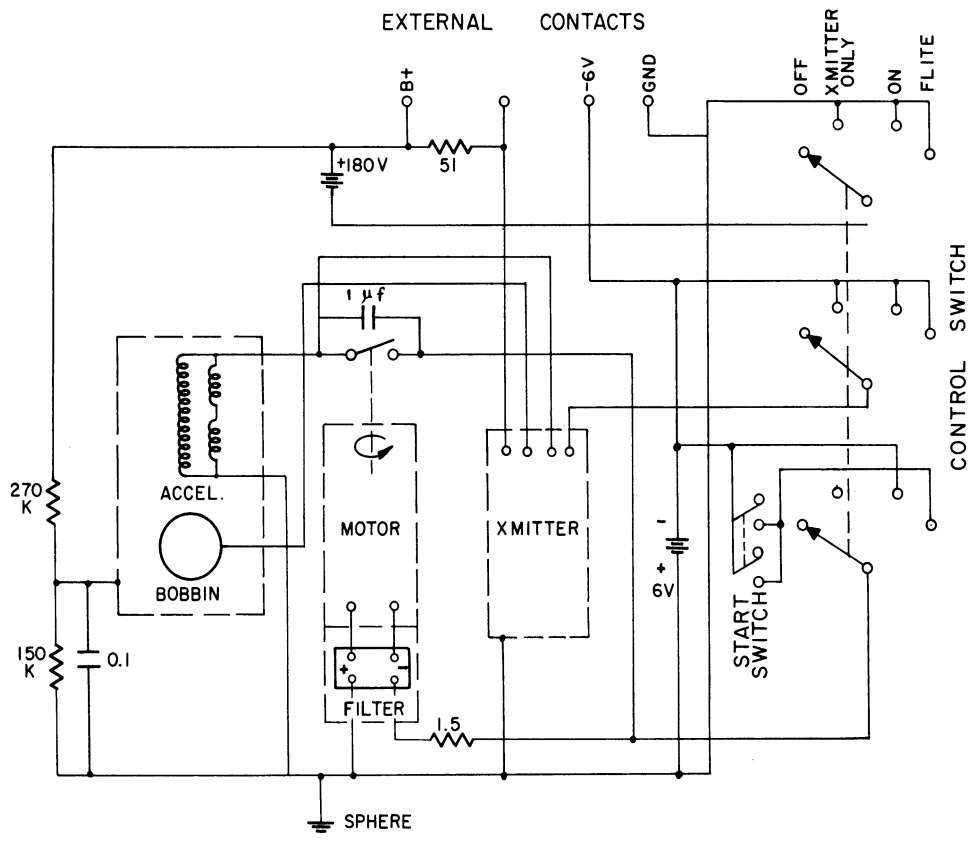

Fig. 12. Schematic of sphere circuit.

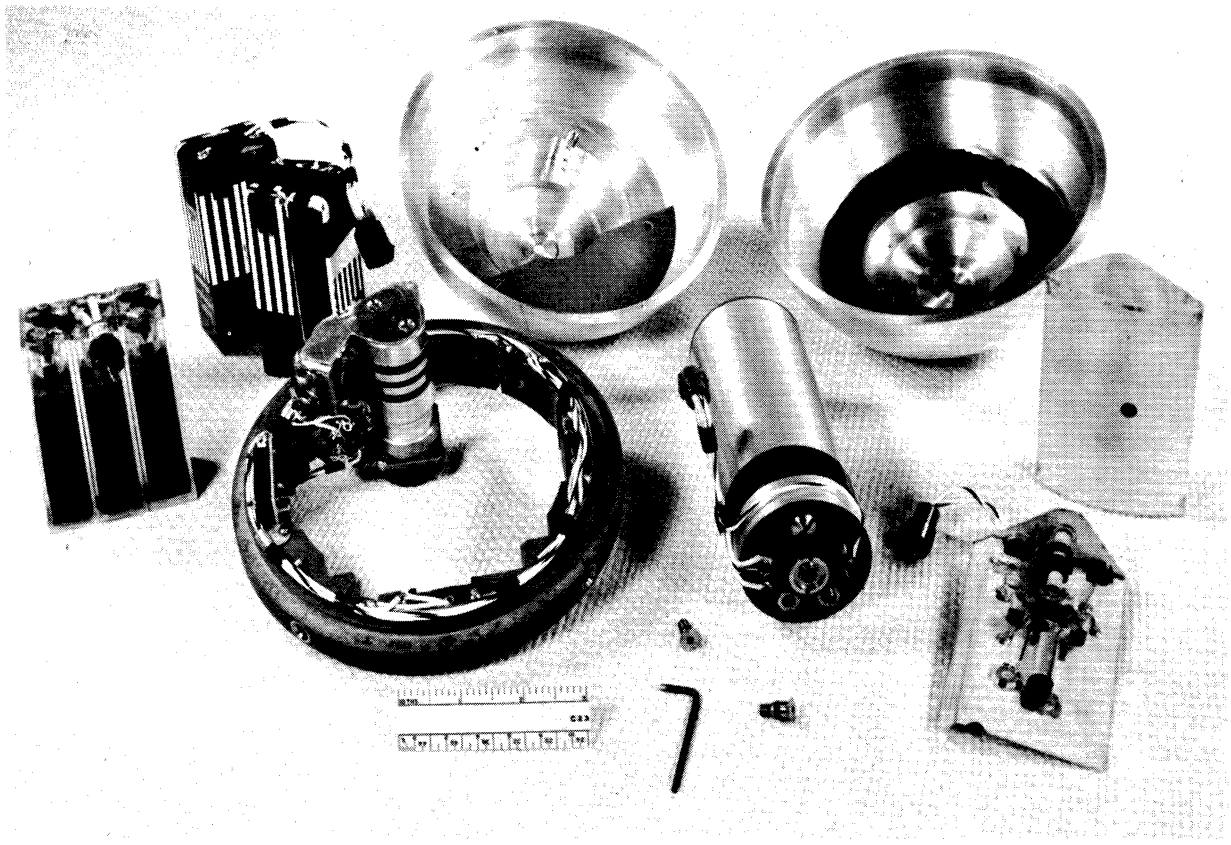

Fig. 13. Sphere components.

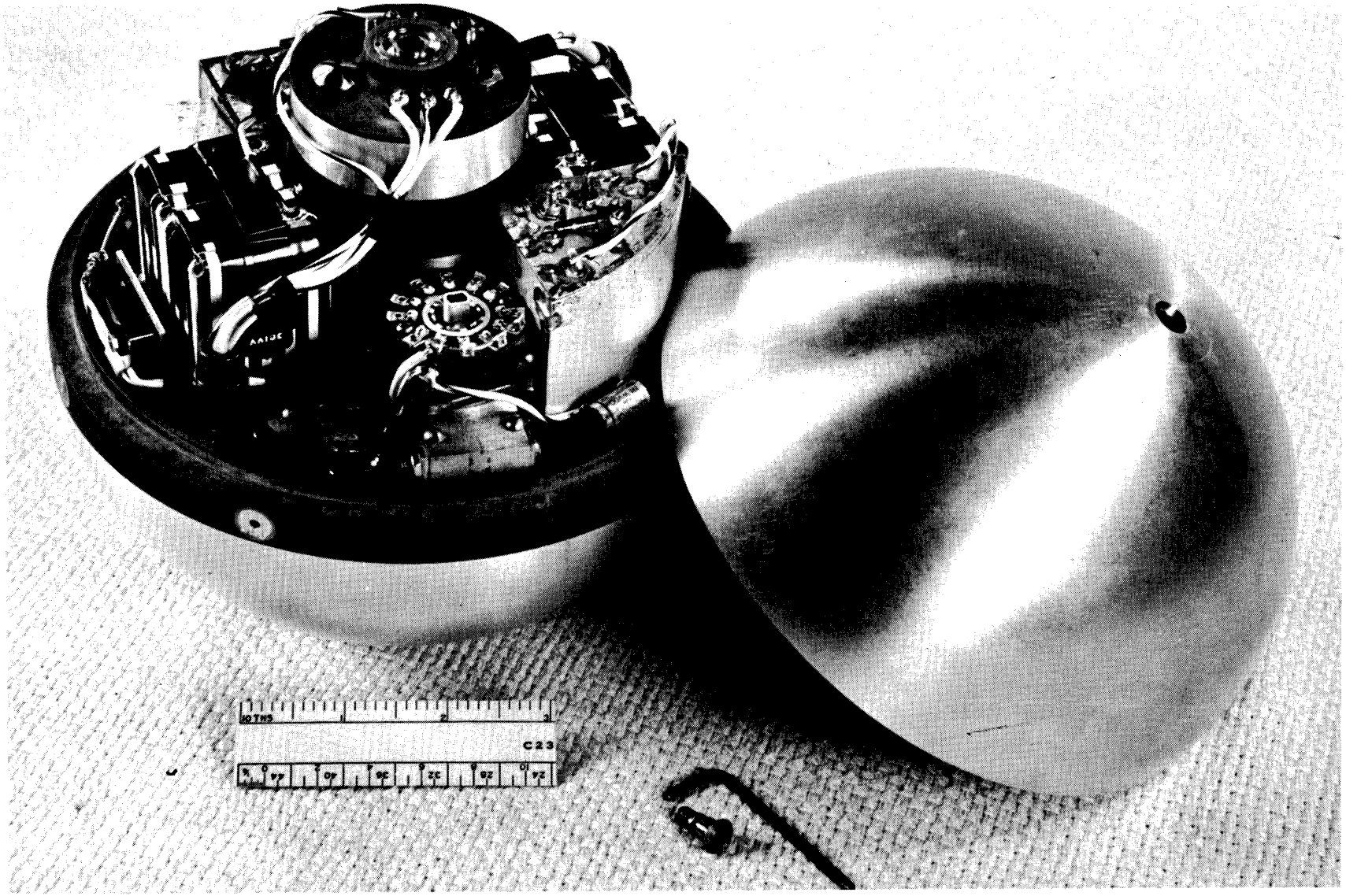

Fig. 14. Sphere assembly.

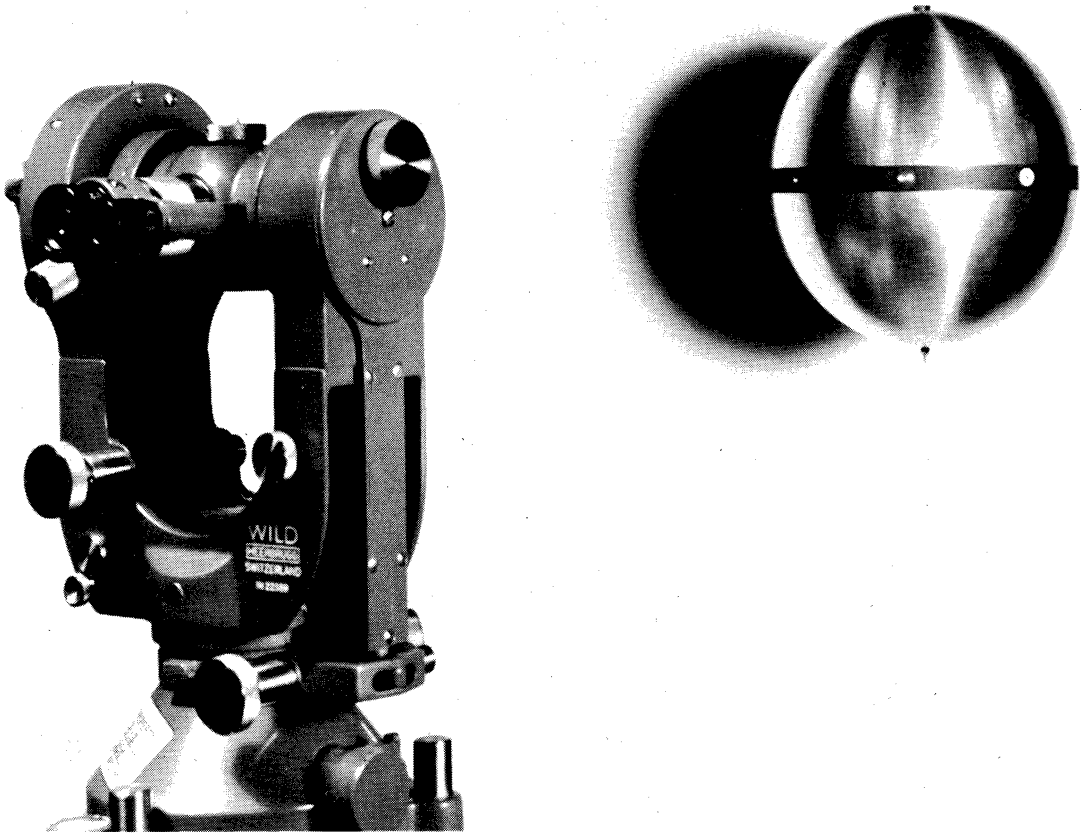

Fig. 15. Balance check of sphere.

member resisting the internal pressure. Figure 16 is a drawing of the sphere assembly as flown. It shows an internal shield can which was added after the photographs were taken. The can provided a space, free of rf fields, for mounting components; rf losses due to induced currents in these components were thereby eliminated.

5.2. TRANSMITTER

The transmitter was a Colpitts oscillator with an output of 2 watts at 217 mc. The radiated power from the sphere was about 0.5 watt, the losses being due to high reactive circulating currents in the coupling network caused by the low sphere impedance as an antenna. Because the Q of the sphere was very high, the oscillator had two possible operating frequencies when load and tank circuits were tuned to the same frequency. This condition was corrected, however, by slight de-tuning of the antenna to discriminate in favor of one of these frequencies.

Radiation tests of the sphere were made on the roof of East Engineering Building. The layout of the YAGI receiving array used in the tests

is shown in Fig. 17. The sphere patterns were compared with a standard dipole designed for 217 mc. Figure 18 is an E-plane pattern for the standard dipole while Figs. 19 and 20 are E-plane and H-plane figures for the sphere. The sphere pattern is seen to be essentially omnidirectional. The units are volts/meter x meters because the 30-meter distance to the receiving array was left in the equations for both the dipole and sphere.

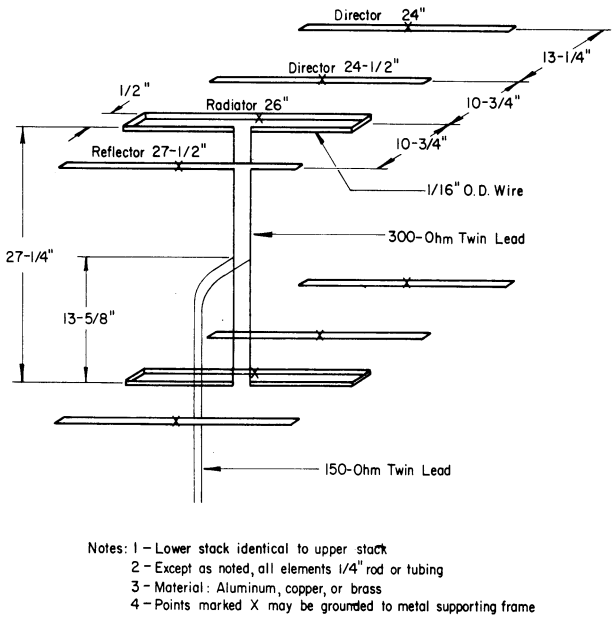

Fig. 17. Receiving antenna array.

Upon completion of the roof tests, which indicated an acceptable radiated power, the sphere was mounted on the Aeronautical Engineering Department airplane (Cessna 180) for distance tests. See Fig. 21. The same receiving array was used. Signals were received up to distances of 400,000 feet, with the plane at an altitude of 16,000 feet. The received signal strength in this situation was 2 μ volts. Although the receiver required 5 μ volts for proper operation of the following equipment, it was felt that the low receiving angle was the cause of the marginal signal at the maximum distance.

The schematic of the transmitter is shown in Fig. 22. Figures 23 and 24 show the construction of the chassis. The shield can is seen in Fig. 13. It was originally intended to use on-off modulation of the transmitter to indicate when the accelerometer bobbin was in transit. This was not feasible, however, because the transmitter would not always turn on at the frequency at which it went off, presumably because of battery changes between the two load conditions. Consequently, frequency-shift modulation was employed. Referring to Fig. 22, the firing of thyratron No. 1 changes the resonant frequency of the tank circuit and thereby shifts the frequency about 300 kc, which takes it out of the pass band of the receiver. The plate supply divider for thyratron No. 1 is de-coupled from the tank circuit by choke Z-235. When the accelerometer intervalometer switch is opened, thus releasing the bobbin, the positive inductive pulse fires thyratron No. 2. Condenser C7 discharges through the common cathode resistor R3, extinguishing No. 1. The transmitter frequency then corresponds to "on." The initial contact of the bobbin with the cavity provides a positive pulse on the grid of thyratron No. 1, thus firing it. The resulting increase in cathode potential extinguishes No. 2. Further bobbin bounce contacts have no effect. The transmitter frequency now corresponds to "off."

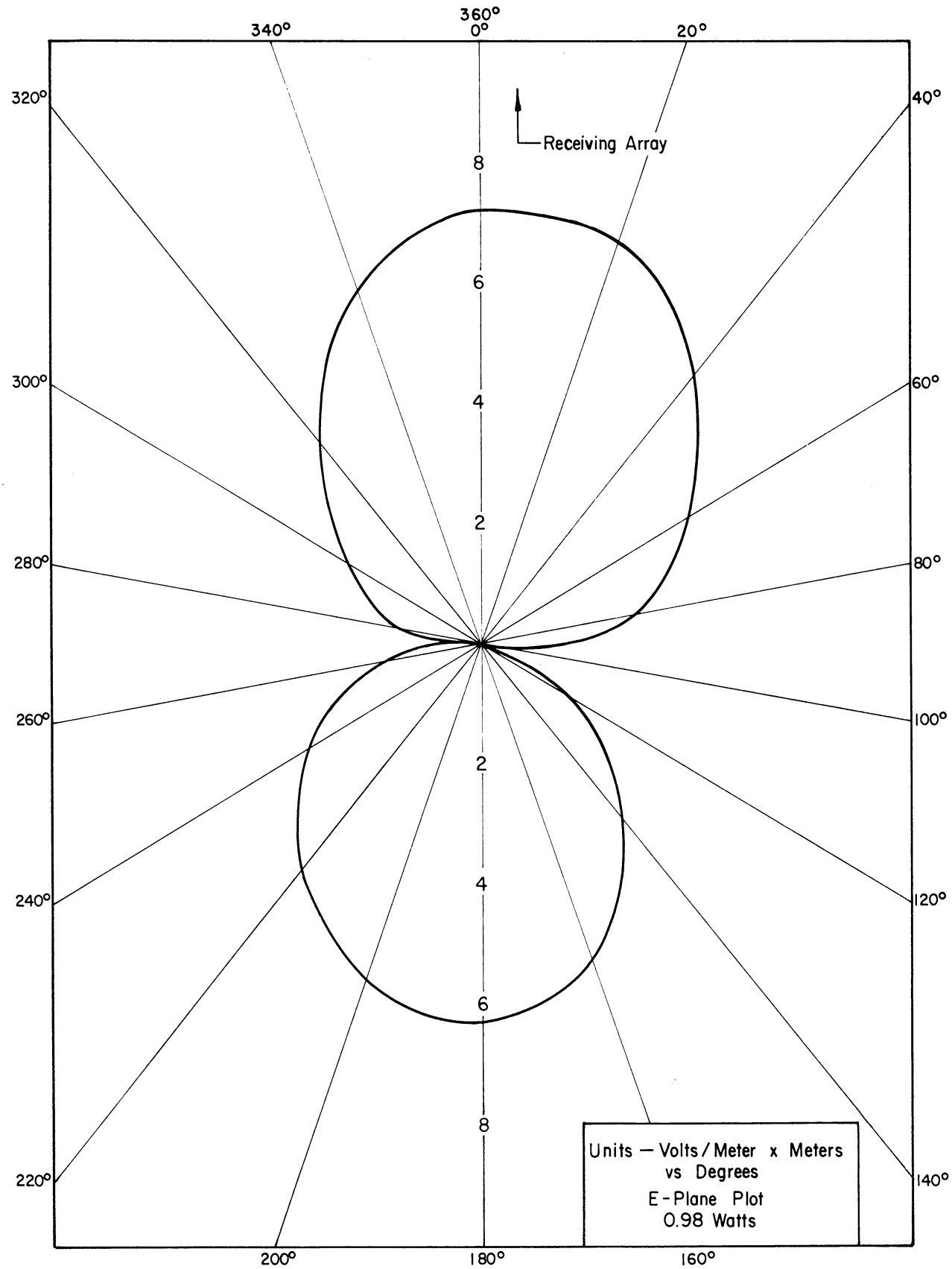

Fig. 18. Standard dipole pattern, E-plane.

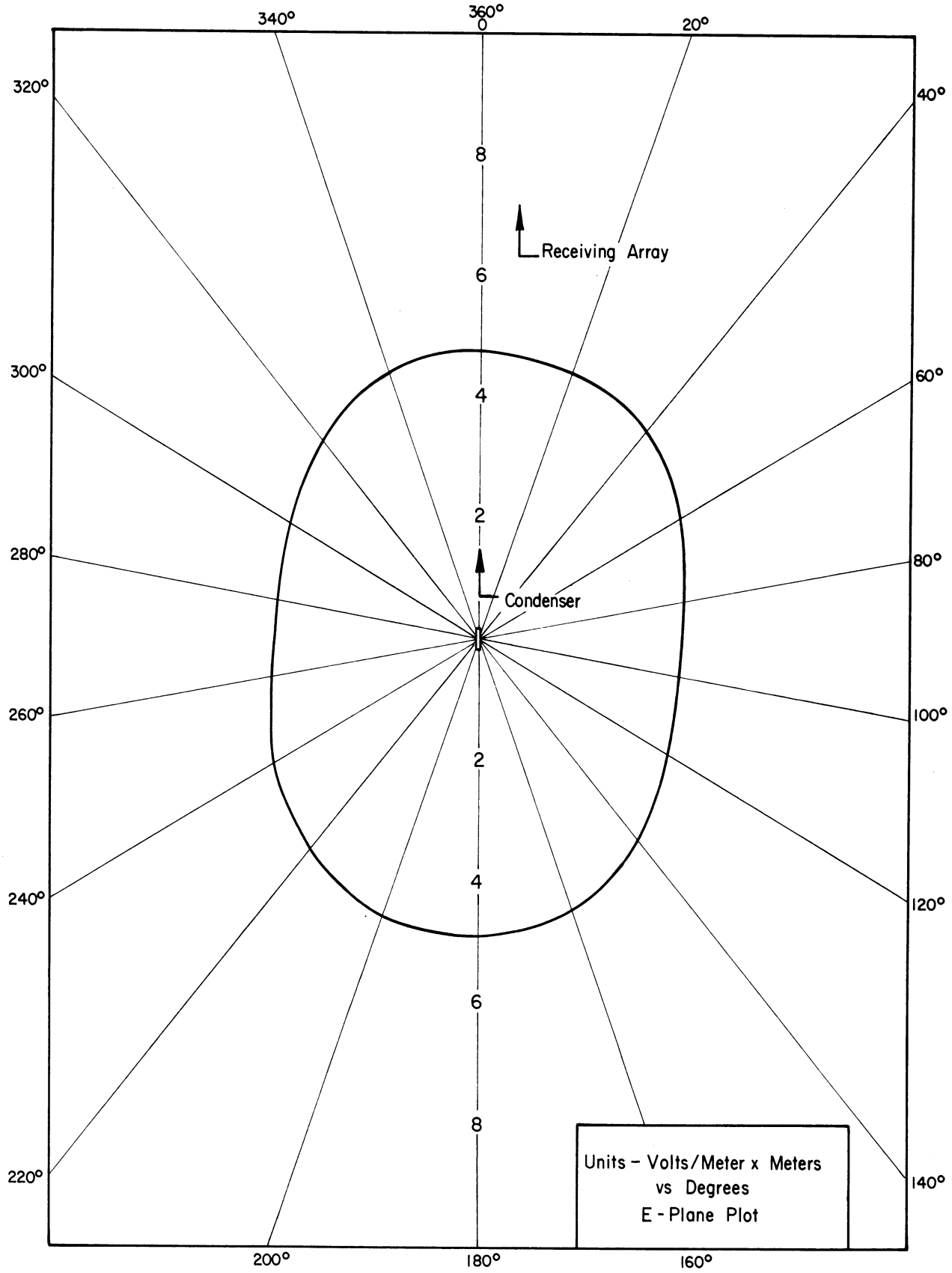

Fig. 19. Sphere pattern, E-plane.

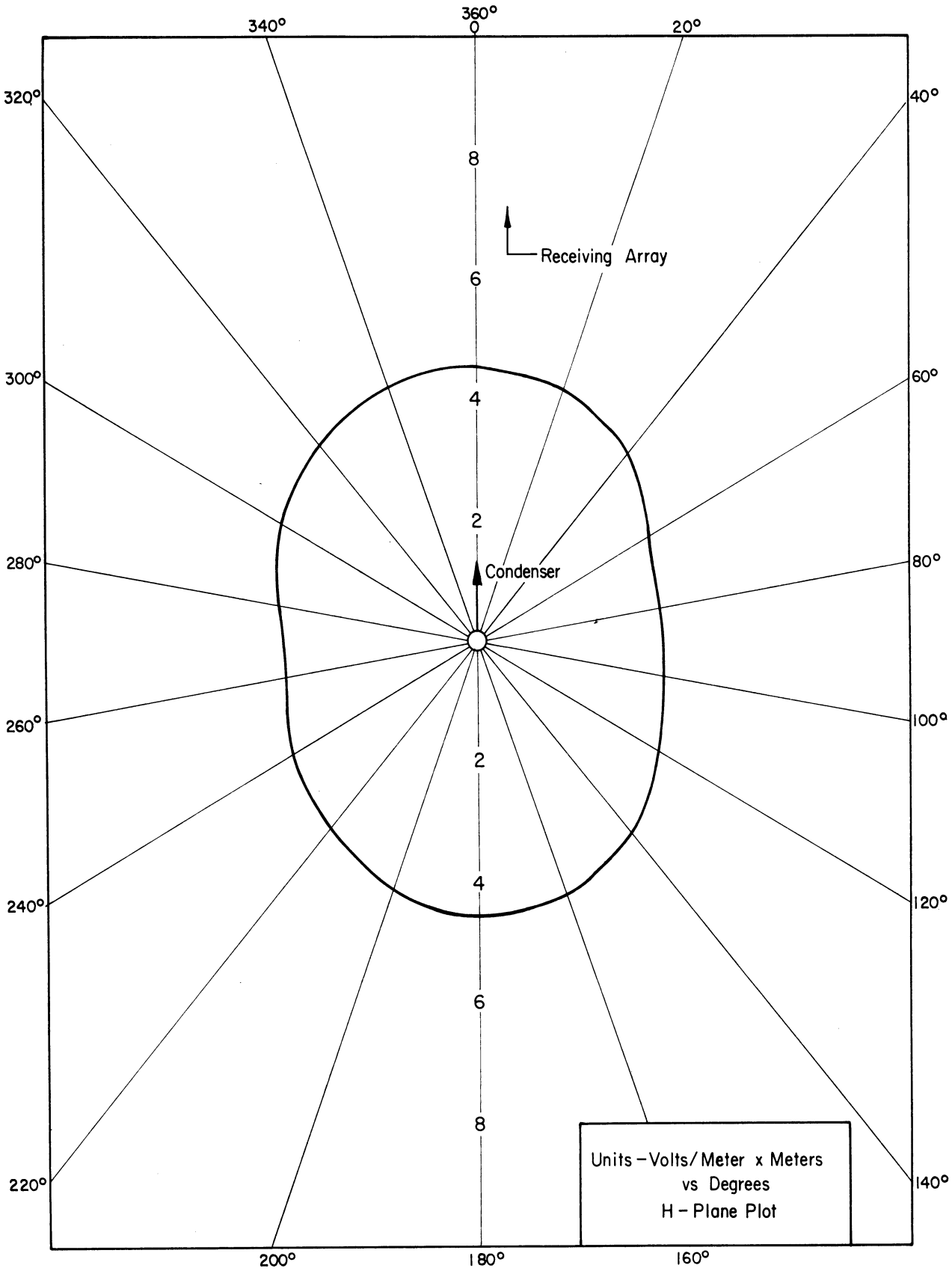

Fig. 20. Sphere pattern, H-plane.

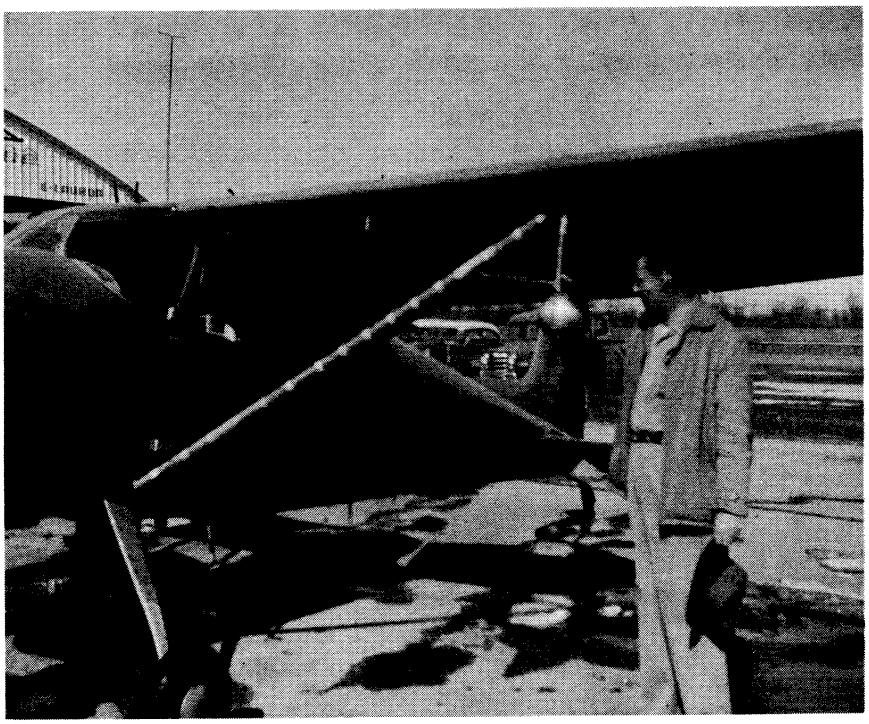

Fig. 21. Sphere mounted for distance check.

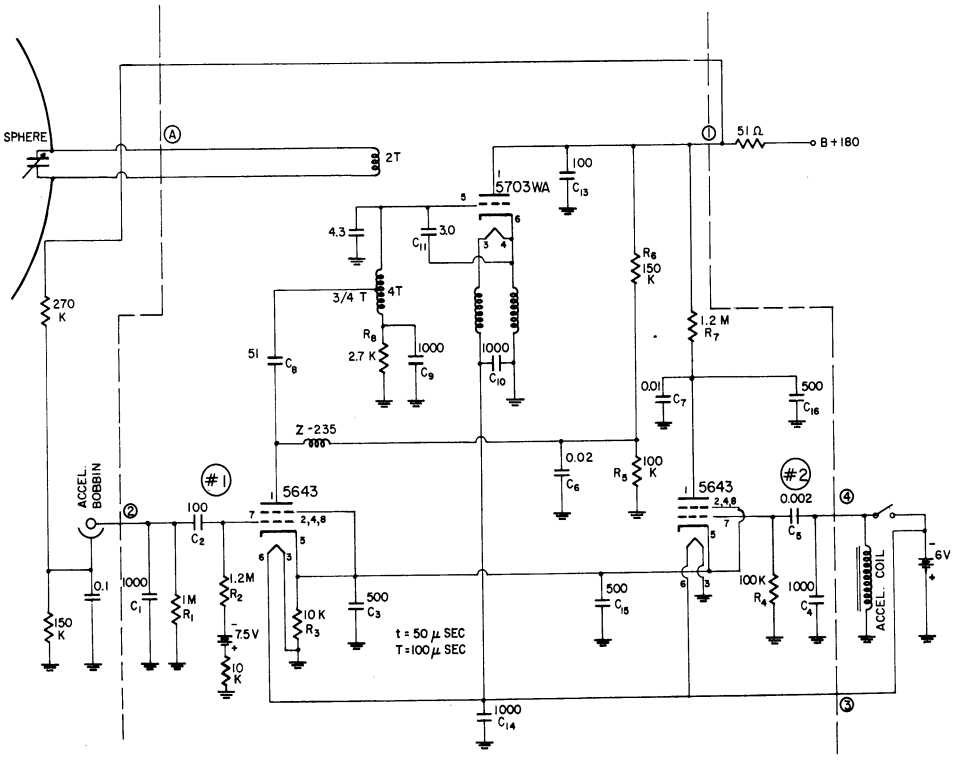

Fig. 22. Schematic of sphere transmitter.

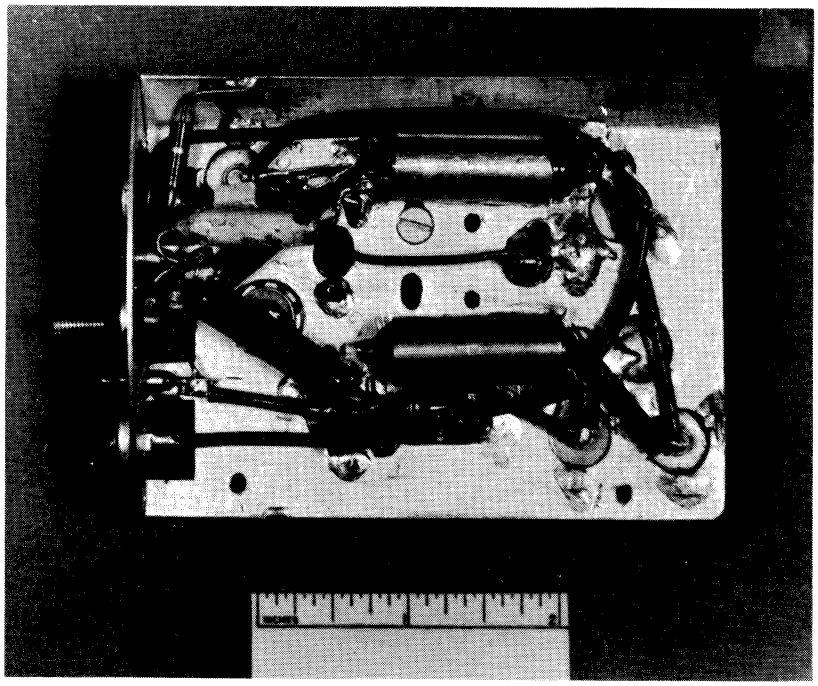

Fig. 23. Construction of sphere transmitter.

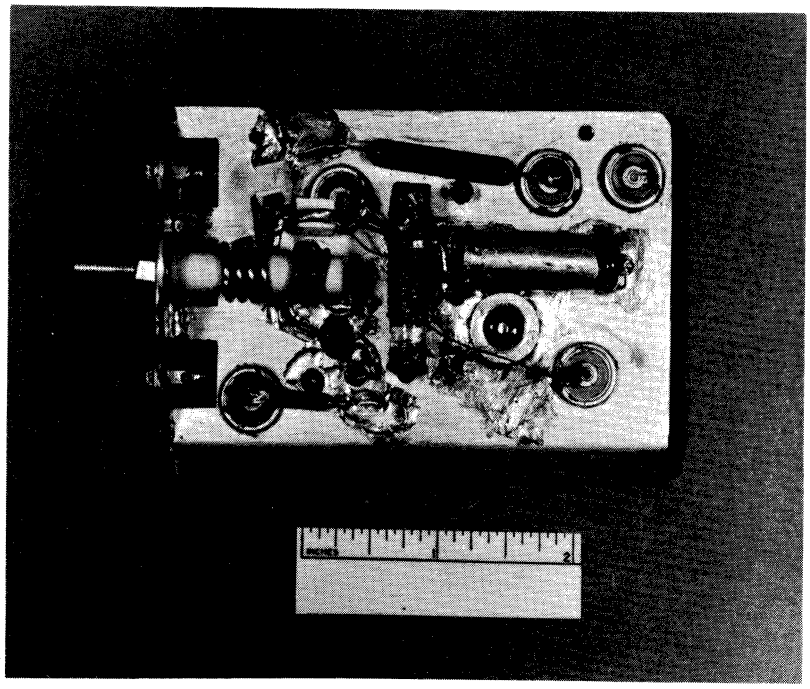

Fig. 24. Construction of sphere transmitter.

5.3. NOSE CONE AND EJECTION SYSTEM

It was required that the sphere be ejected from the nose cone by a simple, reliable, nondestructive device which would not add appreciably to the weight or diameter of the rocket. The ejection device and nose-cone design are shown in Fig. 25, and the completed parts in Fig. 26. The sphere rests in a cast aluminum cup which screws to the front end of the Deacon. A fairly strong spring is compressed between the sphere and the cup. At the top of the cup, located on successive 90° centers, are 4 blasting cap "guns" and 4 partial thread sections. The cup also contains the batteries, timing motor, and pull-away switch for detonating the blasting caps. A second, inverted cup of steel, seen in the center of Fig. 26, is now placed over the sphere with a light spring between the two. The second cup is then clamped to the lower one by means of the threaded clamp ring in the right foreground of the photograph. In operation, the pull-away switch starts the timer at take-off. At altitude the timer applies voltage to the blasting caps which fracture the clamp ring at four pre-weakened spots. The lower heavy spring separates the sphere and nose cone from the lower cup, whereupon the upper light spring eases the sphere out of the upper steel cup.

The nose cone also contained a DPN-19 radar beacon for tracking. The antennas, batteries, and control relay are seen mounted on the steel cup. The beacon and coupling circuit were mounted on an aluminum tripod which was mounted on the steel cup and was covered by the nose cone. A fairing ring and nose tip are also seen in Fig. 26.

The assembled nose cone ready to mount on the Deacon is illustrated in Fig. 27. In this photo it is mounted on a drop platform which was used to test the assembly at 100g acceleration. The platform was calibrated with a conventional accelerometer. The calculated maximum acceleration encountered in flight is 60g.

6. GROUND STATION

The ground-station equipment consisted of a tracking radar, c-w Doppler radar, and telemeter receiving station. The radar, which was a modified SCR-584, and the Doppler radar were NACA equipment and are not described here. The telemeter ground station, with the exception of the antenna and input amplifier, was built and assembled at Michigan. The assembly is seen in Fig. 28. Its overall function was to receive the frequency-shift modulated signals from the sphere and convert them to forms suitable for recording on film, tape, and a Brush Recorder.

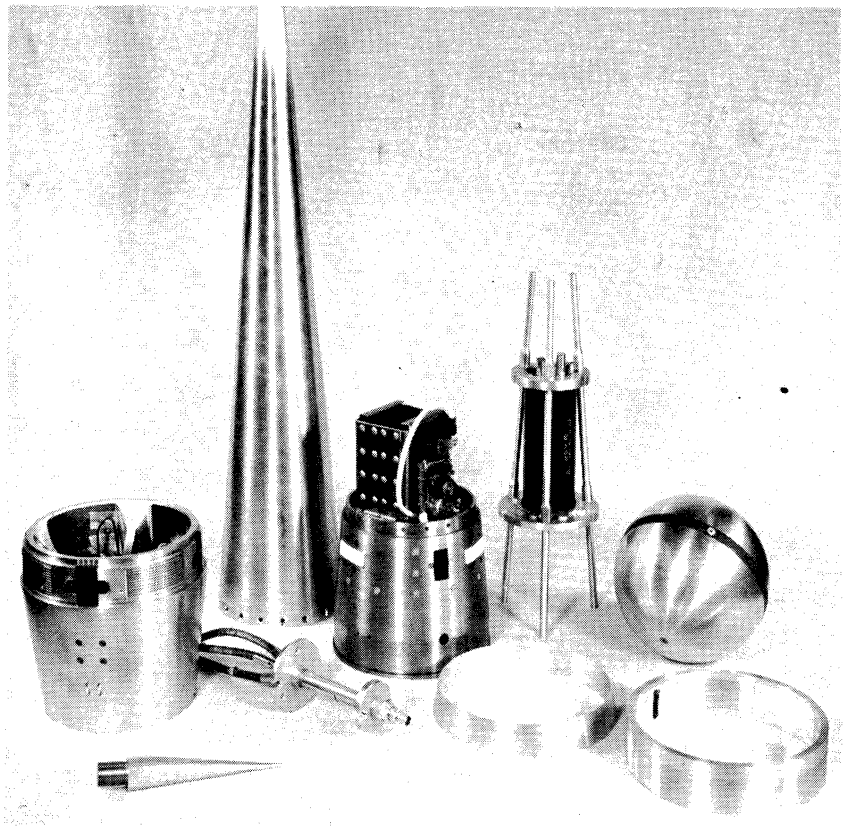

Fig. 26. Nose-cone instrumentation components.

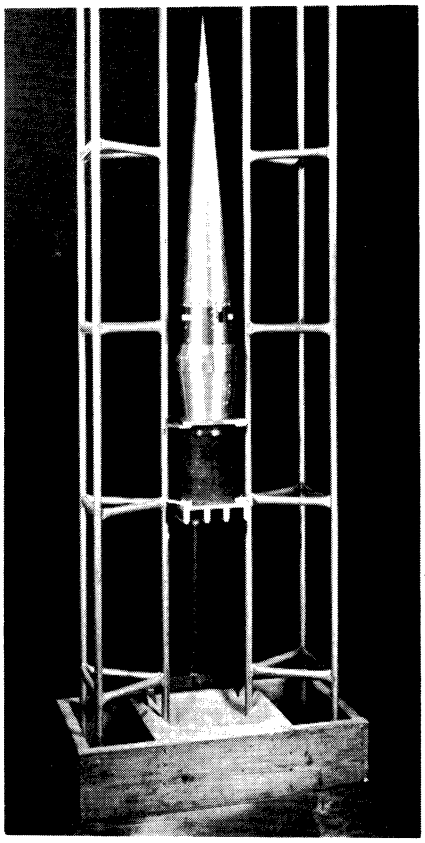

Fig. 27. Assembled nose cone on drop table.

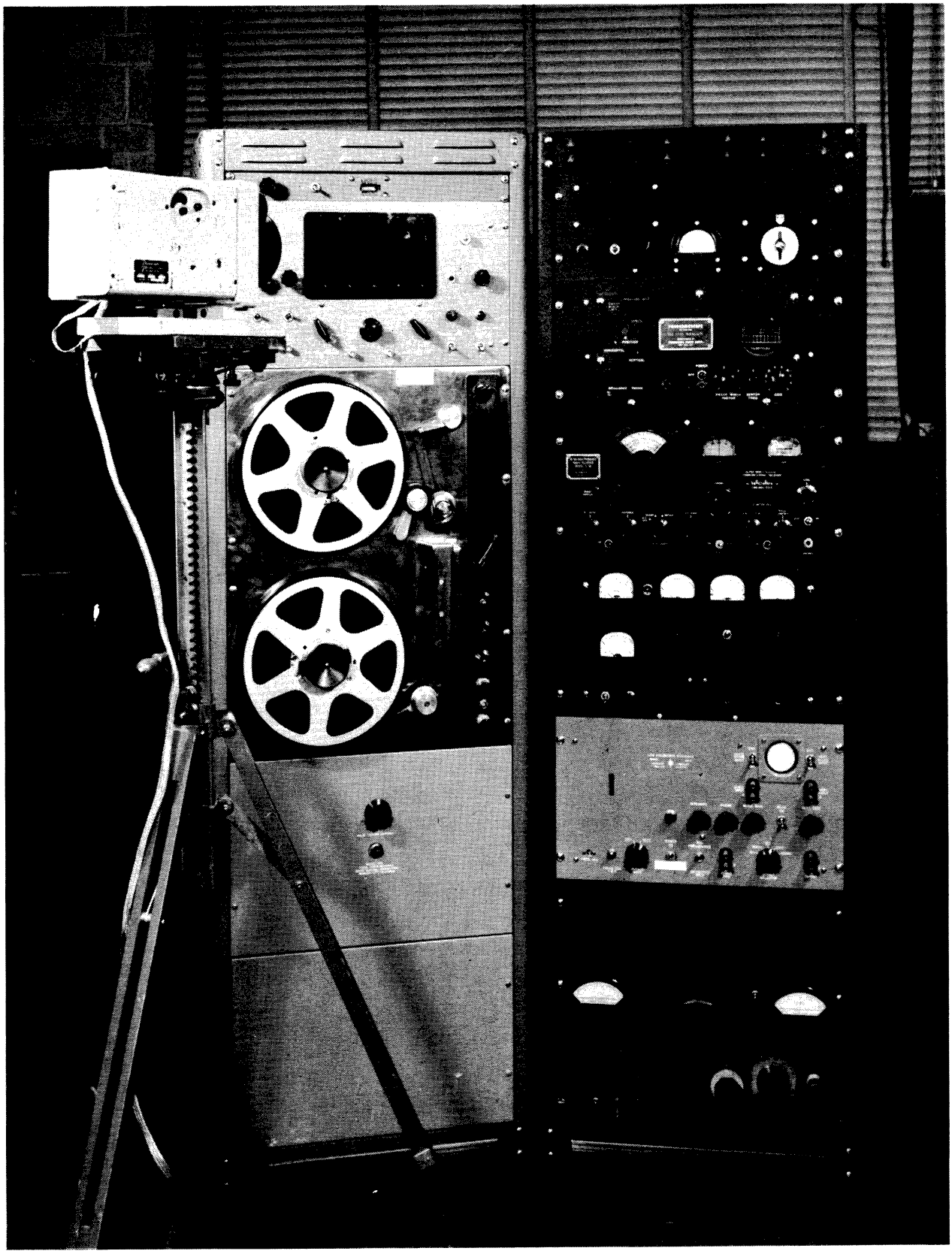

Fig. 28. Telemetering ground station.

6.1. INPUT

The NACA input to the ground station consisted of a steerable helical antenna with a beam width of about 60° and 11 db of gain. The antenna fed into an ASCOP pre-amp (with a gain of 15 db) tuned to 217 mc.

6.2. TUNER

The top right-hand chassis (Fig. 28) is a "Standard" TV cascode tuner. It was used on channel 13 and fine-tuned to 217 mc. Its main purpose was to convert 217 mc to 43.5 mc to operate the Hallicrafter's receiver. This chassis also contains a Michigan-built power supply.

6.3. PANORAMOSCOPE

The next lower chassis is a Panoramoscope by Panoramic Radio Corp., Type SA3 T1000. It was used without modification.

6.4. RECEIVER

The next chassis is a Hallicrafter's Ultra-High-Frequency Radio Receiver, S-36. It was modified as follows:

6.41. The AM detector was modified to improve the response time constant.

6.42. A cathode-follower output was added.

6.43. The I. F. signal was tapped off at the plate of the converter state to provide a signal for the Panoramoscope.

This receiver was used with no automatic volume control or automatic noise limiting.

6.5. PULSE CONTROL

The right center chassis of Fig. 28 contains the pulse-control circuits used to modify the output of the receiver to forms suitable for recording. The schematics are seen in Figs. 29 and 30. Referring to Fig. 29, the 75K resistor is the cathode resistor of the receiver output cathode follower. The input to the Brush Recorder is across this resistor. Meter V_1 monitors the rectified signal strength and is used in tuning and manually directing the antenna. The 6AL5 diodes form a clipping and limiting network whose output is a square wave free of noise. The grid-coupling network of the 6AK5 is a differentiating circuit which converts the square-wave signal

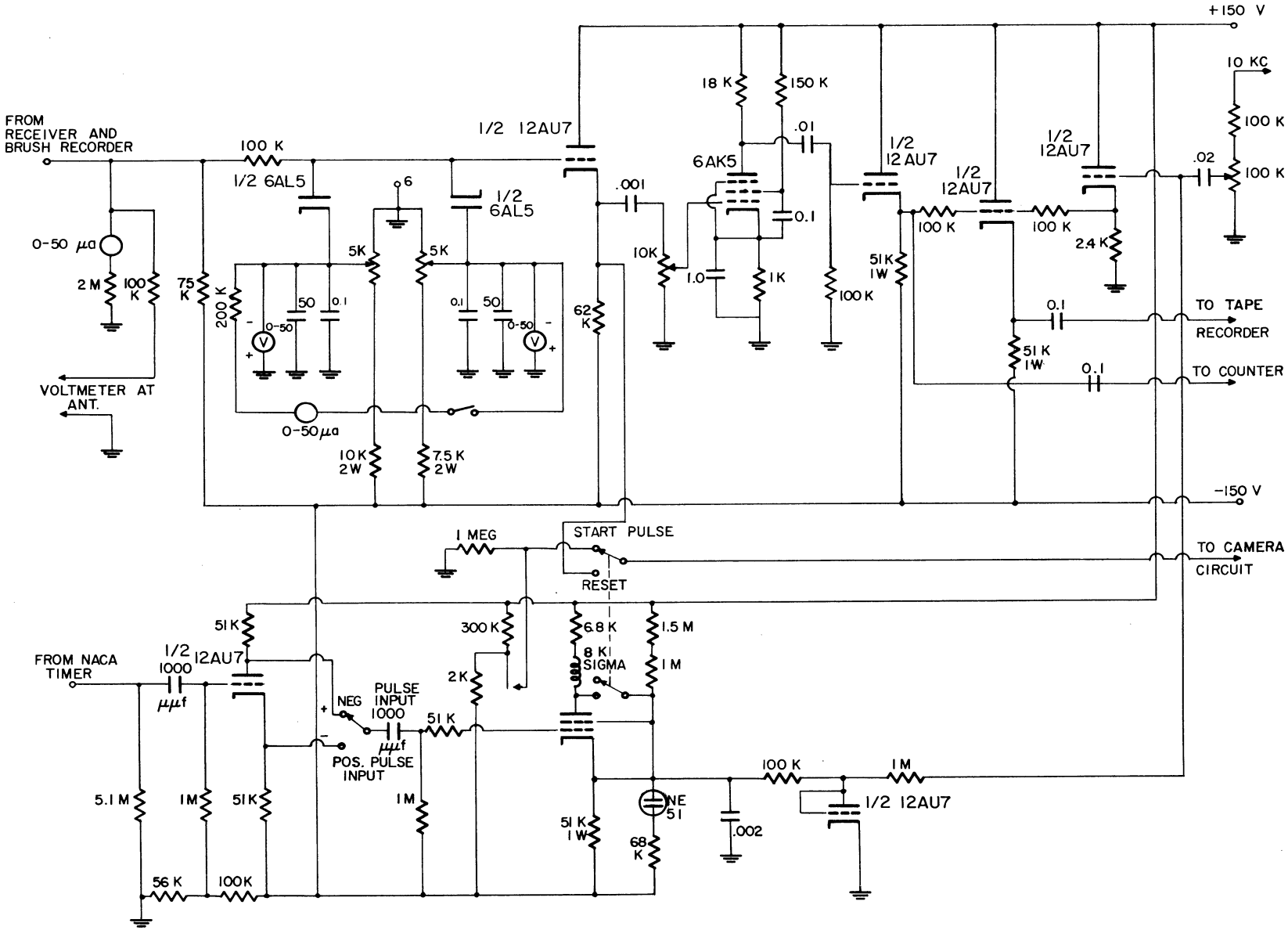

Fig. 29. Schematic of pulse-control circuit.

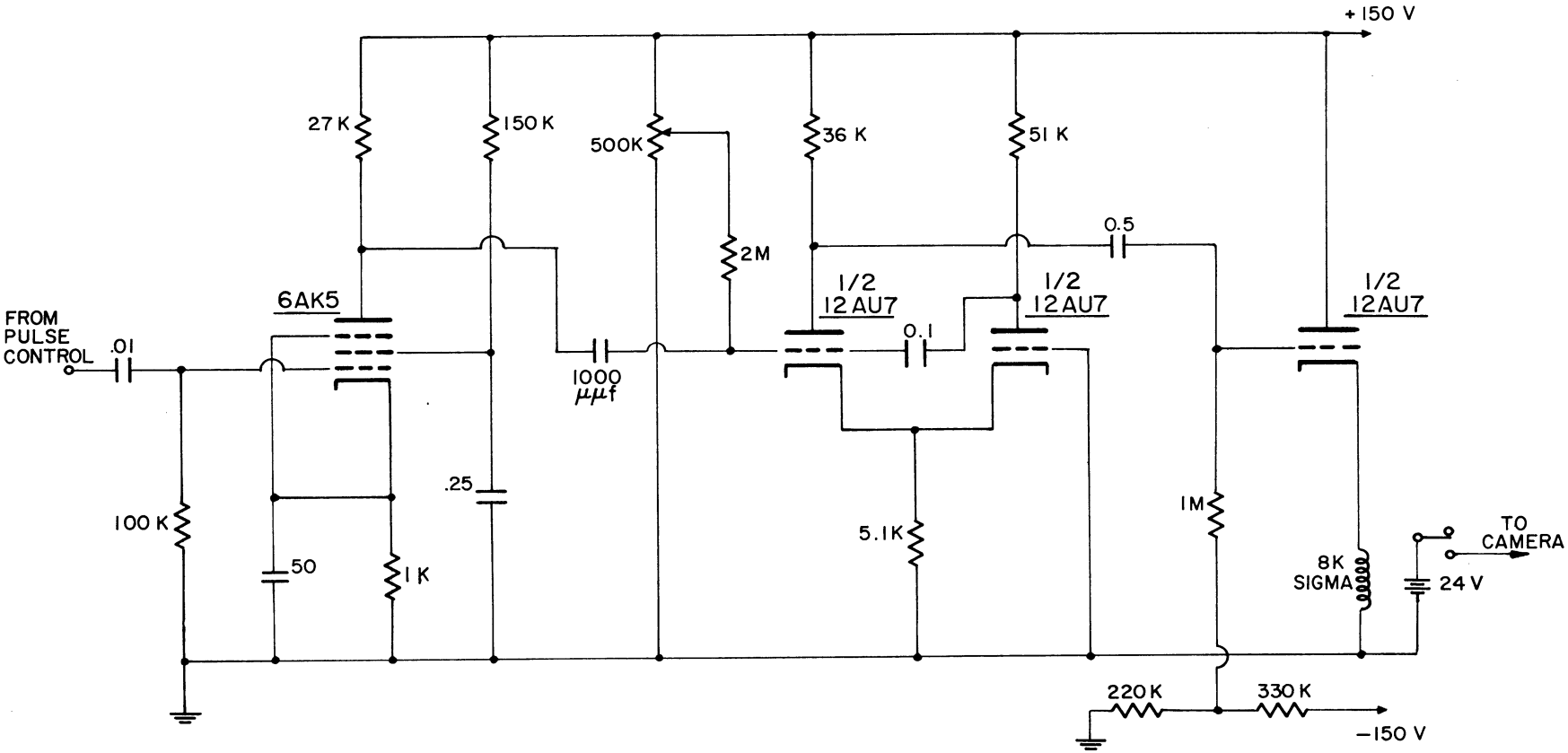

Fig. 30. Schematic of camera circuit.

to alternate positive and negative pulses with a 10-μsec time constant. The 6AK5 section also provides gain control. The three succeeding cathode followers mix the signal pulses with a 10-kc standard frequency from the standard oscillator, thus providing an accurate time base on the tape record. The last cathode follower is biased to cut-off until rocket take-off. By this maans, the 10-kc signal marks take-off. The bias shift is accomplished by the lower circuit of Fig. 29, which also provides a signal to operate the camera at take-off.

The camera circuit of Fig. 30 closes the output relay for 50 milliseconds each time a stop pulse (which also stops the Hewlett-Packard counter) is applied to the input. The relay sequences the camera.

6.6. STANDARD OSCILLATOR

The equipment below the pulse-control chassis is a Hewlett-Packard Low-Frequency Standard Type 100D. It is a crystal oscillator which was used to supply 10 kc as a time base for the tape recorder and 10 cps for the clock circuit.

6.7. CLOCK CIRCUIT

The next lower chassis is the clock circuit, whose schematic is shown in Fig. 31. It takes 10 cps from the Low-Frequency Standard, multiplies the signal by 6 and amplifies it to 14 watts to give 60-cycle power for operating the digital clock.

6.8. SIGNAL GENERATOR

The equipment at the lower right of Fig. 28 is Federal Mfg. and Engineering Corp. Signal Generator Type 804 used for checking the receiver.

6.9. CLOCK, COUNTER, AND CAMERA

The upper two items in the left relay rack are an illuminated digital clock and a Hewlett-Packard Electronic Counter Model 522B. To the left on the tripod is a Beattie Varitron Camera. These three items constituted one of the recording systems. The clock ran continuously, the counter was started and stopped by the signals from the sphere, thus displaying the accelerometer transit time at 0.6-second intervals, while the camera photographed the counter and clock at take-off and at each stop pulse. This arrangement then would give transit times as a function of rocket time.

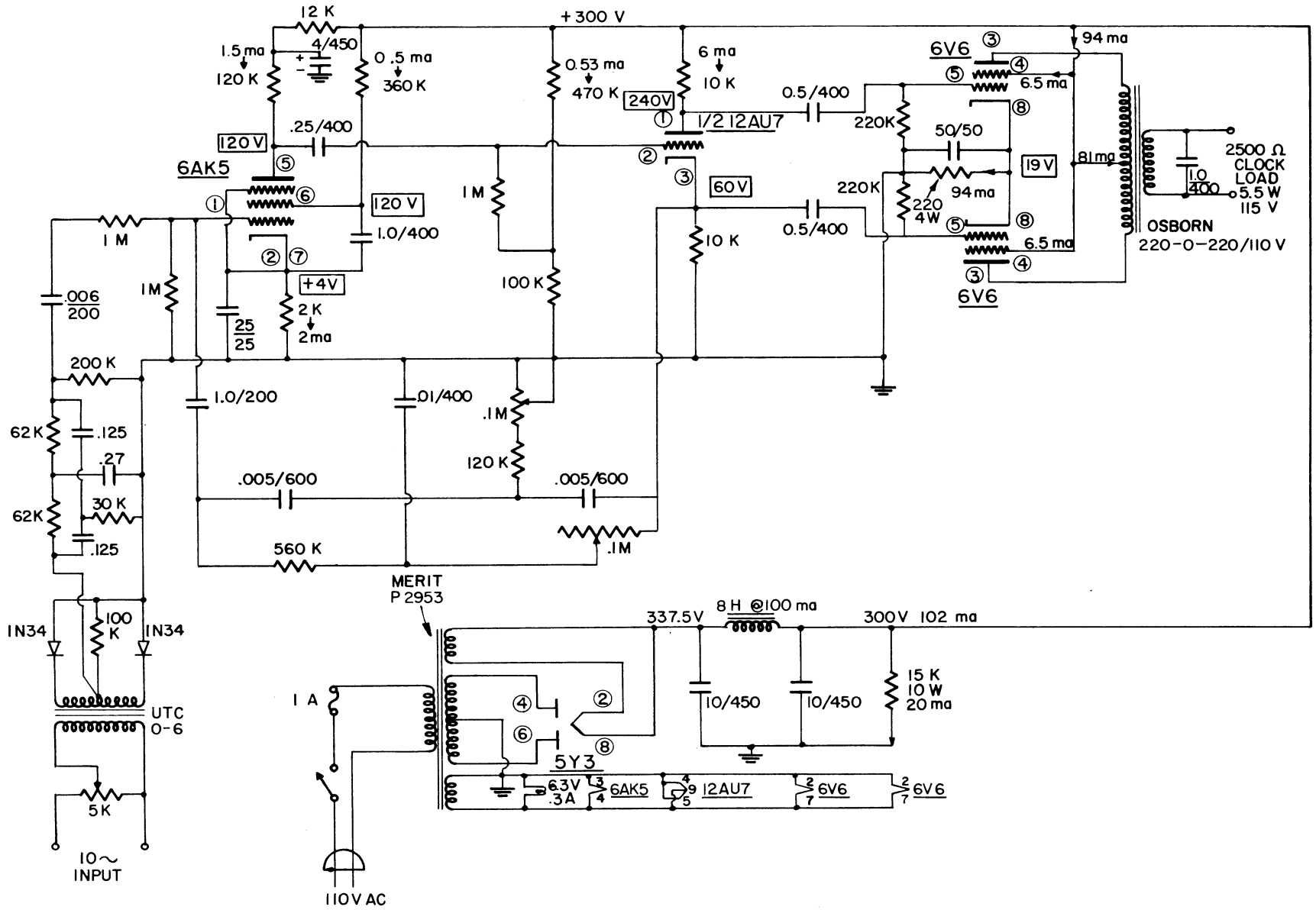

Fig. 31. Schematic of clock circuit.

6.10. TAPE RECORDER

The tape recorder is an Ampex two-channel equipment, Model 309. It recorded accelerometer start and stop pulses superimposed on a 10-kc standard time signal. The recorder constituted the second recording method of the telemeter system.

6.11. BRUSH RECORDER

As noted above, a Brush Recorder was connected across the output of the receiver. It was primarily for the purpose of monitoring signal strength. However, during the flight it actually recorded the entire data sequence, whereas only half the points were recorded on tape and none on the camera film. See Section 8.

7. THE NIKE-DEACON (DAN) SOUNDING ROCKET

The successful development of a synoptic method for upper-air density is as much dependent on a suitable rocket as on the measuring instrumentation. Following the successful use by Van Allen of the Rockoon[12] (Deacon and balloon) as a sounding vehicle, we began to investigate the possibility of using the Deacon or similar rocket in a two-stage boosted combination. The objective was to find an inexpensive vehicle for carrying 50 pounds to an altitude of 50 to 100 miles. It was desired that the rocket should be capable of being fired at a predetermined time on a predictable trajectory. At the invitation of the Pilotless Aircraft Research Development group at the NACA laboratory at Langley Field, we examined their use of the Deacon rocket boosted by a Nike booster. In the NACA work the combination had been used successfully to achieve high Mach numbers at low altitudes. In a cooperative project with NACA the rocket was modified for high-altitude use by providing larger, lighter fins and a long coasting period (about 15 seconds) for the Deacon. Two successful flights were carried out at the NACA test site at Wallops Island, Va., on 8 April 1955 and 24 June 1955.[13,14]

We are indebted to Mr. J. A. Shortal and his group at NACA for arranging the cooperative effort which resulted in the flights. NACA provided Deacon rockets, designs, and parts as well as the firing range, crew, and tracking facilities. Michigan designed and built the Deacon fins and built or had built most of the auxiliary parts, including the nose-cone instrumentation and booster fins. Boosters were provided by the Ordnance Corps and the DPN-19 beacons by the Signal Corps.

7.1. COSTS

One requirement of a synoptic vehicle is low cost. The DAN is a combination vehicle which must be purchased in parts and assembled by the user. Considerable effort went into this process for the first two DAN's, so the costs are not representative. However, after the first two missiles were used it was calculated that they could be copied for about $4000 apiece plus the cost of the Nike booster which is also about $4000. These costs do not include the cost of the scientific instrumentation. Subsequent procurement efforts on about 12 DAN's show that these costs can be held.

7.2. LAUNCHING OPERATIONS

Another requirement of a synoptic vehicle is that it be relatively easy to handle and fire. In this respect the all-solid-propellant rocket is vastly superior to a liquid-propellant one. Ideally, a sounding rocket would be small enough and light enough to be completely man handled. The Deacon meets this requirement, as its complete take-off weight with instrumentation is about 220 pounds. It is 6 inches in diameter and about 12.5 feet long. The Nike booster, however, must be handled with special equipment, as it is considerably heavier. It is also about 12.5 feet long and is 16.5 inches in diameter. At Wallops Island the rockets were fired from a modified experimental model Terrier launcher seen in Fig. 32. The Nike is suspended from an overhead tiltable arm. It is free after about one inch of movement. The Deacon is supported only by the coupling device between it and the booster. Preparation for firing 6 additional DAN's has led to the development of methods for handling and launching the vehicle with the use of hand-operated equipment only. These may not be relied upon exclusively, however, if power devices are available.

Experience with the first two DAN's showed that, after construction, the missiles could be prepared, both mechanically and electrically, for launching with an expenditure of 7 man days of effort. The actual firing operations were accomplished by a crew of about 5 in a time of less than 3 hours.

7.3. DESIGN AND CONSTRUCTION

The design factors were the usual ones of strength and rigidity to resist aerodynamic and acceleration loads, stability, and drag. Calculations showed that only nominal aerodynamic heating would be encountered in any of the parts. The overall assembly of the DAN is illustrated in Figs. 32 and 33. Starting with the front end, the main features are:

7.31. Nose Cone.—The nose cone, which is described in Section 5, screws onto the front end of the Deacon.

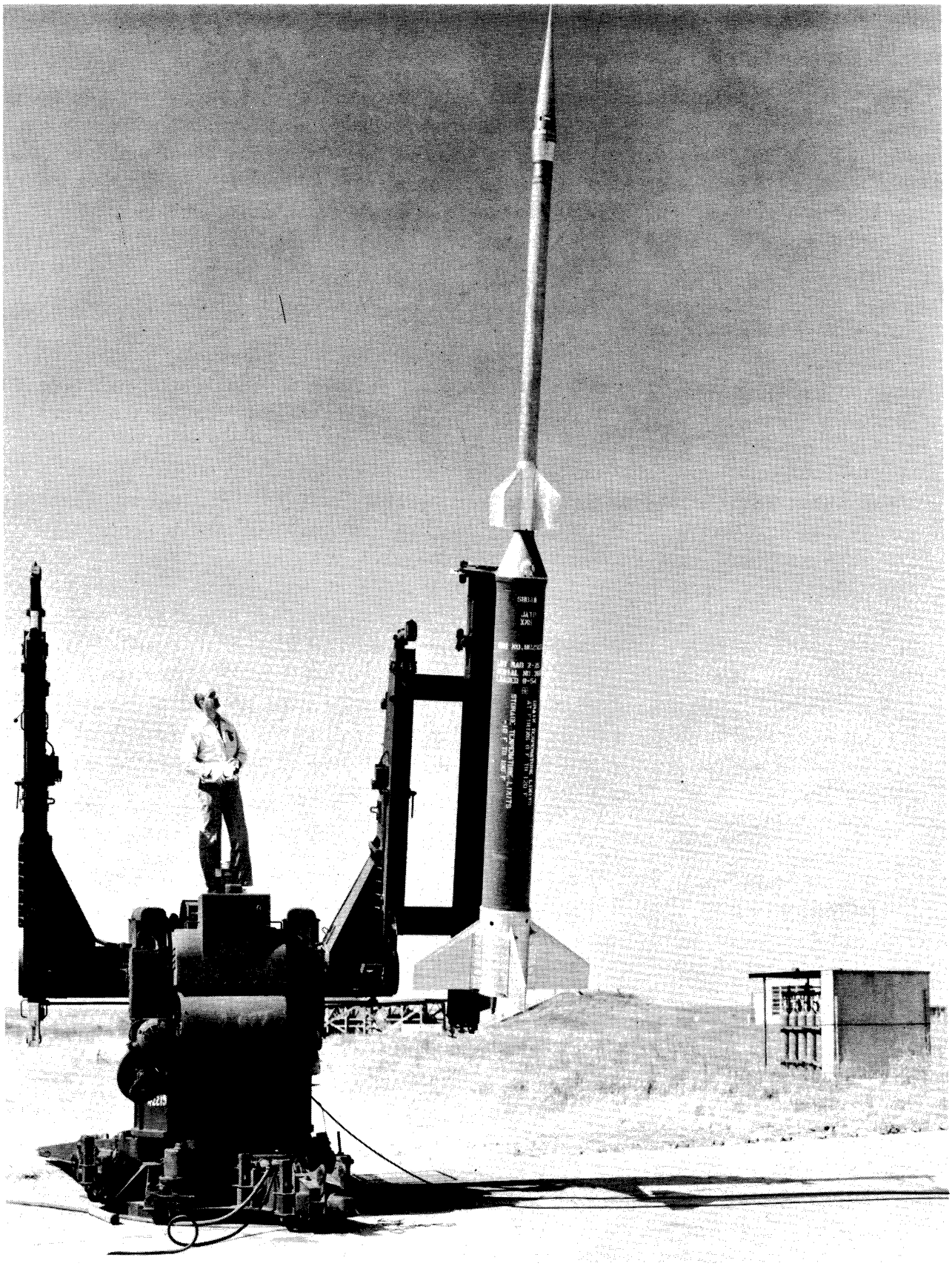

Fig. 32. Nike-Deacon (DAN) rocket on launcher.

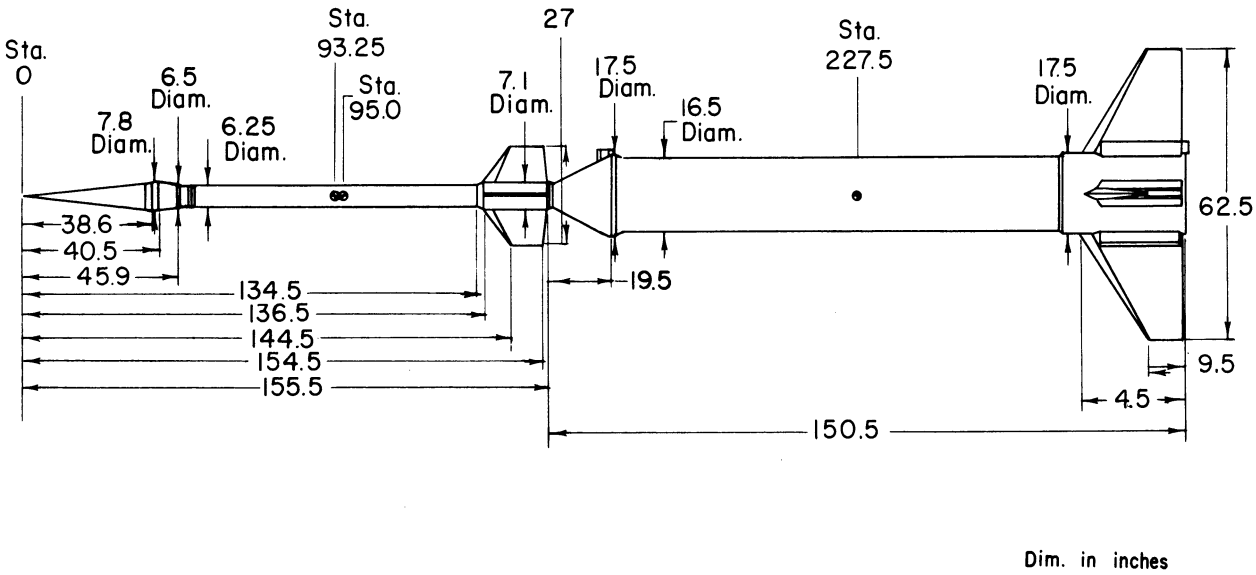

Fig. 33. Dimensions of Nike-Deacon rocket.

7.32. Deacon Rocket.—The Deacon is 6.25 inches in diameter and 107 inches long, exclusive of attachments. Loaded, it weighs 151.5 pounds. For complete operational and performance characteristics see the SPIA Manual.[15]

7.33. Deacon-Fins.—The Deacon fins presented a considerable problem in design and manufacture. Because of the long coasting period, fins of fairly large area were required. Because of the rather high velocities, the aerodynamic loads, under assumed yaw angles, were large. These loads presented a problem in rigidity rather than ultimate strength. In order to meet the stability requirements with the light payload, it was required that the fins be of minimum weight. All of these criteria were finally met with the fin assembly of Figs. 34 and 35. The fins were machined from Dural plate and bolted to a cylindrical shroud machined from a Dural tube.

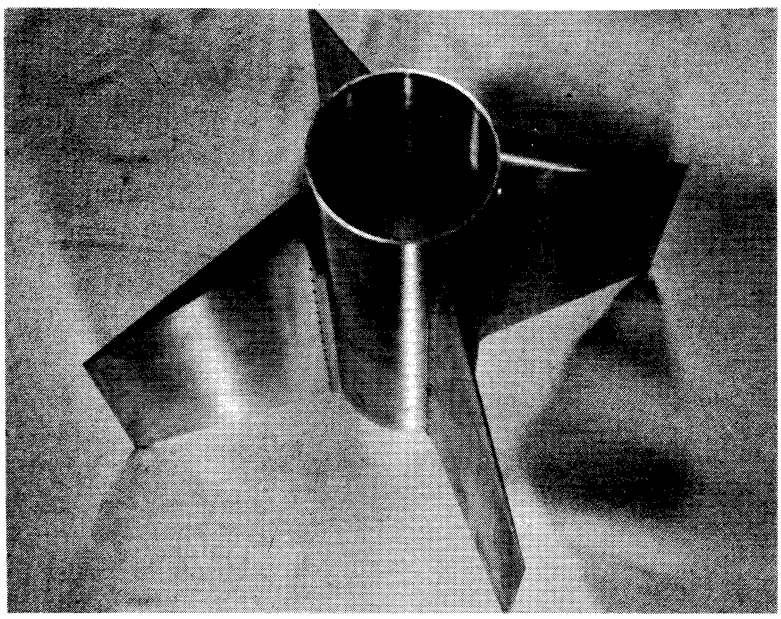

Fig. 34. Deacon fin assembly.

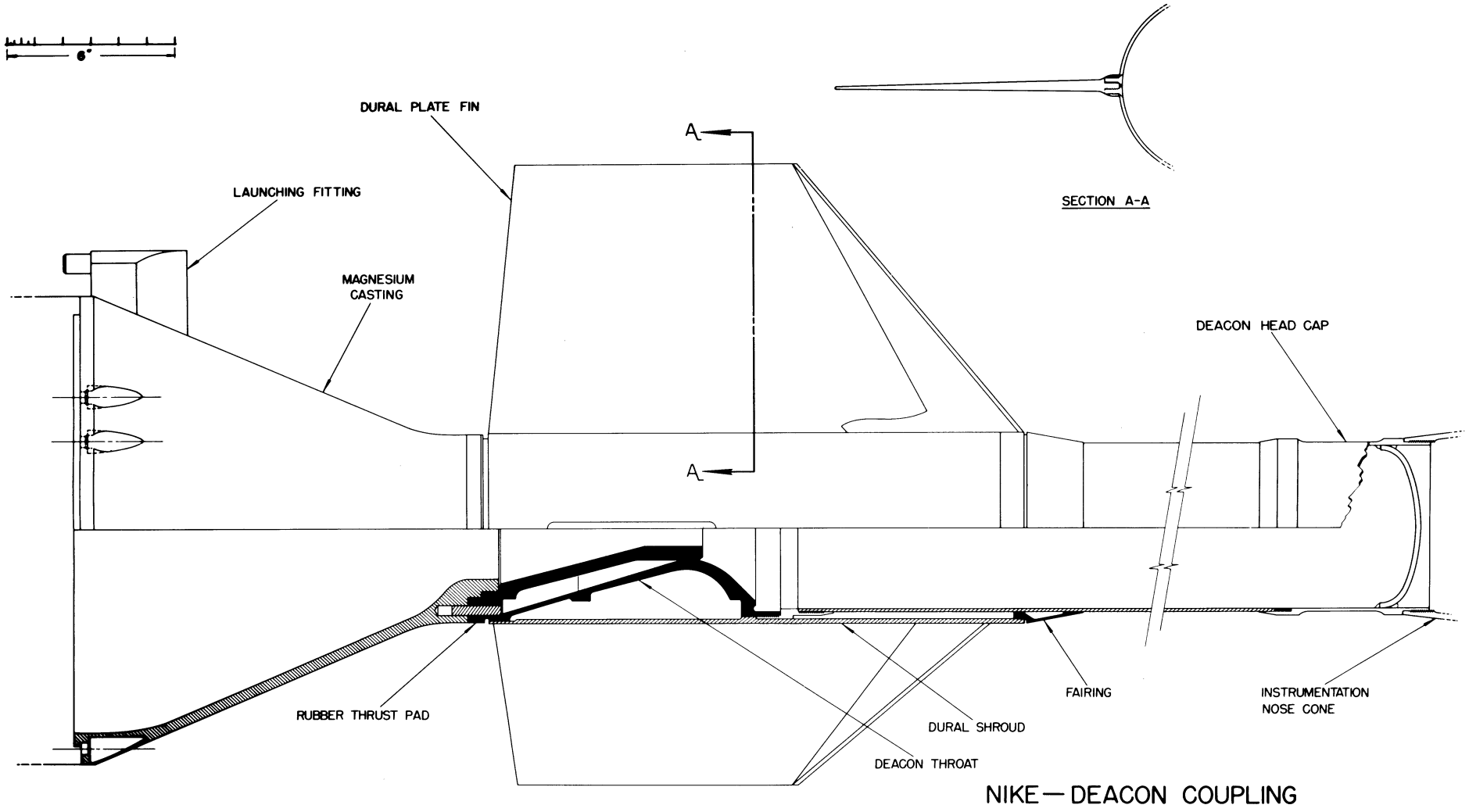

Fig. 35. Nike-to-Deacon coupling.

7.34. Nike-to-Deacon Coupling.—This device, of NACA design, consists of a cone mounted on the front end of the Nike, the cone being surmounted by a cylindrical section which plugs into the Deacon throat. The coupling is illustrated in Fig. 35. In operation the Deacon merely slips off the Nike at booster burn-out, the force being the difference in the Nike and Deacon drag forces.

7.35. Nike Booster.—See Reference 15.

7.36. Nike Fins.—Because of the lighter weight of the Deacon compared to the Nike missile, the acceleration of the DAN is greater than that of a complete Nike. The resulting greater aerodynamic loads were calculated to be too great for the standard Nike booster fins. NACA designed new fins and employed four instead of three. The assemblies were procured by Michigan. The fin construction is seen in Fig. 36. The fins were bolted in slots welded to a welded magnesium shroud which is seen in Fig. 32. Alignment of the fins was accomplished with the aid of a potting compound in which the fins were set before the bolts were tightened.

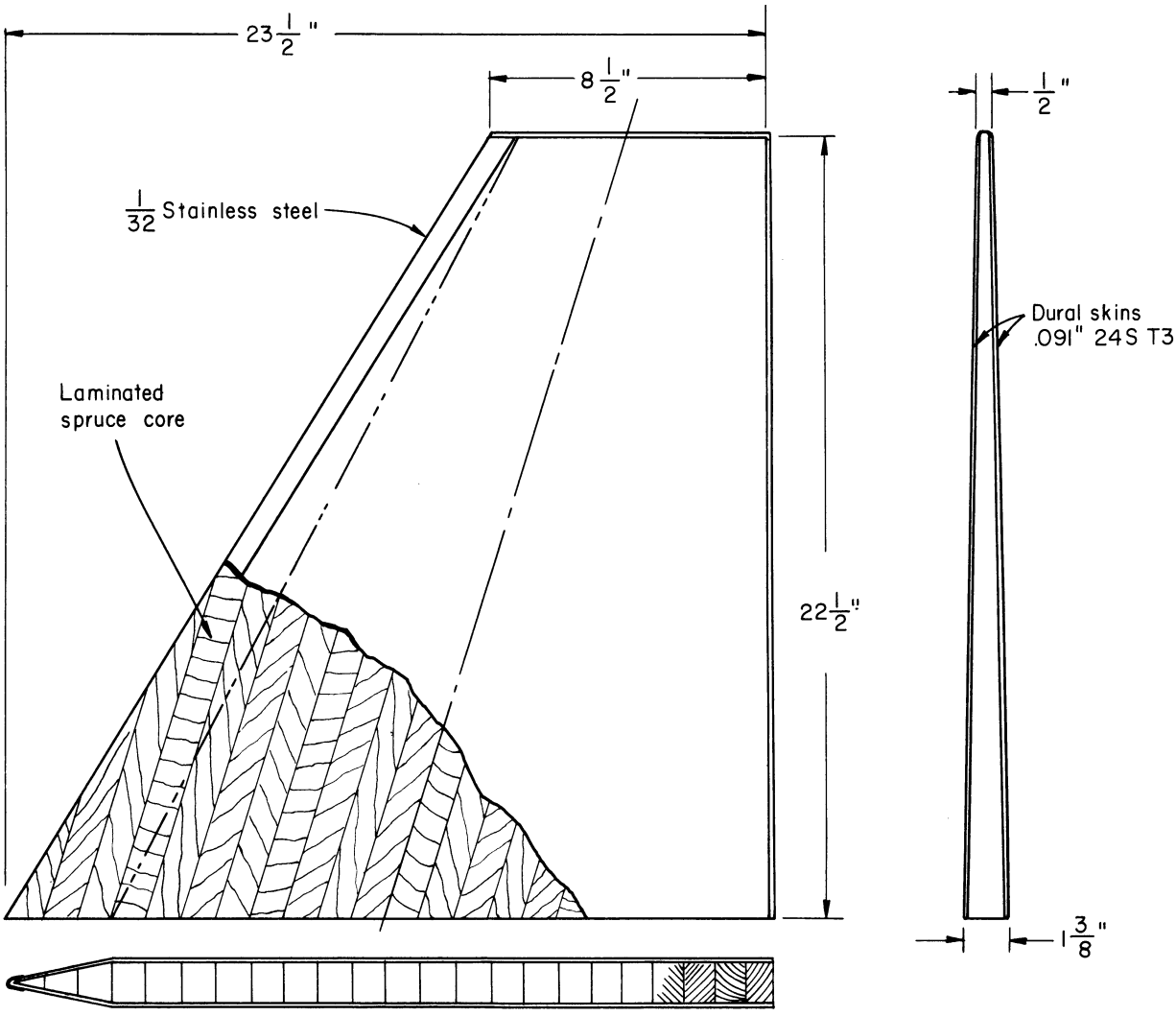

Fig. 36. Nike fin construction.

8. FLIGHTS*

The two DAN flights were similar in most respects. In DAN No. 1 the sphere did not contain an accelerometer because its operation caused rf interference with the transmitter. Therefore, no upper-air data were expected. The purpose of the flight was to test the rocket and sphere ejection system and to measure received signal strength. In DAN No. 2 an internal shield isolated the transmitter so that the accelerometer was flown and upper-air densities measured. The coasting period of the first rocket was longer than that of the second.

8.1. DAN NO. 1

Total Take-Off Weight: _____ pounds
Nike Complete: _____ pounds
- Fins and shroud: 100 pounds
- Coupling: 35 pounds
- CG (loaded): 78.5 inches from rear end

Deacon Complete: _____ pounds
- Fins and shroud: 25.5 pounds
- Nose cone and instrumentation, including sphere: 34.75 pounds
- CG (loaded): 60.5 inches from rear end

Firing Date: 8 April 1955
Take-Off Time: 10:19 EST
Firing Angle: 75°
Booster Burn-Out:
- Time: 3.3 seconds
- Velocity: 3200 feet/second
- Altitude: 4900 feet

Deacon Ignition:
- Time: 17.0 seconds
- Velocity: 1584 feet/second
- Altitude: 36,000 feet

Deacon Burn-Out:
- Time: 20.8 seconds
- Velocity: 5150 feet/second
- Altitude: 47,060 feet

Sphere Ejection:
- Time: 52 seconds
- Altitude: 174,000 feet

---

*Much of the flight data of this section was provided by NACA either in private communications or Research Memorandum SL55L27.

Peak (of Nose Cone):
Time: 161 seconds
Altitude: 356,000 feet
Horizontal Range: estimated 340,000 feet

8.2. DAN NO. 2

Total Take-Off Weight: _____ pounds
Nike Complete: _____ pounds
Fins and shroud: 100 pounds
Coupling: 35 pounds
CG (loaded): 77 inches from rear end
Deacon Complete: _____ pounds
Fins and shroud: 25.5 pounds
Nose cone and instrumentation, including sphere: 39.75 pounds
CG (loaded): 62.25 inches from rear end
Firing Date: 24 June 1955
Take-Off Time: 13.04 EST
Firing Angle: 75°
Booster Burn-Out:
Time: 3.3 seconds
Velocity: 3300 feet/second
Altitude: 5,200 feet
Deacon Ignition:
Time: 12.8 seconds
Velocity: 1980 feet/second
Altitude: 28,000 feet
Deacon Burn-Out:
Time: 16.0 seconds
Velocity: 5289 feet/second
Altitude: 39,339 feet
Sphere Ejection:
Time: 52 seconds
Altitude: 182,000 feet
Peak (of Nose Cone):
Time: 156.0 seconds
Altitude: 347,339 feet
Horizontal Range: estimated, 320,000 feet

Figures 37 to 41, taken from Reference 14, are plots of various flight parameters. A discussion of the method of obtaining peak time and altitude for DAN No. 2 and the difference in these quantities between the sphere and nose cone is contained in the next section.

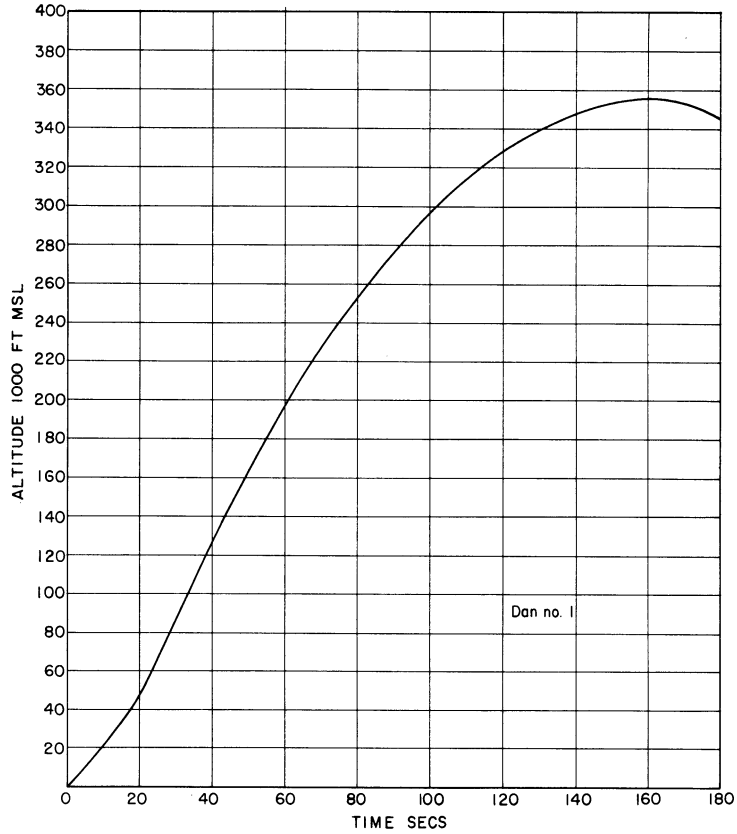

Fig. 37. Altitude vs time, DAN No. 1.

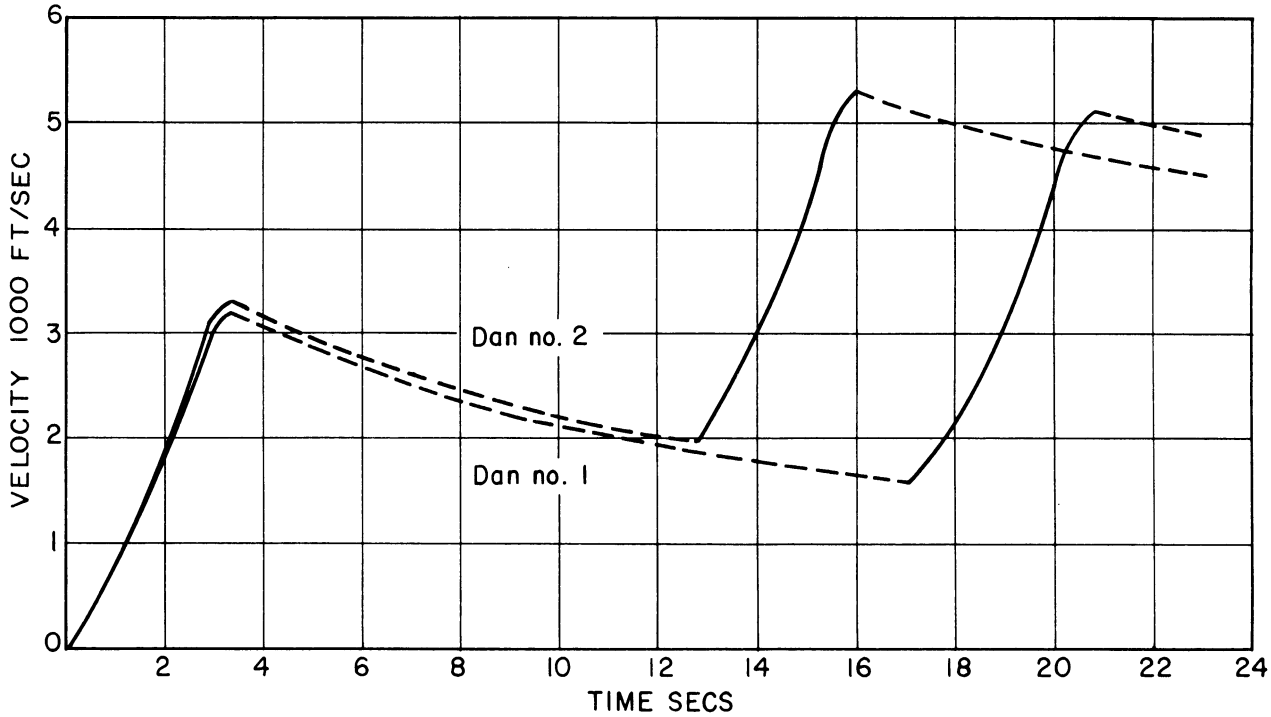

Fig. 38. Velocity vs time, DAN's 1 and 2.

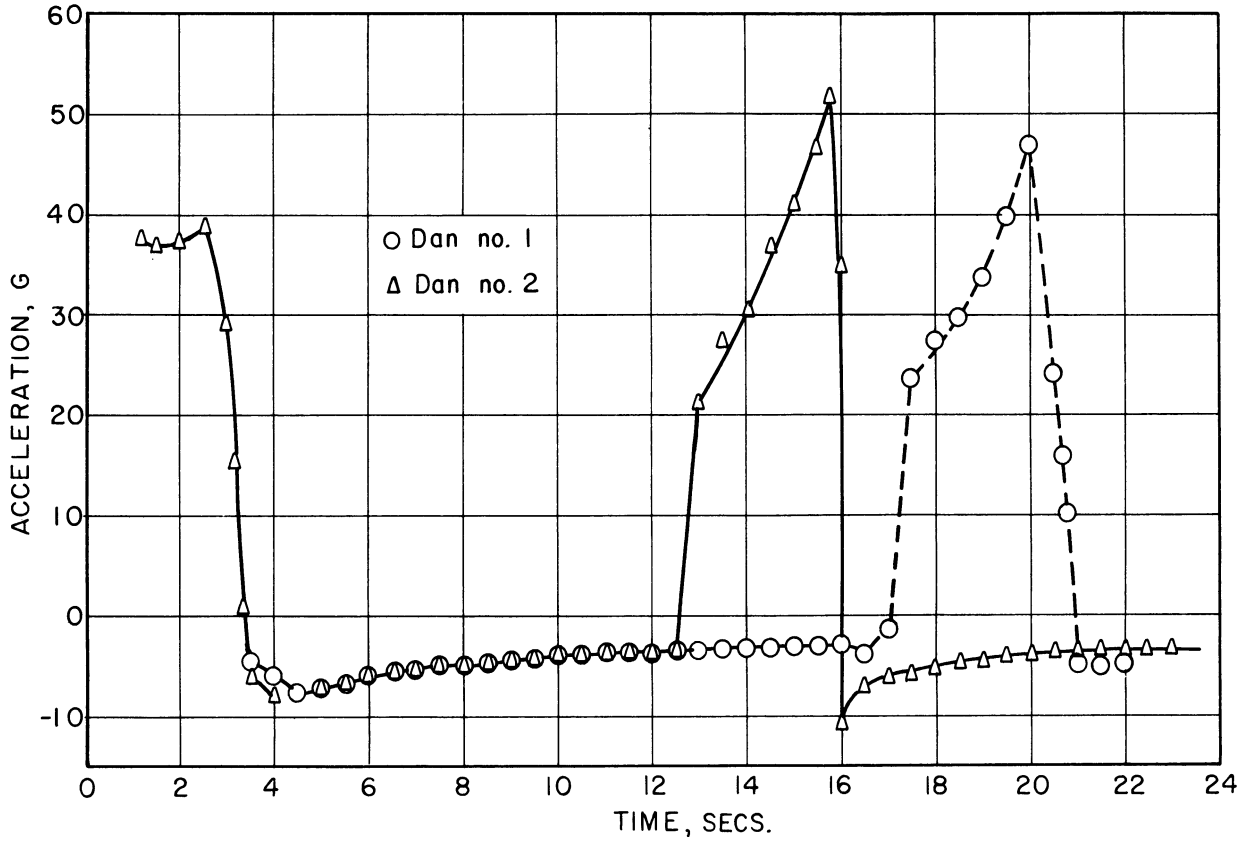

Fig. 39. Acceleration vs time, DAN's 1 and 2.

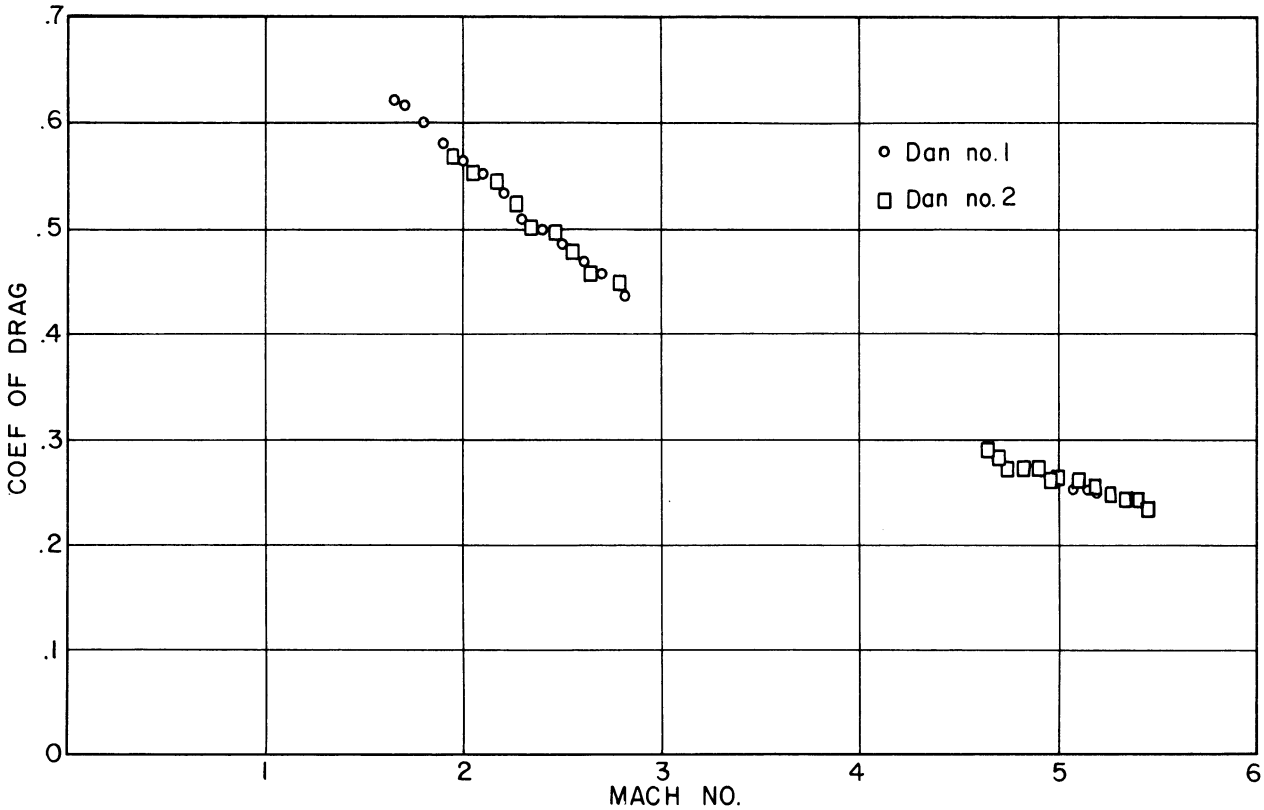

Fig. 40. Rocket coefficient of drag vs Mach number.

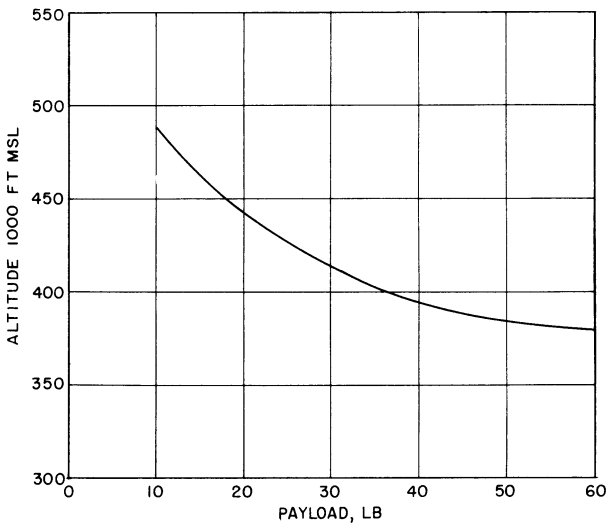

Fig. 41. Altitude vs payload weight.

9. DATA REDUCTION AND RESULTS

In the following, the coordinates (x,y) are those of a right Cartesian coordinate system with origin at the rocket launcher; x is horizontal range in the plane of the trajectory (east-southeast) and y is altitude above a plane tangent to the earth's surface at the launcher.

9.1. THE RAW DATA

The raw data consists of the following:

(a.) Time intervals from the time-of-flight accelerometer.

(b.) Radar measurements of the position of the rocket nose cone as a function of time for a portion of the rocket trajectory.[14]

Because of the low signal-to-noise ratio of the signal from the sphere transmitter, the electronic counter and camera data recording system did not record properly. However, the accelerometer signals were recorded on both the Brush Recorder and the magnetic tape recorder.

To see why the camera and electronic counter system did not work properly, refer to Section 6.5. Because of the low signal-to-noise ratio, the signal output from the differentiator was not free of noise as had been expected. Thus the signal to the Hewlett-Packard electronic counter consisted of a random series of start and stop pulses. Similarly, the camera signal consisted of a random series of stop pulses. Under these conditions, the counter and camera could not function properly.

Figure 42 is a copy of a section of the Brush record showing the first eight accelerometer signals obtained on the upleg of the trajectory. In this figure time increases from right to left, as indicated by the time scale at the top. The speed of the Brush Recorder was 5 divisions per second (25 mm/second). The width of a pulse is a measure of the corresponding accelerometer time interval. Because of the finite time of rise and fall of the Brush pen, the pulse width at the top or at the bottom of the pulse do not indicate correctly the accelerometer time interval. The correct distance is the horizontal distance between the two points at which the pen begins its upward and downward motion, respectively. These points are indicated by the words start and stop for the fifth accelerometer signal on the figure. This record does not represent the optimum type of recording of accelerometer time intervals. The speed of the Brush record was not sufficient to determine the time interval with the desired accuracy. The record does provide flight-time monitoring of the experiment and a reliable backup of the other recording method. The original intended purpose of this record was to record the time variation of received signal strength, which is indicated by the variation in pulse amplitude of the pulses in the figure.

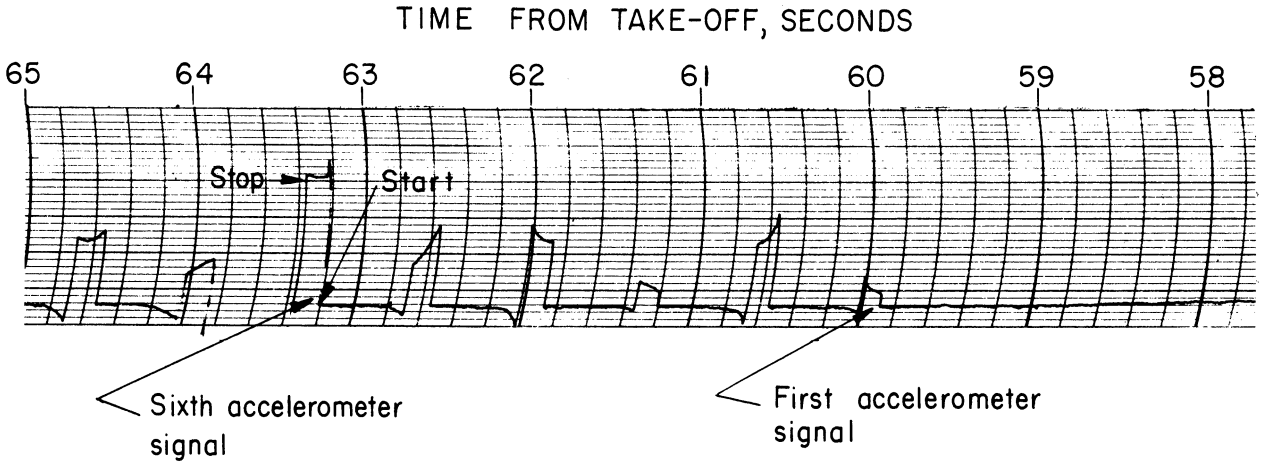

Fig. 42. Portion of Brush Recorder record.

The magnetic tape recording of the accelerometer time signals consisted of a signal which was the sum of the 10-kc standard-frequency sine wave plus the output of the signal differentiator (see Section 6.5). Ideally then, for large signal-to-noise ratio, the recorded signal would have been the sum of a 10-kc sine wave plus sharp pulses of opposite polarity defining the beginning and end of the accelerometer time interval. Because of the low signal-to-noise ratio, the signals actually consisted of the sum of a 10-kc sine wave plus a series of sharp random pulses, some positive, some negative, which appeared during the accelerometer time interval. This recording ideally would contain the time interval with the beginning and end each defined within one cycle of the 10-kc standard frequency (.01 millisecond). Because of the low signal-to-noise ratio, the beginning and end of the signals actually recorded were not defined that well. In the ideal case, this record would have been played back into the electronic counter and camera data recording unit to ob-

tain the accelerometer time intervals. Again, because of the low signal-to-noise ratio of the recorded accelerometer time intervals, this was not possible. Accordingly, an alternate method of playback was devised.

Figure 43 is a block diagram of the playback apparatus. The output of the tape-recorder playback unit was applied to one channel of a dual-beam oscilloscope. It was also amplified and then fed into a 10-kc band-pass filter to obtain the 10-kc signal, which was then divided down to 1 kc. This 1-kc signal was fed into the second channel of the dual-beam oscilloscope and into the x input of an auxiliary monitor oscilloscope. The output of a local oscillator (100 cps) was fed into the y input of the monitor oscilloscope and into the sweep synchronizing input of the dual-beam oscilloscope. During the playback, the Lissajous figure on the monitor oscilloscope was observed by an operator who adjusted the dial on the 100-cps local oscillator to keep it synchronized with the 1-kc frequency. The sweep control on the dual-beam oscilloscope was adjusted to get one sweep every 20 milliseconds synchronized by the 100-cps input from the local oscillator. The face of the dual-beam scope was photographed by a continuously running 35—mm-film camera.

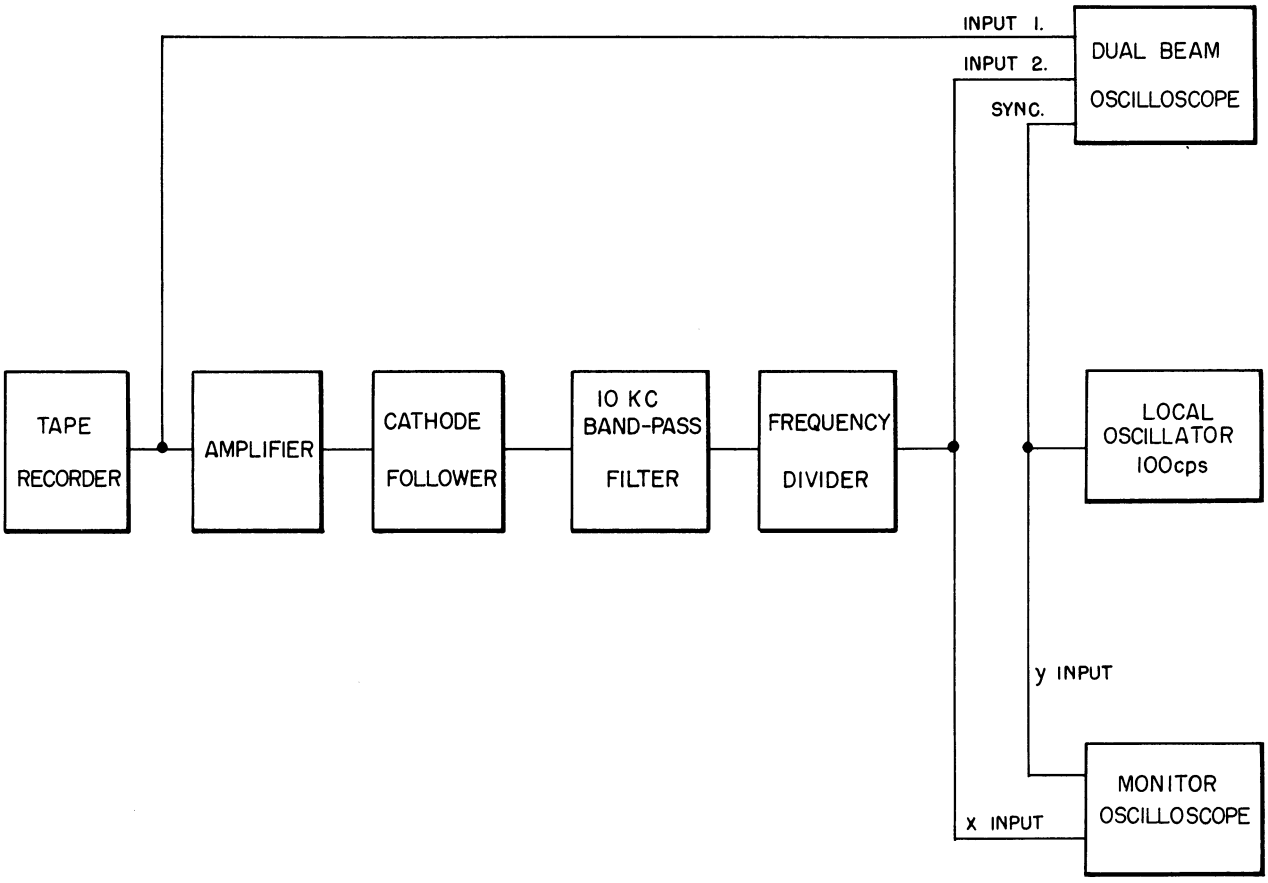

Fig. 43. Block diagram of playback system.

Figure 44 is a copy of a section of the 35—mm-film record obtained in the playback of the magnetic tape recording. It shows the signal from the magnetic tape displayed on one trace of the dual-beam oscilloscope in 20-

millisecond segments adjacent to 20-millisecond segments of the second trace of the scope. During the time when the accelerometer signal does not appear on the signal trace, the second trace records 20 cycles of the 1-kc output of the frequency divider. During the time that an accelerometer signal appears on the signal trace, the 1-kc signal disappears on the second trace and reappears later. The length of the trace in this case is still 20 milliseconds because the sweep is synchronized by the 100-cps signal from the local oscillator. It is believed to be extremely unlikely that the sweep would lose synchronism by as much as one cycle of the 100-cps "sync" signal.

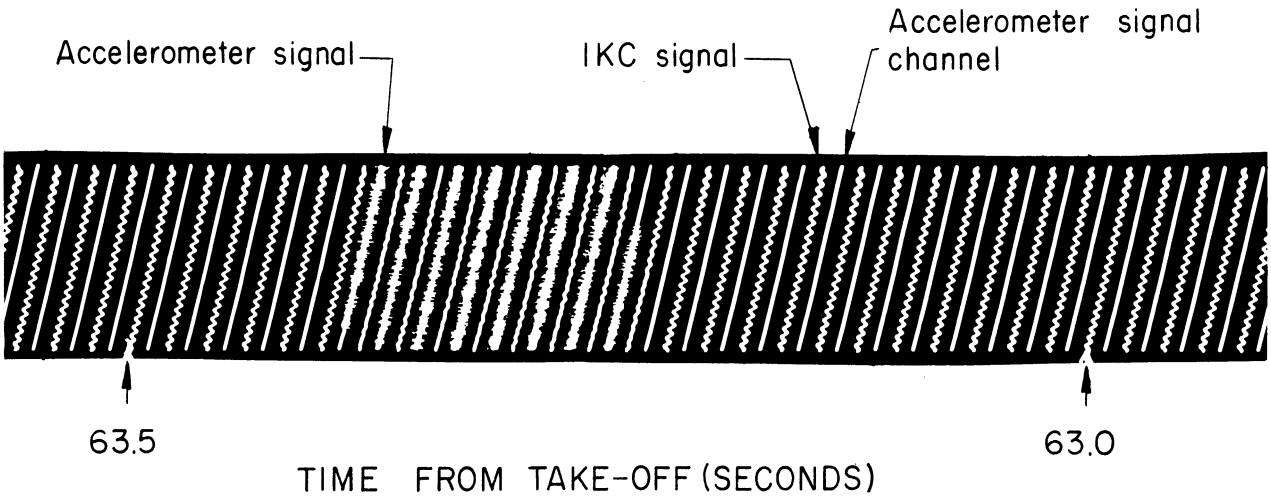

Fig. 44. Portion of film record.

The accelerometer time intervals were obtained by the following procedure. The time of the start and stop of each accelerometer signal was obtained by summing the whole number of sweeps from the start of the record, and by obtaining fractional parts of a 20-millisecond sweep by reference to a sweep containing 20 cycles of the 1-kc signal. This fractional part was estimated to the nearest 0.1 cycle (i.e., nearest 0.1 millisecond). The time interval of the signal was taken as the difference between stop and start time.

It had been intended that the 10-kc standard-frequency signal appear on the magnetic tape exactly at take-off, thus defining take-off time and providing a real-time reference point for the accelerometer time intervals. Because of a broken cable the 10-kc signal was not automatically applied at take-off. It was applied manually by an operator at a time estimated to be about 1.5 seconds after take-off time. The accelerometer time signals obtained from the magnetic tape recording are related to real time by assuming that the 10-kc signal started exactly at 1.5 seconds after take-off.

A modified SCR 584 tracking radar was used by NACA to track a signal from an AN/DPN-19 radar beacon housed within the nose cone of the rocket. The primary radar data are slant range, azimuth angle, and angle of elevation as a

function of time. Altitude, horizontal range, and velocity components can be calculated from these primary data. During the flight the beacon was tracked intermittently on the upleg, data being obtained only for 0.5 second of time around 29,000 feet of altitude. The beacon was not tracked again until just before peak. From this point on, radar data were obtained continuously down to 144,000 feet.

The upleg portion of the trajectory was calculated by NACA starting at 29,000 feet, using velocity data obtained from a c-w Doppler velocity radar unit (Velocimeter) along with the altitude, range, and flight-path angle obtained from the SCR 584 tracking radar at this altitude. The calculation included missile drag considerations and yielded a calculated upleg portion of the trajectory which matched reasonably well with the radar data obtained for the peak of the trajectory.

9.2. SPHERE DRAG-ACCELERATION DATA

Following are the details of the procedure used to calculate sphere drag accelerations from the accelerometer time intervals.

As noted in Section 9.1, the time interval of a given signal was taken as the difference between stop and start time. The time of the accelerometer signal, i.e., the time at which the sphere is assumed to have experienced the corresponding drag acceleration, was taken to be the average of the stop and start time.

The drag acceleration, a_D, corresponding to a given accelerometer signal of length t is given by equation (15) above (see Section 4.3).

$$a_D = \frac{2(s - v_o t)}{t^2} \tag{15}$$

In calculating a_D, it was assumed that v_o was always equal to zero and thus equation (15) becomes

$$a_D = \frac{2s}{t^2} \tag{15a}$$

The distance s for the accelerometer used on the flight was 0.188 inch (0.01567 foot). Substituting this value in the equation, we obtain

$$a_D = \frac{0.03133}{t^2} \text{ ft/sec}^2 . \tag{15b}$$

Before flight, this equation was programmed for a digital computer and a table of values of a_D as a function of t was prepared. In this table, 0.0001-second

increments in t were used for t in the range of 0.0010 to 0.0999 second. By noting the proper shift in decimal points, the same table was used for 0.001-second increments in t for t in the range of 0.010 to .999 second. After the time intervals were read from the records the corresponding drag accelerations were obtained by referring to the table.

It next became necessary to correlate in time the drag accelerations obtained from the Brush and film records. Although a common reference time marker had not been applied to each of the records, it is obvious that the accelerometer time-interval signals or the corresponding drag accelerations themselves provide the basis for time correlation of the two records. A graph of acceleration vs time was prepared for each of the two sets of acceleration data. The data from the film record had the estimated 1.5-second point as reference time. The data from the Brush record had an arbitrary zero placed on the record as reference time. When these two graphs were superimposed one upon the other over a light table, they could be made to come into rough agreement by displacing one time scale with respect to the other. This comparison also showed that the time scale on the Brush record seemed to be stretched slightly, as would be the case if the Brush Recorder had been running at a speed slightly lower than normal. The amount of the displacement and stretching of time scales was obtained as follows:

Let t' and t be film time and Brush time, respectively. Then $\delta t = t - t'$ is the amount to be subtracted from the Brush time to bring it into agreement with film time. If the Brush scale was stretched with respect to film time, then δt would be a linear function of time, i.e., we could write

$$\delta t = at + b , \tag{23}$$

and an equation to convert Brush time into film time would be

$$\begin{aligned} t' &= t - \delta t \\ &= (1 - a)t - b. \end{aligned} \tag{24}$$

The coefficients a and b were evaluated by selecting corresponding points at the beginning and end of the records. The results obtained were

$$a = 0.00236$$

$$b = 141.715 .$$

Thus equation (24) becomes

$$t' = 0.99764t - 141.715 . \tag{24a}$$

The stretching of Brush time corresponds to what would be obtained if the Brush Recorder speed were low, by 0.236%, that is, if the power line frequency were 59.86 cps instead of 60 cps. A check of the Delaware Power and Light Co. frequency record indicates a line frequency of 59.9 cycles at the time of the rocket flight. The theory of the stretching of the time scale of the Brush Recorder would, therefore, appear to be well substantiated.

The times of the acceleration data from the Brush Recorder were corrected as indicated above and the acceleration data from both records were then plotted on one graph as shown in Fig. 45. The first drag-acceleration data point, 2.29 feet/second^2, was obtained at 59.95 seconds shortly after the estimated time of ejection (58 seconds) of the sphere from the rocket. The drag acceleration gradually decreased until the value 0.147 feet/second^2 (.004g) was reached. At this point the "recycling cut-off" of the accelerometer was reached, the drag-acceleration time intervals had become longer than the accelerometer recycling time would allow to be recorded. The fingers picked up the bobbin before it had completed its travel to the cavity.

The accelerometer time intervals for the next 130 seconds, during which time the sphere went up over the peak of its trajectory and started down again, were therefore not useable. At about 230 seconds, the drag accelerations again became large enough so that they could be measured. From this point on, the drag acceleration increased until, at about 282 seconds, it had increased to 122.5 feet/second^2 (about 4g). At this point the accelerometer again began to give improper readings. It is believed that the voltage of the battery operating the pickup fingers had decreased to the point where the fingers were not able to pick up the bobbin properly against the 4g drag acceleration. At about 300 seconds, when the drag acceleration had decreased, good acceleration data were again obtained. However, the battery voltage was falling off continuously, and from about 310 seconds on, the pickup fingers were not able to pick up the bobbin properly, although the drag acceleration had decreased to about 1g.

In the figure the solid line indicates the drag accelerations that should have been recorded in the last period of flight. During this time the sphere was below 100,000 feet where the densities are well known so that there can be no doubt of the malfunctioning of the accelerometer.

9.3. CALCULATION OF THE SPHERE TRAJECTORY

The trajectory of the sphere was calculated as follows. The peak time, horizontal velocity at peak, and peak altitude were determined from the raw data of Section 9.1. Numerical integration of the equations of motion of the sphere both forward and backward in time from peak then yielded velocity as a function of time. A second integration produced position vs time. The details of these calculations follow.

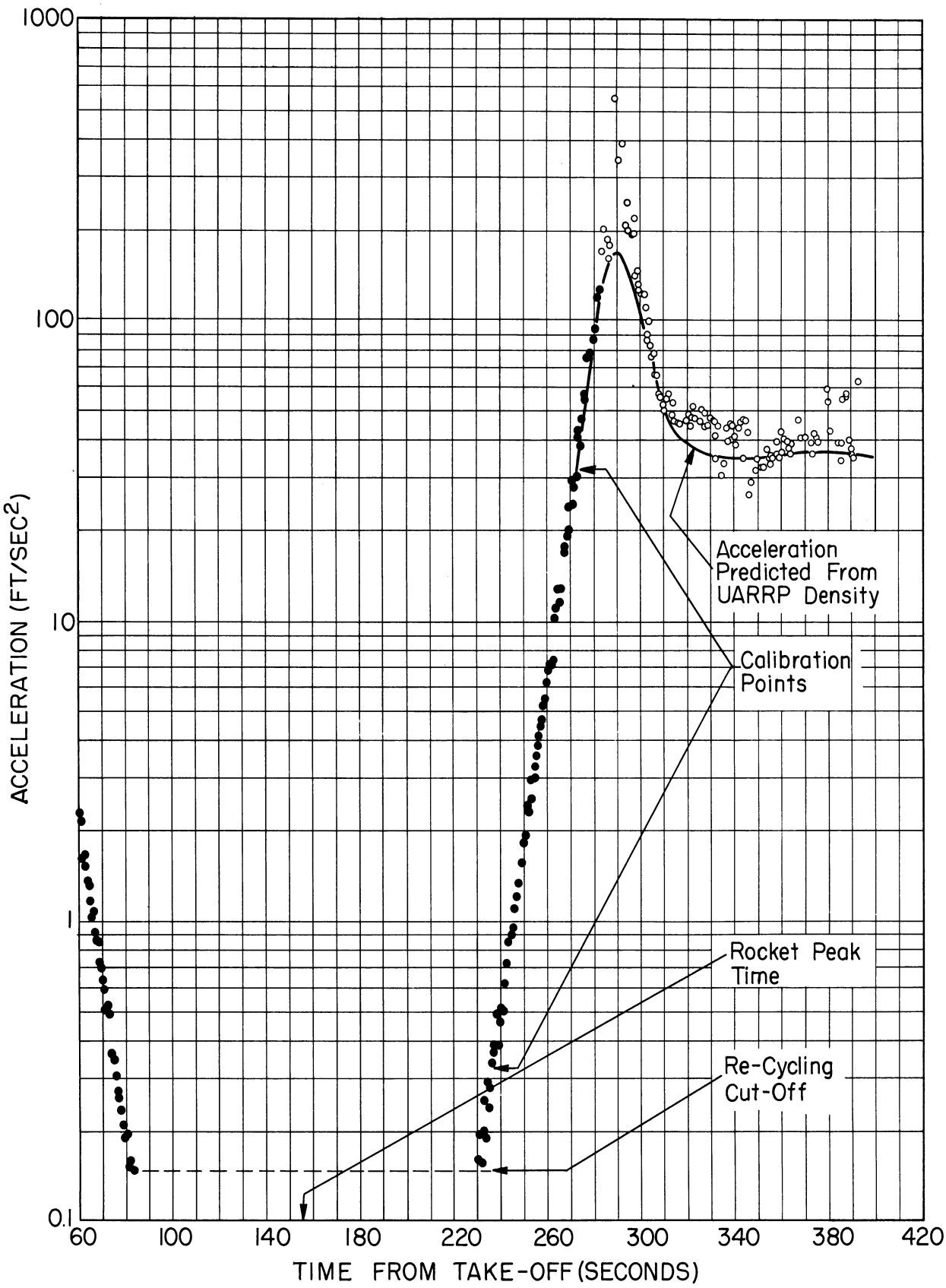

Fig. 45. Acceleration vs time, DAN No. 2.

The sphere peak time was obtained from the drag-acceleration data. Note that the plot of drag acceleration vs time for a_D less than 2 feet/second^2 (Fig. 45) is remarkably symmetrical about a vertical line which bisects the space between the upleg and downleg data. The curve for drag acceleration vs time would be symmetrical about peak time if the curve for velocity vs time were symmetrical about peak time. To a first approximation this is true for the region of data considered. The drag acceleration is small compared to the acceleration of gravity, and the horizontal velocity is approximately constant. Thus, except for the fact that on the upleg we have a small drag force in approximately the same direction as the gravitational acceleration, whereas on the downleg we have a small drag force in a direction opposite to the acceleration of gravity, we have almost the same equation of motion on the upleg as we do on the downleg in this region of the trajectory. We can therefore find peak time by bisecting the space between the two curves. This was done by selecting an acceleration less than 2 feet/second^2 and taking the average of the times at which this acceleration was experienced by the sphere on the upleg and downleg. This was done for 14 values of acceleration in the range of 2-0.15 feet/second^2. The sphere peak time obtained was 155.68 $\pm$ 0.1 second.

The sphere peak altitude was then obtained by a process consisting of three steps:

1. The peak altitude of the nose cone was obtained from the NACA tracking-radar data.

2. An estimate of the difference in peak altitude between the sphere and the nose cone was obtained by consideration of the difference in drag force on the two bodies.

3. The sphere peak altitude was then obtained by subtracting the estimated difference in peak altitudes from the peak altitude of the nose cone.

Because of the large amount of scatter in the radar data, a parabola was fitted to the altitude-vs-time data and the peak altitude of the parabola, 347,340 feet, was taken to be the nose-cone peak altitude.

The difference in peak altitude of the nose cone and sphere was arrived at by the following procedure. The sphere drag-acceleration measurements indicate that the sphere had a peak altitude which was about 4800 feet less than it would have been in a perfect vacuum. The air drag acceleration on the cone is estimated to be about one-sixth of the air drag acceleration on the sphere. Thus the cone would have a peak altitude about 800 feet lower than the peak of the vacuum trajectory and the sphere peak would be 4000 feet lower than the nose-cone peak.

The peak altitude of the sphere according to this reasoning was therefore 343,340 feet.

The horizontal range and velocity of the sphere at peak was obtained by a procedure similar to that for the peak altitude:

1. The horizontal range and velocity of the nose cone at peak were obtained from the NACA tracking-radar data.

2. An estimate of the difference in horizontal range and velocity at peak between the sphere and the nose cone was obtained by estimating the difference in drag force on the two bodies.

3. The horizontal range and velocity of the sphere at peak were then obtained by subtraction of the corresponding estimated difference of part (2).

In step (1) the straight line fitted to the range-vs-time data (see Fig. 46) indicated that, at peak, the nose cone had a horizontal range of 173,400 feet and a horizontal velocity of 1081 feet/second. The drag considerations indicate that, at peak, the range of the sphere would be about 1600 feet less than the range of the nose cone and that the horizontal velocity of the sphere would be about 15 feet/second less than that of the nose cone. Thus the horizontal range of the sphere at peak was 171,800 feet, while its horizontal velocity at this time was 1066 feet/second.

A vacuum trajectory was calculated for the sphere for the 147-second time interval to about peak (82.82 - 230.27 seconds) during which drag-acceleration measurements were not obtained and where the drag acceleration was less than 0.13 feet/second^2. For a vacuum trajectory, the vertical component of velocity, $\dot{y}$, is given by

$$\dot{y} = -g(t - T_o) , \tag{25}$$

the vertical position, y, by

$$y = y_o - \frac{1}{2} g (t - T_o)^2 , \tag{26}$$

where

g = the acceleration of gravity in feet/second^2,
t = time, seconds,
y_o = sphere peak altitude, feet, and
T_o = sphere peak time, seconds.

The horizontal range, x, of the sphere, for this vacuum trajectory, is given by

$$x = x_o + \dot{x}_o(t - T_o) , \tag{27}$$

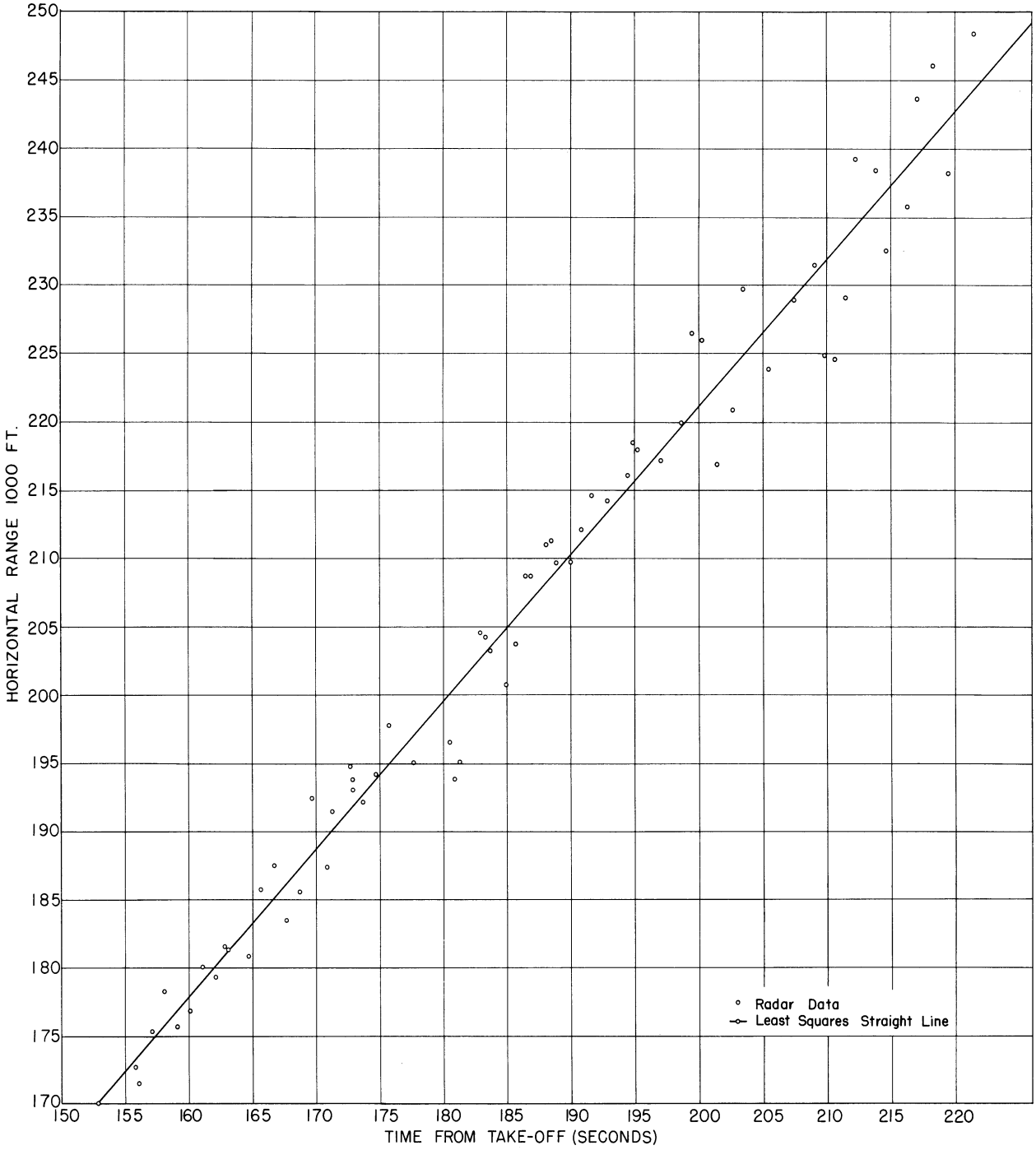

Fig. 46. Horizontal range vs time, DAN No. 2.

where

x_o = horizontal range of sphere at peak, feet, and
$\dot{x}_o$ = horizontal velocity of sphere at peak, feet/second.

For the period of time from 59.95 to 82.82 seconds on the upleg of the trajectory, the trajectory calculation included the drag accelerations measured by the accelerometer. The starting point for this calculation was at 82.82 seconds, and the trajectory was developed by working backward in

time. The process used can be best explained by referring to Table I, which shows in general notation a part of a calculation sheet.

The first two columns contain the measured values of drag acceleration, a_D, and the times at which these drag accelerations were measured. As noted above, x is horizontal range with respect to the launcher and y is altitude above a plane tangent to the earth's surface at the launcher. A dot above a variable indicates differentiation with respect to time, a subscript D refers to drag, V is the net velocity, and g is the acceleration of gravity. When a quantity is preceded by a Δ, this indicates that we have taken the difference between two values, and the subscript on the symbol following the Δ will refer to the second of the two quantities. If a quantity has a bar placed over it, this indicates that we have taken the average of two values, and again the subscript refers to the second of the two values. The time being considered is indicated by placing that value of time in parentheses. Examples of this notation are: $\ddot{x}_D(T_o)$, the horizontal component of drag acceleration at the time T_o, ΔT_2, the increment of time $T_2 - T_1$; $\bar{\ddot{y}}_2$, the average net vertical component of acceleration in the time interval T_1 to T_2.

For the upleg portion of the trajectory, the time T_o would be 82.82 seconds, the times T_1, T_2, etc., would then decrease to 59.95 seconds, for we are working backward in time. At the start of the calculation the values of T_i and a_{D_i} for this time interval and the initial conditions x_o, $\dot{x}_o$, y_o, $\dot{y}_o$, and V are known. The procedure followed for the time interval T_o to T_1 is as follows:

1. Resolve $a_D(T_o)$ into horizontal and vertical components $\ddot{x}_D(T_o)$ and $\ddot{y}_D(T_o)$ by the equations

$$\ddot{x}_D(T_o) = -\frac{\dot{x}(T_o)}{V(T_o)} a_D(T_o) \tag{28}$$

$$\ddot{y}_D(T_o) = -\frac{\dot{y}(T_o)}{V(T_o)} a_D(T_o) \ . \tag{29}$$

2. Find the velocities $\dot{x}(T_1)$, $\dot{y}(T_1)$, $V(T_1)$ at the time T_1 by the following set of successive approximations.

a. Estimate the average values $\bar{\ddot{x}}_1$, $\bar{\ddot{y}}_1$ in the time interval T_1 to T_2.

b. Calculate corresponding values of $\dot{x}(T_1)$ and $\dot{y}(T_1)$, using the equations

$$\dot{x}(T_1) = \dot{x}(T_o) - \bar{\ddot{x}}_D \cdot \Delta T_1 \tag{30}$$

TABLE I

TRAJECTORY CALCULATION SHEET

Time	a_D	ΔT	$\dot{x}$	$\dot{y}$	V	$\ddot{x}_D$	$\ddot{y}_D$	g	$\ddot{y}_D$-g	Δy	y	Δx	x
T_o	$a_D(T_o)$		$\dot{x}(T_o)$	$\dot{y}(T_o)$	$V(T_o)$	$\ddot{x}_D(T_o)$	$\ddot{y}_D(T_o)$	$g(T_o)$	$\ddot{y}_D(T_o)-g(T_o)$		$y(T_o)$		$x(T_o)$
		ΔT_1	$\bar{\dot{x}}_1$	$\bar{\dot{y}}_1$		$\bar{\ddot{x}}_1$			$\bar{\ddot{y}}_1$	Δy_1		Δx_1	
T_1	$a_D(T_1)$		$\dot{x}(T_1)$	$\dot{y}(T_1)$	$V(T_1)$	$\ddot{x}_D(T_1)$	$\ddot{y}_D(T_1)$	$g(T_1)$	$\ddot{y}_D(T_1)-g(T_1)$		$y(T_1)$		$x(T_1)$
		ΔT_2	$\bar{\dot{x}}_2$	$\bar{\dot{y}}_2$		$\bar{\ddot{x}}_2$			$\bar{\ddot{y}}_2$	Δy_2		Δx_2	
T_2	$a_D(T_2)$		$\dot{x}(T_2)$	$\dot{y}(T_2)$	$V(T_2)$	$\ddot{x}_D(T_2)$	$\ddot{y}_D(T_2)$	$g(T_2)$	$\ddot{y}_D(T_2)-g(T_2)$		$y(T_2)$		$x(T_2)$

$$\dot{y}(T_1) = \dot{y}(T_o) - \bar{\ddot{y}}_D \cdot \Delta T_1 . \tag{31}$$

c. Calculate $V_1 = \sqrt{\dot{x}^2(T_1) + \dot{y}^2(T_1)}$. (32)

d. Resolve $a_D(T_1)$ into horizontal and vertical components by

$$\ddot{x}_D(T_1) = - \frac{\dot{x}(T_1)}{V(T_1)} a_D(T_1) \tag{33}$$

$$\ddot{y}_D(T_1) = - \frac{\dot{y}(T_1)}{V(T_1)} a_D(T_1) . \tag{34}$$

e. Calculate $\ddot{y}(T_1) = \ddot{y}_D(T_1) - g(T_1)$. (35)

f. Check the average values $\bar{\ddot{x}}_1$ and $\bar{\ddot{y}}_1$ estimated in (a) above by calculating the averages

$$\bar{\ddot{x}}_1 = \frac{\ddot{x}_D(T_o) + \ddot{x}_D(T_1)}{2} \tag{36}$$

$$\bar{\ddot{y}}_1 = \frac{\ddot{y}(T_o) + \ddot{y}(T_1)}{2} \tag{37}$$

g. Repeat steps (a) to (f) until the values of $\bar{\ddot{x}}_1$ and $\bar{\ddot{y}}_1$ estimated in (a) agree with the values of $\bar{\ddot{x}}_1$ and $\bar{\ddot{y}}_1$ calculated in (f).

3. Calculate the average values of the velocity components,

$$\bar{\dot{x}}_1 = \frac{\dot{x}(T_o) + \dot{x}(T_1)}{2} \tag{38}$$

$$\bar{\dot{y}}_1 = \frac{\dot{y}(T_o) + \dot{y}(T_1)}{2} , \tag{39}$$

and the horizontal range and altitude at the time T_1 by the equations

$$x(T_1) = x(T_o) + \Delta x_1 \tag{40}$$

$$y(T_1) = y(T_o) + \Delta y_1 , \tag{41}$$

where

$$\Delta x_1 = - \bar{\dot{x}}_1 \Delta T \tag{42}$$

$$\Delta y_1 = - \bar{\dot{y}}_1 \Delta T . \tag{43}$$

These steps were repeated for each time interval on the upleg.

The trajectory for the time intervals 230.27 to 282.30 seconds and 302.24 to 310.59 seconds on the downleg was also calculated in this fashion; however, since we were working forward in time, there were changes of sign in some of the equations used. Equations (30) and (31) of part 2b become

$$\dot{x}(T_1) = \dot{x}(T_0) + \bar{\ddot{x}}_D \, \Delta T \tag{44}$$

$$\dot{y}(T_1) = \dot{y}(T_0) - \bar{\ddot{y}}_D \, \Delta T \tag{45}$$

and equations (42) and (43) of part (3) become

$$\Delta x_1 = \bar{\dot{x}}_1 \, \Delta T \tag{46}$$

$$\Delta y_1 = \bar{\dot{y}}_1 \, \Delta T \, . \tag{47}$$

It was apparent that the time-of-flight accelerometer was not working properly during the time intervals 282.30 to 302.24 seconds and 310.59 to 404.87 seconds (the last data point). In order to fill in the trajectory in these time intervals, the drag acceleration was calculated from the drag formula at regular intervals and resolved into components proportional to the velocity components. These calculated drag-acceleration components were then used instead of measured values in a numerical process similar to that described above.

The calculated sphere-trajectory data are given in Figs. 47, 48, and 49, showing, respectively, sphere altitude vs time, sphere altitude vs horizontal range, and velocity components vs time. In the figures the NACA radar data and estimated upleg trajectory for the rocket nose cone are shown for comparison with the calculated sphere trajectory. The regions corresponding to the different types of calculations described above are indicated on the figures. The overall trajectory calculation process appears to be satisfactory. One check on the process is the sphere impact time. The trajectory calculations indicate that the sphere range at impact was almost exactly 60 miles. The last signal was received from the sphere at 404.9 seconds. At this time the altitude of the sphere, according to the calculated trajectory, was 1500 feet above the plane tangent to the earth at the launcher. At this range the surface of the earth would lie 2400 feet below the tangent plane, while the line of sight from the telemeter antenna (30 feet above launching plane at launcher) would be about 500 feet below the tangent plane. Thus at this time the calculated sphere altitude was 2000 feet above the line of sight tangent to the earth from the telemeter antenna, and 3900 feet above sea level.

If the last sphere signal indicates sphere impact with the ocean, then the calculated sphere altitude would be in error by 3900 feet at impact time. However, it is not certain that the sphere telemeter signal should have been received up until impact. The question of the propagation of the

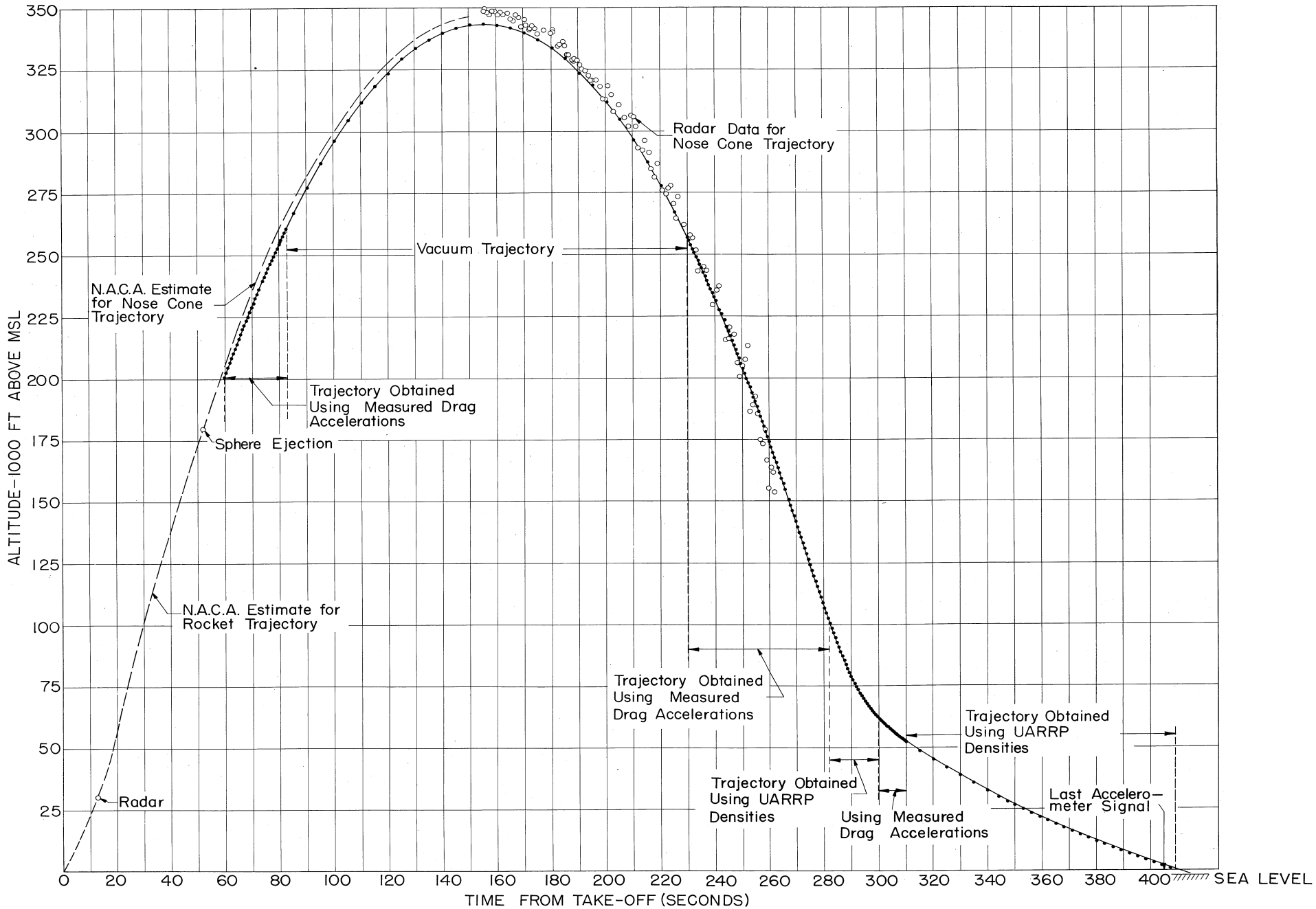

Fig. 47. Sphere altitude vs time, DAN No. 2.

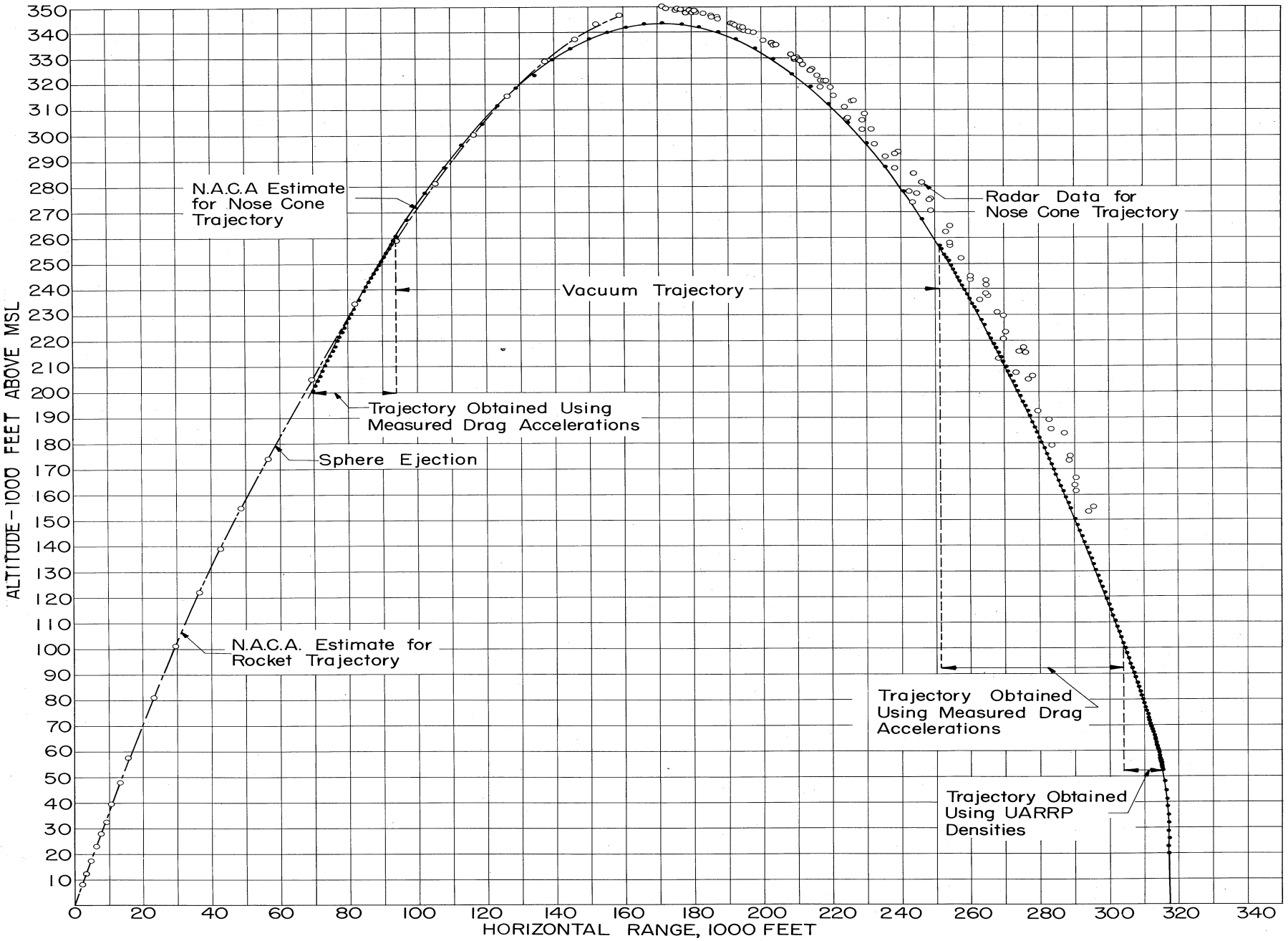

Fig. 48. Sphere altitude vs horizontal range, DAN No. 2.

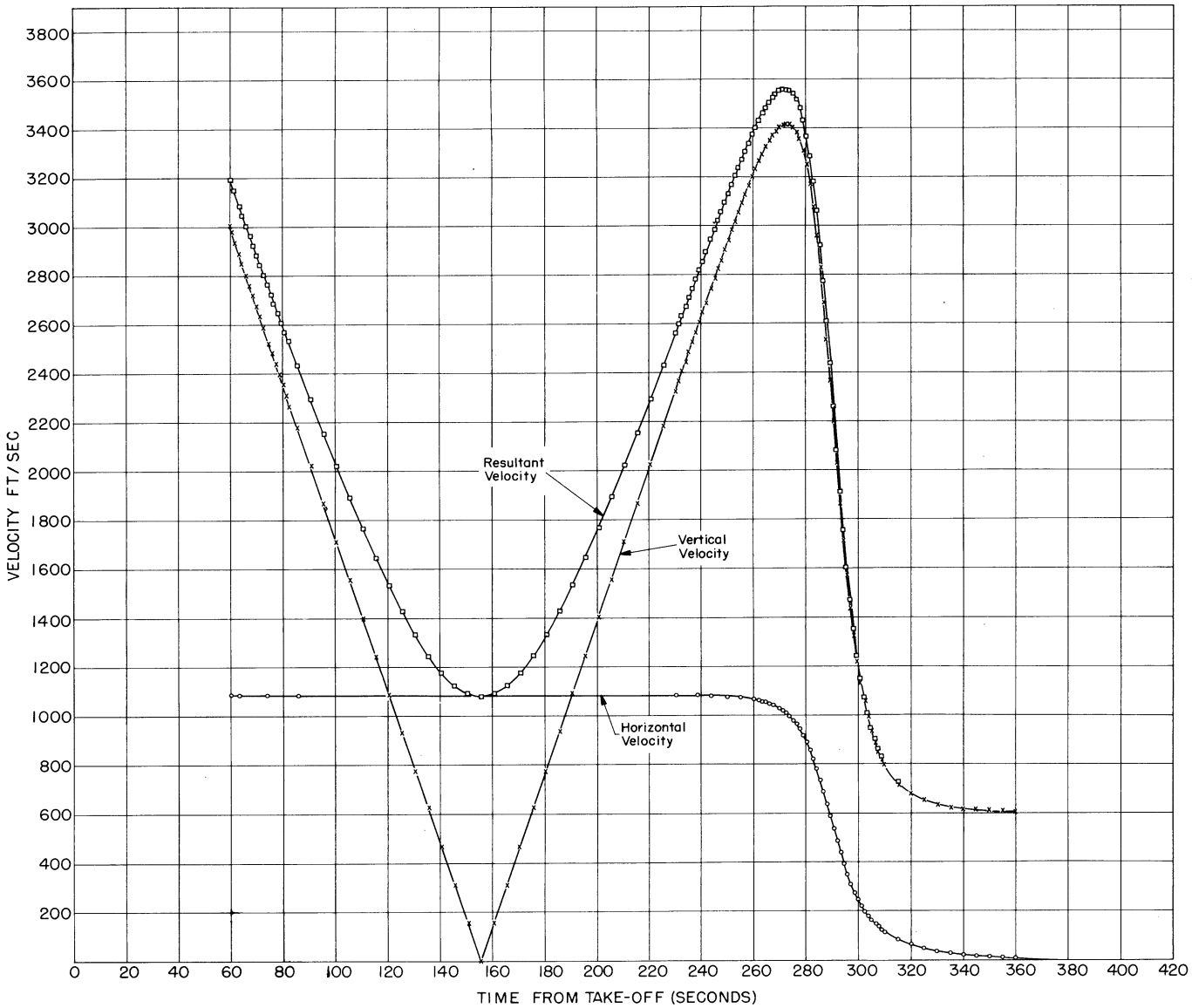

Fig. 49. Sphere velocity components vs time, DAN No. 2.

relatively weak 220-mc signal for 60 miles over the ocean from a source not more than 3900 feet above sea level is difficult to resolve. Loss of signal due to absorption or multipath transmission is possible.

The possibility of a 3900-foot error in altitude at impact appears to be unlikely considering the good agreement of the calculated densities with balloon sonde densities at the 50,000-60,000—foot altitude region (see Fig. 50). However, the drag accelerations had poor accuracy in the low-altitude regions, and the drag coefficients used in calculating drag accelerations for the latter part of the trajectory were in the high Reynolds number, low Mach number region and could have considerable error.

9.4. DENSITY AND TEMPERATURE CALCULATIONS

The equation for drag acceleration was used to calculate density. From Section 2 above, we have

$$\rho = \frac{2m}{A} \frac{a_D}{C_D V^2} \tag{1}$$

where the symbols are as defined in Section 2, i.e.:

ρ = air density, slugs/foot^3,
m = sphere mass, slugs,

$A = \frac{\pi d^2}{4}$ = sphere cross-sectional area,

a_D = drag acceleration feet/second^2,
V = sphere velocity, and
C_D = sphere drag coefficient, a function of Mach number, M, and Reynolds number, Re; these in turn are defined by

$$M = \frac{V}{a} \tag{48}$$

$$Re = \frac{\rho V d}{\mu} , \tag{49}$$

where

a = velocity of sound,
d = sphere diameter, and
μ = air viscosity.

To obtain temperature, we combine the hydrostatic equation and the equation of state of a perfect gas:

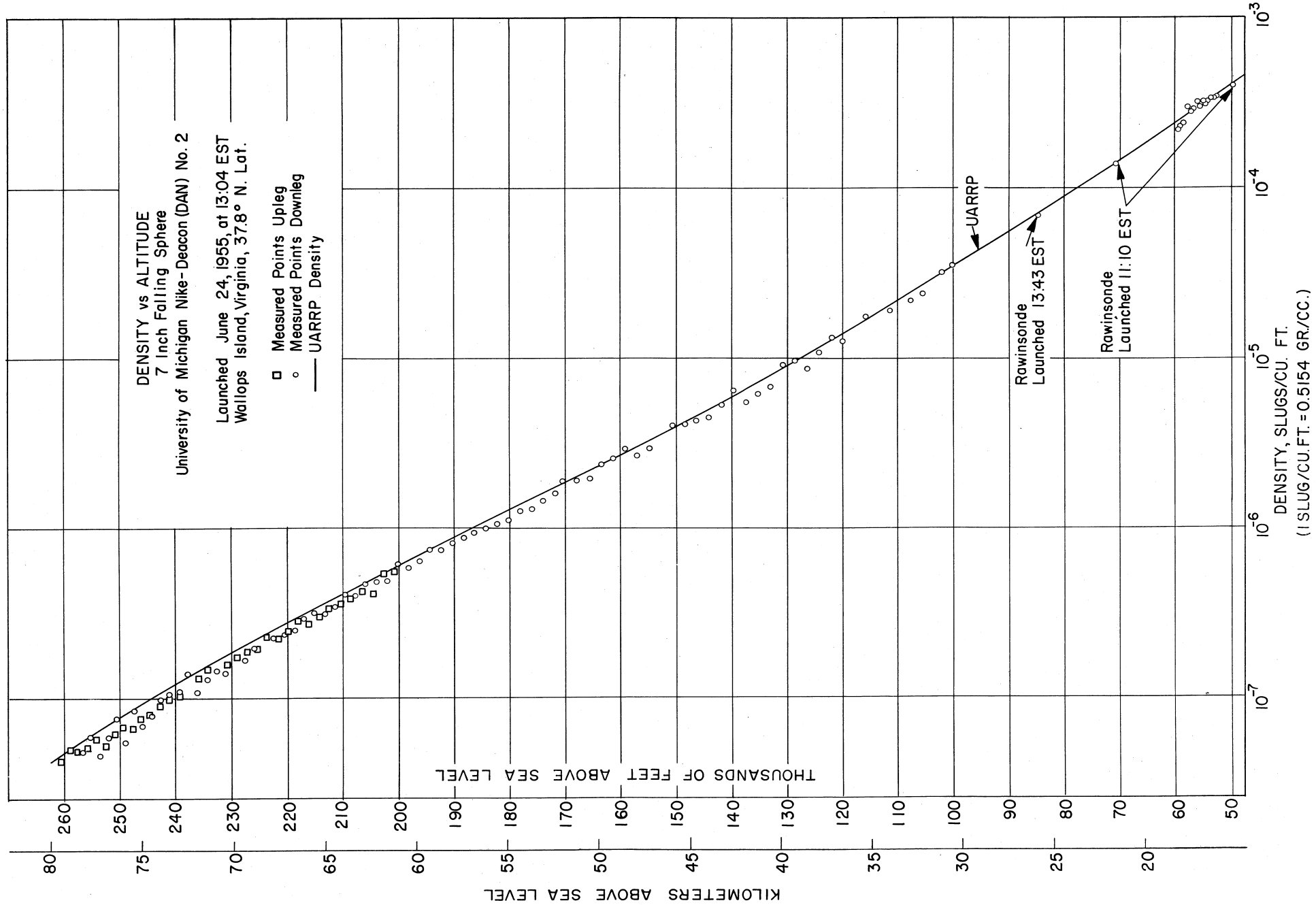

Fig. 50. Atmospheric density vs altitude, DAN No. 2.

$$dp = -g\rho \, dy \tag{50}$$

$$p = \rho \frac{R}{M_a} T , \tag{51}$$

where

p = ambient pressure,
R = universal gas constant, and
M_a = average molecular weight of air.

Integrating equation (50), we obtain

$$p(h) = -\int_{y(0)}^{y(h)} g\rho \, dy + p(0) \tag{52}$$

where

$$p(0) = \rho(0) \frac{R}{M_a} T(0) = \text{pressure at altitude } y(0),$$

$$p(h) = \rho(h) \frac{R}{M_a} T(h) = \text{pressure at altitude } y(h),$$

then

$$T(h) = -\frac{\int_{y(0)}^{y(h)} g\rho \, dy}{\rho(h) \frac{R}{M_a}} + \frac{\rho(0)}{\rho(h)} T(0) \tag{53}$$

or

$$T(h) = I(h) + \frac{\rho(0)}{\rho(h)} T(0) \tag{54}$$

where

$$I(h) = -\frac{\int_{y(0)}^{y(h)} g\rho \, dy}{\rho(h) \frac{R}{M_a}} \tag{55}$$

Equation (54) can be used to calculate temperature at the altitude $y(h)$ from the measured densities in the altitude range $y(0)$ to $y(h)$, provided $T(0)$ at $y(0)$ is known. Since $T(0)$ is not known, a reasonable value is assumed. If the assumed value is in error, $T(h)$ will also be in error. However, since $T(h)$ is the sum of two terms, the error in $T(h)$ caused by the error in $T(0)$ will decrease as the calculation proceeds and $I(h)$ becomes the dominant term. At about 45,000 feet below $y(0)$, $I(h)$ is nearly 10 times as large as

$$\frac{\rho(0)\ T(0)}{\rho(h)} \quad ,$$

and the error in T(h) due to the error in T(0) becomes negligible.

The detailed calculation procedure is the following. For each accelerometer data point, the information at hand consists of values of A, m, and d measured before the flight, accepted values of g, C_D, and μ, and assumed values of ρ, T, and a.[5] At each data point, the following series of calculations are made:

1. μ is determined from the assumed value of T.

2. $M = V/a$ and $Re = \rho Vd/\mu$ are calculated.

3. C_D is read from the chart of C_D as a function of M and Re.

4. $\rho(h)$ is calculated using equation (1).

5. T(h) is calculated using equation (54). I(h) in this equation is obtained by numerical integration of the values $\rho(h)$, g(h) using the relation

$$I(h) = \sum_{k=1}^{h} \frac{[y(k) - y(k-1)][\rho(k)g(k) - \rho(k-1)g(k-1)]}{\ln \frac{\rho(k)g(k)}{\rho(k-1)g(k-1)}} \qquad (56)$$

This formula results from assuming that in a plot of $\rho(h)g(h)$ vs h, the values are connected by exponentials. This implies that temperature is constant in the layer $x_3(k) - x_3(k-1)$.

6. The calculated values of $\rho(h)$ and T(h) will in general, differ from the assumed values. Steps (1) to (5) are then repeated, using the newly calculated values of $\rho(h)$ and T(h) in place of the assumed values. This process "converges" rapidly, because C_D does not vary rapidly with M and Re, so that usually within one to three tries agreement is reached between initial and final values of $\rho(h)$ and T(h).

The results of these calculations are shown in Figs. 50, 51, and 52. Figure 50 shows the individual calculated values of density which were obtained for the altitude range 100,000 to 260,000 feet. For the 200,000-260,000—foot region, densities were calculated on both the upleg and downleg of the trajectory and the results are seen to be in agreement. Additional density points were obtained for the 50,000-60,000—foot altitude region; these were calculated from the valid acceleration data obtained in the time interval 302 to 310 seconds. Inasmuch as the velocities used in calculating these points depend on the trajectory calculations in the interval 282 to 302

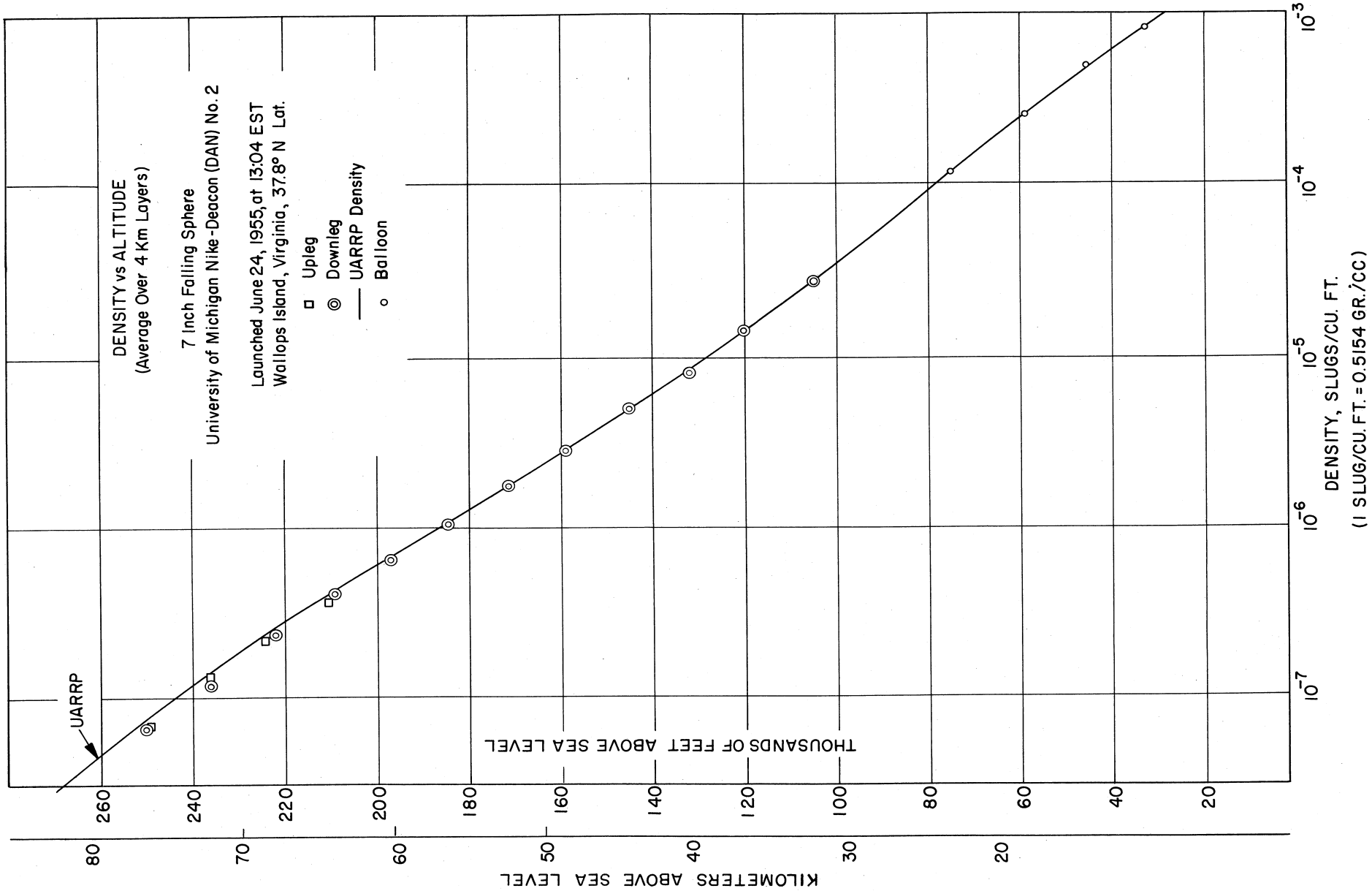

Fig. 51. Atmospheric density averaged over 4-kilometer layers vs altitude, DAN No. 2.

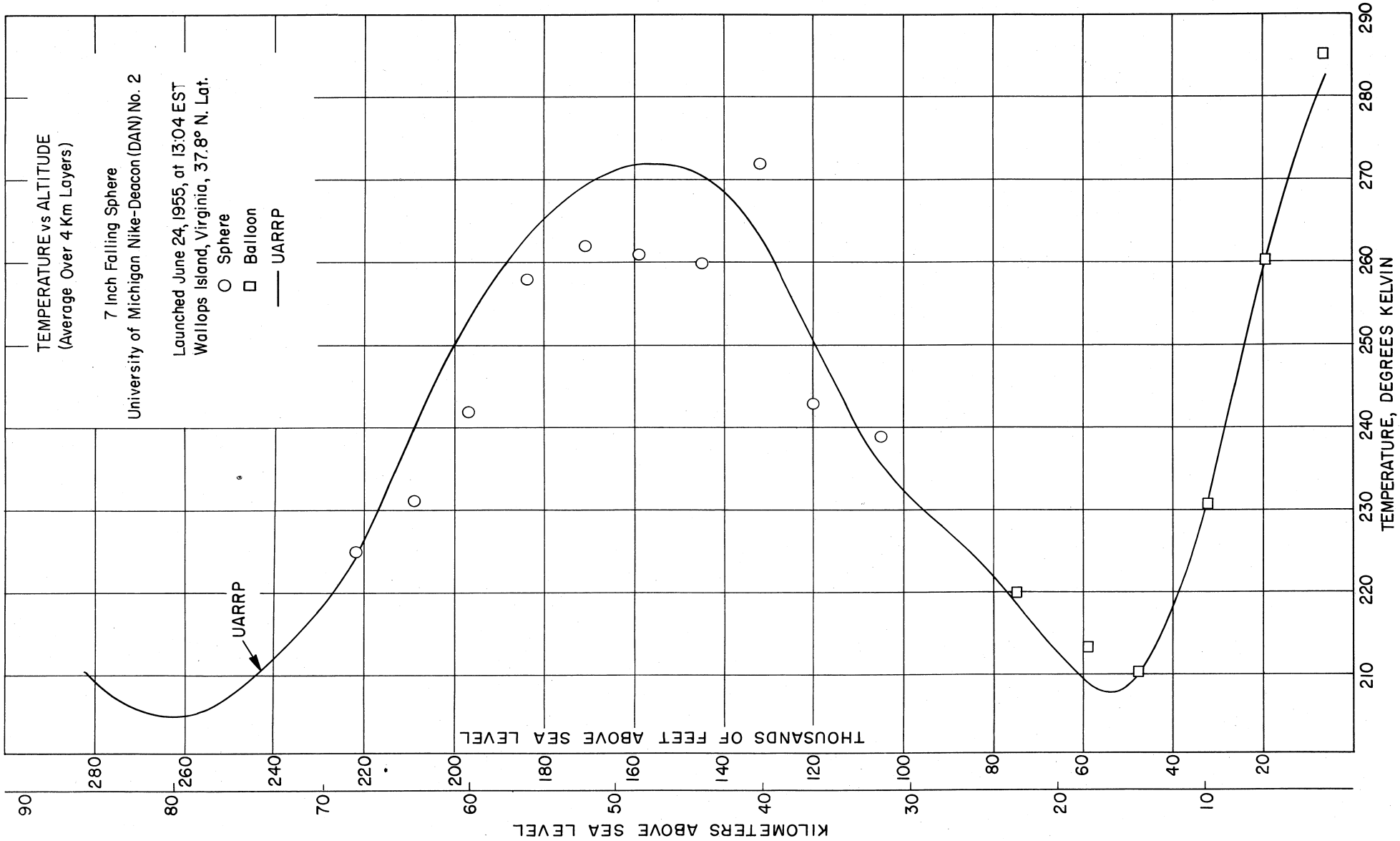

Fig. 52. Atmospheric temperature averaged over 4-kilometer layers vs altitude, DAN No. 2.

seconds which were based on the UARRP densities, they are not completely independent results; however, they are based on measured drag accelerations and therefore demonstrate the validity of the experiment in this altitude region. Rawinsonde density data and the UARRP density data are also shown in the figure for comparison.

Figure 51 shows average densities taken over 4-kilometer altitude layers. The agreement with the expected density is indicated by comparison with the UARRP data, which are also shown on the figure.

Average temperatures over 4 kilometer layers are shown in Fig. 52. The results are in agreement with UARRP density data, although in general they are slightly lower than the UARRP temperatures.

The tabulated values of density and temperature averaged over 4 kilometer layers are given in Table II. The individual calculated densities are given in Table III. The probable-error figures given in the tables are discussed in the next section.

TABLE II

AVERAGE AIR DENSITY AND TEMPERATURE
IN 4-KM LAYERS ABOVE WALLOPS ISLAND, VA.

University of Michigan Nike-Deacon (DAN) No. 2
Launched 24 June 1955 at 1304 Hours EST

Altitude				Density		Temperature	
Upleg		Downleg		Upleg	Downleg	Upleg	Downleg
km	10^3 ft	km	10^3 ft	slugs/ft^3		°K	
		32.1	105		$2.62 \pm .22 \times 10^{-5}$		239 ± 21
		36.7	120		$1.34 \pm .07$		243 ± 17
		40.1	132		$7.66 \pm .28 \times 10^{-6}$		272 ± 16
		44.1	145		$4.76 \pm .14$		260 ± 10
		48.5	159		$2.69 \pm .06$		261 ± 8
		52.0	171		$1.69 \pm .03$		262 ± 5
		56.1	184		$1.01 \pm .02$		258 ± 4
		60.0	197		$6.38 \pm .09 \times 10^{-7}$		242 ± 4
64.1	210	63.9	209	$3.56 \pm .04 \times 10^{-7}$	$3.90 \pm .04$		231 ± 3
68.1	224	67.7	222	$2.19 \pm .02$	$2.29 \pm .02$		225 ± 2
71.9	236	72.1	236	$1.30 \pm .01$	$1.16 \pm .01 \times 10^{-7}$		
75.8	249	76.2	250	$6.87 \pm .05 \times 10^{-8}$	$6.53 \pm .05 \times 10^{-8}$		

TABLE III

AIR DENSITY ABOVE WALLOPS ISLAND, VA.

University of Michigan Nike-Deacon (DAN) No. 2
Launched 24 June 1955 at 1304 Hours (EST)

DOWNLEG

Altitude km	Altitude ft	Density slugs/ft³		Temp °K
30.52	100143	3.50	x 10^{-5}	219
31.07	101937	3.18		222
32.22	105696	2.37 ± 0.40		251
32.79	107595	2.16		255
33.99	111501	1.88		249
35.22	115563	1.75		224
36.49	119723	1.25		262
37.13	121822	1.30		231
37.78	123962	1.07 ± 0.12		256
38.44	126107	8.65	x 10^{-6}	292
39.11	128323	9.67		240
39.81	130612	9.21		227
40.46	132732	6.79		283
41.13	134954	6.20		286
41.79	137105	5.46		301
42.48	139356	6.56 ± 0.56		230
43.13	141502	5.35		257
43.80	143713	4.52		279
44.50	145988	4.30		270
45.15	148121	3.82	x 10^{-6}	279
45.82	150315	4.02		243
47.14	154648	2.91		283
47.80	156821	2.65 ± 0.15		287
48.47	159018	2.93		239
49.11	161108	2.57		249
49.75	163222	2.39		245
50.41	165392	1.96		275
51.07	167552	1.90		261
51.71	169637	1.91		238
52.35	171744	1.60		261
52.99	173840	1.47 ± 0.06		262
53.62	175926	1.29		276
54.25	178001	1.25		263
54.88	180064	1.11		273
55.50	182084	1.07		262
56.12	184124	1.01		257
56.74	186153	9.41	x 10^{-7}	254
57.35	188169	8.85 ± 0.35		249
57.96	190143	8.10	x 10^{-7}	251
58.56	192136	7.46		251
59.18	194146	7.47		231
59.77	196084	6.43		247
60.37	198069	5.83		252
60.91	199833	6.17		220
61.54	201913	4.94		251
62.14	203861	4.87 ± 0.16		234
62.72	205779	4.63		226
63.29	207643	4.00		241
63.86	209523	4.05		219
64.43	211391	3.45		236
64.98	213190	3.14		241
65.55	215061	3.18		218
66.11	216892	2.93		217
66.65	218681	2.50 ± 0.07		235
67.21	220513	2.38		228
67.77	222331	2.28		219
68.83	225819	1.96		216
69.36	227571	1.68	x 10^{-7}	233
70.43	231063	1.39		
70.94	232750	1.44 ± 0.03		
71.46	234450	1.29		
71.96	236085	1.08		
72.49	237837	1.39		
72.98	239446	1.10		
73.49	241094	1.05		
73.98	242729	9.77	x 10^{-8}	
74.48	244351	7.82 ± 0.17		
74.96	245935	6.78		
75.45	247555	8.42		
75.91	249040	5.42		
76.42	250706	7.56		
76.89	252262	5.84		
77.34	253735	4.54		
77.82	255312	5.85		
78.27	256782	4.80 ± 0.11		

TABLE III (Concl.)

UPLEG

Altitude km	Altitude ft	Density slugs/ft³	Altitude km	Altitude ft	Density slugs/ft³
61.14	200605	$5.78 \pm 0.2 \times 10^{-7}$	70.90	232606	1.41×10^{-7}
61.76	202639	5.42	71.44	234390	1.45
62.35	204569	4.13	71.97	236133	1.32
62.96	206572	4.24	73.01	239550	1.02
63.56	208532	3.85	73.54	241275	9.99×10^{-8}
64.15	210477	3.62	74.07	243010	8.84 ± 0.19
64.74	212407	3.35	74.59	244705	8.03
65.31	214266	3.04	75.08	246337	7.51
65.90	216196	2.72 ± 0.07	75.61	248052	6.63
66.47	218083	2.82	76.12	249727	6.73
67.06	220011	2.43	76.56	251172	6.18
67.58	221730	2.23	77.08	252889	5.31
68.14	223547	2.29	77.58	254522	5.71 ± 0.13
68.69	225376	1.94	78.08	256163	5.15
69.26	227245	1.87	78.55	257696	4.84
69.83	229099	1.72	79.02	259238	4.90
70.36	230834	1.59 ± 0.04	79.50	260811	4.34 ± 0.10

10. ERROR ANALYSIS

The sources of error in the densities calculated are

1. The neglect of winds in equation (1).

2. Errors in the measured values of A, m, and a_D. Errors in A and m are negligible.

3. Errors in the C_D data.

4. Errors in the calculation of the trajectory; errors in altitude affect the position of the data on the figure, and errors in velocity which enter into equation (1).

The temperatures calculated from the density-vs-altitude data have additional error sources:

5. Error in the assumed T(0).

6. Errors in the numerical integration process for I(h).

10.1. WIND ERRORS

The errors caused by neglecting winds of known velocities can be calculated from equation (1). Neglecting a vertical wind component would cause a larger error than would the neglect of a horizontal wind of the same magnitude. A neglected vertical wind of 50 feet/second would cause a maximum error of about 5% in the altitude range of the experiment, whereas neglecting a horizontal wind of 100 feet/second would cause only a 1% error. It is known that horizontal winds of the order of magnitude of 10 to 200 feet/second usually do exist in the upper atmosphere,[16] however there are no data on vertical winds in the altitude range of the experiment that are known to the writers.

10.2. ERRORS IN THE MEASURED VALUES OF a_D

There are two sources of errors in the measured values of a_D used in this experiment, the transit-time accelerometer and the errors in reading the time intervals on the records.

As indicated above in Section 4.4, laboratory tests on the accelerometer showed that systematic errors and the standard deviations of random errors would be $\pm$ 1% or less for the range of accelerations from 0.01g to 5g (.32 to 160 feet/second). The accelerometer data for the one rocket flight indicated that the fingers were not picking up the bobbin of the accelerometer correctly at accelerations greater than 4g; however, for the range of the data in this experiment the figure of 1% applies.

As indicated in Section 9.1 the electronic counter and camera data recording system did not function because of low signal-to-noise ratio. The Brush record and the magnetic-tape 35-mm playback record did not yield data free of error as the counter and camera system would have done. The process of measuring the widths of signals on these records introduced errors in the accelerometer data. Laboratory tests made of the reading process indicated that the standard deviations of readings for both the Brush and film records were 0.002 second. Combining the two sources of error gives the net percent error as a function of acceleration shown in Table IV.

10.3. ERRORS IN DRAG COEFFICIENT, C_D

For most of the altitude range of the experiment, where $M > 1$ and $Re > 400$, the maximum error in drag coefficient is estimated to be less than 2%. At high altitudes, where $M > 2$ and $Re < 400$, the error in drag coefficient may be as high as 5%.

TABLE IV

ERROR IN DRAG ACCELERATION FOR DAN 2

Based on: 1% standard deviation in a single accelerometer signal
0.002 second standard deviation in reading
Probable error = 0.6745 σ

Width of Time Interval ΔT, sec	Acceleration a_D, ft/sec^2	Reading σ % of ΔT	Reading σ % of a_D	Accelerometer σ % of a_D	Net σ in Drag Accelerations % of a_D	Net Probable Error in Drag Acceleration % of a_D
.015	139.	13.3	26.6	1	26.6	18
.025	50.	8.0	16.0	1	16.04	11.1
.050	12.5	4.0	8.0	1	8.1	5.5
.070	6.39	2.9	5.72	1	5.8	3.9
.100	3.13	2.0	4.0	1	4.1	2.8
.250	0.501	0.8	1.6	1	1.9	1.3
.500	0.125	0.4	0.8	1	1.3	1.0

10.4. ERRORS IN THE TRAJECTORY CALCULATIONS

The error in altitude of any point on the sphere trajectory is the sum of the errors from two sources. The first of these, the error in nose-cone peak altitude, is estimated to be 500 feet, based on known tracking-radar accuracies. The second error is in the estimate of the difference in sphere and nose-cone peak altitudes, which may be wrong by as much as 1000 feet. The net maximum error in altitude is therefore estimated to be less than 1500 feet.

The velocity at any point on the trajectory has also two main sources of error, the horizontal velocity at peak and the error due to integration of the drag accelerations. The least-square curve fitting of the straight line indicated that there was about a 2% standard deviation in the radar velocity at peak. This in turn produces less than 1% error in velocity for all of the calculated trajectory.

10.5. ERRORS IN T(0) AND I(h)

It was noted above that an error in assumed T(0) for use in equation (54) would cause an error in the top 45,000 feet of calculated temperatures. Accordingly, temperature results are presented starting 45,000 feet below the density results and the error in temperature due to the error in T(0) is negligible. The error in the integral I(h) can be shown to be less than the

error in $\rho(h)$, the density at the same altitude.

10.6. NET ERROR IN DENSITY AND TEMPERATURE

The individual errors were combined according to error theory. The values of probable errors in individual density data points are given at regular intervals in Table III. The errors in the 4-kilometer average densities and temperatures are shown in Table II. The probable error in the average was taken to be the probable error in an individual point divided by the square of the number of points included in the average.

The probable errors increase in percent as the altitude decreases. The error in density varies from about 2% at 260,000 feet to 18% at 100,000 feet; the error in average density varies from about 1% at 260,000 feet to 7% at 100,000 feet; the error in average temperature, from 1% to 210,000 to 8% at 100,000 feet. The increase in percent error at low altitudes is due to the increase in the percent reading error, for as the altitude decreased, the drag acceleration increased, the accelerometer time interval decreased, and, therefore, the percent reading error in accelerometer time interval increased.

If the signal-to-noise ratio of the telemeter signal had been sufficient to operate the primary data recording system, the maximum error in density would have been approximately equal to the error in drag coefficient, i.e., ± 5% above 250,000 feet altitude and ± 2% below 250,000 feet altitude.

11. CONCLUSIONS

The small-sphere experiment for density resulted in significant data. Because of the low signal-to-noise ratio, the reading errors of the secondary recording system were, for the most part, the controlling errors.

With a reasonable increase in radiated power and with essentially the same primary recording system as used in DAN 2, the reading errors can be made negligibly small so that the error in coefficient of drag will be the controlling error.

The operational procedures of the experiment and of the rocket firing were simple enough so that the combination may be considered a long step forward in the achievement of a synoptic method.

The process of reproducing the sphere trajectory from peak altitude, velocity at peak, and drag acceleration was successful and introduced no significant errors in the densities and temperatures beyond those contributed by errors in the data.

Sufficient data were obtained to test the process of obtaining density and temperature without the use of the radar-tracking data. This will be attempted.

BIBLIOGRAPHY

1. The Rocket Panel (UARRP), Phys Rev., 88, 1027-1032 (1952).

2. R. A. Minzner and W. Ripley, ARDC Model Atmosphere, Geophysics Research Directorate, AFCRC, June, 1956.

3. Manual of the ICAO Standard Atmosphere-Calculations by NACA, International Civil Aviation Organization, Montreal, Canada, and Langley Field, Va., May, 1954.

4. F. L. Bartman et al., J. Atmos. and Terr. Physics, Spec. Suppl. 1 (1954).

5. F. L. Bartman, L. W. Chaney, L. M. Jones, and V. C. Liu, "Upper Air Density and Temperature by the Falling Sphere Method," J. Appl. Phys., June, 1956.

6. D. Hoffleit, "DOVAP—A Method for Surveying High Altitude Trajectories," Scientific Monthly, 68, 172 (1949).

7. F. L. Bartman, V. C. Liu, and E. J. Schaefer, "An Aerodynamic Method of Measuring the Ambient Temperature of Air at High Altitudes," Eng. Res. Inst., Univ. of Mich., Signal Corps Contract No. W-36-039 SC-32 307 (1950), p. 33.

8. A. May and W. R. Witt, Jr., "Free Flight Determinations of Drag Coefficients of Spheres," U. S. Naval Ordnance Laboratory, NAVORD Report 2352 (1952).

9. E. D. Kane, "Drag Forces on Spheres in Low Density Supersonic Gas Flow," Univ. of Calif., Eng. Projects Report HE-150-65, February, 1950.

10. F. S. Sherman,and E. D. Kane, "Supplementary Data on Sphere Drag Tests," Univ. of Calif., Eng. Projects Report HE-150-71, August, 1950.

11. F. L. Bartman, "D. C. Analog Computer Survey of Trajectories of Spheres Falling Through the Upper Atmosphere," Assn. for Comp. Mach., Ann Arbor meeting, June, 1954.

12. J. A. Van Allen and M. B. Gottlieb, "The Inexpensive Attainment of High Altitudes with Balloon-Launched Rockets," J. Atmos. and Terr. Physics, Spec. Suppl. 1 (1954).

13. L. M. Jones and W. H. Hansen, "The Nike Deacon Sounding Rocket," an informal report, Eng. Res. Inst., Univ. of Mich. (1955).

14. R. H. Heitkotter, "Flight Investigation of the Performance of a Two-Stage Solid Propellant Nike-Deacon (DAN) Meteorological Sounding Rocket," NACA Research Memorandum SL55L27 (1955).

15. Solid Propellant Information Agency Manual, Mlb-fw/B, Johns Hopkins University.

16. W. G. Stroud, W. Nordberg, and J. R. Walsh, "Atmospheric Temperatures and Winds Between 30 and 80 km," J. Geophysical Research, 61:45-56, (1956).